Physica D 56 (1992) 303–367
North-Holland

PHYSICA D

Fronts, pulses, sources and sinks in generalized complex Ginzburg–Landau equations

Wim van Saarloos
AT&T Bell Laboratories, Murray Hill, NJ 07974, USA
and Instituut-Lorentz, University of Leiden, Nieuwsteeg 18, 2311 SB Leiden, The Netherlands*

and

P.C. Hohenberg
AT&T Bell Laboratories, Murray Hill, NJ 07974, USA

Received 14 August 1991
Accepted 16 January 1992
Communicated by H. Flaschka

An important element in the long-time dynamics of pattern forming systems is a class of solutions we will call "coherent structures". These are states that are either themselves localized, or that consist of domains of regular patterns connected by localized defects or interfaces. This paper summarizes and extends recent work on such coherent structures in the one-dimensional complex Ginzburg–Landau equation and its generalizations, for which rather complete information can be obtained on the existence and competition of fronts, pulses, sources and sinks. For the special subclass of uniformly translating structures, the solutions are derived from a set of ordinary differential equations that can be interpreted as a flow in a three-dimensional phase space. Fixed points of the flow correspond to the two basic building blocks of coherent structures, uniform amplitude states and evanescent waves whose amplitude decreases smoothly to zero. A study of the stability of the fixed points under the flow leads to results on the existence and multiplicity of the different coherent structures. The dynamical analysis of the original partial differential equation focusses on the competition between pulses and fronts, and is expressed in terms of a set of conjectures for front propagation that generalize the "marginal stability" and "pinch-point" approaches of earlier authors. These rules, together with an exact front solution whose dynamics plays an important role in the selection of patterns, yield an analytic expression for the upper limit of the range of existence of pulse solutions, as well as a determination of the regions of parameter space where uniformly translating front solutions can exist. Extensive numerical simulations show consistency with these rules and conjectures for the existence of fronts and pulses. In the parameter ranges where no uniformly translating fronts can exist, examples are shown of irregularly spreading fronts that generate strongly chaotic regions, as well as nonuniformly translating fronts that lead to uniform amplitude states. Recent perturbative treatments based on expansions about the nonlinear Schrödinger equation are generalized to perturbations of the cubic-quintic and derivative Schrödinger equations, for which both pulses and fronts exist in the unperturbed system. Comparison of the results with the exact solutions shows that the perturbation theory only yields a subset of the relevant solutions. Nevertheless, those that are obtained are found to be consistent with the general conjectures, and in particular they provide an analytic demonstration of front/pulse competition. While the discussion of the competition between fronts and pulses focusses on the complex Ginzburg–Landau equation with quintic terms and a subcritical bifurcation, a number of results are also presented for the cubic equation. In particular, the existence of a family of moving source solutions derived by Bekki and Nozaki for this equation contradicts the naive counting arguments. We attribute this contradiction to a hidden symmetry of the solution but have not been able to show explicitly how this symmetry affects the phase space orbits.

*Present address.

Contents

1. Introduction 304
2. The generalized complex Ginzburg–Landau equations and the three-mode dynamical system 310
2.1 Definitions of the PDE's and ODE's 310
2.1.1. General case 310
2.1.2. The complex Ginzburg-Landau equation 311
2.1.3. Other special cases 311
2.2. Fixed points and their stability for the complex Ginzburg–Landau equation 312
2.2.1. Fixed points 312
2.2.2. Stability in the PDE dynamics 314
2.2.3. Stability in the ODE dynamics 316
2.3. Coherent structures 318
2.3.1. Definitions of fronts, pulses, sources and sinks 318
2.3.2. Counting arguments for the existence of coherent structures 319
2.3.2.1. Fronts 319
2.3.2.2. Pulses 320
2.3.2.3. Sources and sinks 320
2.3.2.4. Summary of counting arguments 322
2.3.3. The nonlinear diffusion equation 322
3. Analytic results 324
3.1. Symmetries and conservation laws 324
3.1.1. Conservation laws 324
3.1.2. Continuous symmetries 325
3.2. Integrability of the ODE's 325
3.2.1. General integrability conditions 325
3.2.2. Solitons in the nonlinear Schrödinger equation 326
3.2.3. Pulses and fronts in the quintic-cubic and generalized derivative Schrödinger equations 327
3.2.3.1. Generalized derivative Schrödinger equation 327
3.2.3.2. The quintic-cubic equation 328
3.3. Exact solutions of the complex Ginzburg–Landau equation 330
3.3.1. Nonlinear front 330
3.3.2. Exact pulse solution 333
3.3.3. Sources and sinks 335
4. Marginal stability conjectures and selection criteria 340
4.1. Linear marginal stability 340
4.2. Nonlinear selection 342
4.3. Effect of Benjamin–Feir instability 346
4.4. Implications of the terms f_2 and f_3 in eq. (2.1) 346
5. Perturbation expansions 347
5.1. Perturbing about the quintic derivative Schrödinger limit 347
5.2. Pulses and fronts in the perturbed quintic-cubic Schrödinger equation 351
6. Numerical results 355
7. Conclusion 361
7.1. Comparison with experiment 362
7.2. Open theoretical problems 363
Acknowledgements 364
Appendix. Signs of the real parts of the roots of a cubic equation 365
References 365

1. Introduction

A number of nonequilibrium pattern forming systems are known to display solutions we can call "coherent structures". These states are either themselves localized in space or they consist of a spatially extended regular pattern with a localized defect [1]. Examples are fronts, pulses, sources or sinks in one-dimensional systems, and targets, spirals, dislocations or grain boundaries in two dimensions. Such structures have been identified in experiments on thermal convection in pure fluids and binary mixtures [1, 2], on parametric surface waves in fluids [3], on Taylor–Couette flow between rotating cylinders [4, 5], in nonlinear light-wave propagation in fibers [6], and in oscillatory chemical reactions [7]. They play an important role in the dynamics of nonequilibrium pattern forming systems, for example in the selection of a final steady pattern at long times, and in the time evolution of periodic, quasiperiodic or disordered (chaotic) patterns.

The simplest set of models that account for this type of behavior, at least semi-quantitatively, are the so-called Ginzburg–Landau models, of which a prototype is the complex Ginzburg–Landau equation

$$\partial_t A = \varepsilon A + (1 + \mathrm{i}c_1)\partial_x^2 A + (1 + \mathrm{i}c_3)|A|^2 A - (1 - \mathrm{i}c_5)|A|^4 A, \tag{1.1}$$

where $A(x,t)$ is a complex function and ε, c_1, c_3 and c_5 are real coefficients. (Most, but not all, of our discussion will concern the case illustrated in eq. (1.1), where the bifurcation at $\varepsilon = 0$ is subcritical.)

The present study will confine itself to spatially infinite systems in *one dimension* and will focus primarily on temporally periodic or quasiperiodic solutions, with only limited attention given to chaotic

states that arise for many regions of the parameter space (ε, c_i). Our primary interest is to describe coherent structures, i.e solutions or features of solutions that are *localized* in space. These features can be stationary, uniformly translating (with constant velocity v) or time dependent, with a velocity $v(t)$ that is either periodic or chaotic in time. A brief account of this work was published earlier [8].

The main physical question we wish to answer can be phrased as follows: Suppose we start with the uniform $A = 0$ state at time $t = 0$, and introduce a small *localized* perturbation at $x = 0$. What will the system look like at long times? The most likely outcomes are:

(i) The system decays back to $A = 0$,

(ii) A localized pulse, or a set of pulses are formed. If so, is the velocity zero, constant, periodic or chaotic?

(iii) A stable finite-amplitude state can grow in the system by the creation and propagation of a *front* that invades the $A = 0$ state. For this case, we may ask what the wavevector and frequency of the finite amplitude state will be, as well as the velocity of the moving front.

(iv) The system can become chaotic everywhere.

For any of the above examples we may ask how sensitive the outcome will be to the particular initial disturbance.

The present paper contributes to answering the above set of questions for the complex Ginzburg–Landau model, eq. (1.1) and extensions thereof, by formulating a set of conjectures which generalize the "marginal stability" [9–11] and "pinch-point" [12–14] hypotheses of earlier authors for front dynamics, and reduce to these in appropriate special cases. Moreover, we verify our conjectures by carrying out detailed numerical computations as well as by an analytic perturbation expansion near the *dissipationless* limit of eq. (1.1), obtained by letting $|c_1|, |c_3|, |c_5| \to \infty$, where exact front and pulse solutions are available. In contrast to the expansion about the nonlinear Schrödinger limit $c_5 = 0$, $|c_3|$, $|c_1| \to \infty$ given earlier [15–18], our unperturbed system has *both* fronts and pulses, and we can therefore study the front–pulse competition analytically.

In order to formulate our selection hypotheses we first provide a detailed analysis of *uniformly translating solutions* of the partial differential equation (PDE) (1.1). These can be obtained from a set of three ordinary differential equations (ODE's) in the variable $\xi = x - vt$. Specifically, we set [19–21]

$$A(x,t) = \mathrm{e}^{-\mathrm{i}\omega t}\hat{A}(x - vt), \tag{1.2a}$$

$$\hat{A}(\xi) = a(\xi)\,\mathrm{e}^{\mathrm{i}\phi(\xi)}, \tag{1.2b}$$

and define the variables $q(\xi) = \partial_\xi \phi$, and $\kappa(\xi) = \partial_\xi a/a$. Insertion of eqs. (1.2) into (1.1) leads to the ODE's

$$\partial_\xi a = \kappa a, \quad \partial_\xi q = \mathscr{Q}(a,q,\kappa), \quad \partial_\xi \kappa = \mathscr{K}(a,q,\kappa), \tag{1.3}$$

which can be considered as a *dynamical system* in the pseudo-time ξ (the functions $\mathscr{Q}$ and $\mathscr{K}$ are calculated below). This system has parameters ε, c_1, c_3, c_5, v and ω, the first 4 of which are fixed by the starting PDE, and the last two can be varied to find different solutions. Fixed points of eq. (1.3) are nonlinear wave states of eq. (1.1) with uniform envelope, and *heteroclinic orbits* of eq. (1.3), joining different fixed points, are the coherent structures we seek to characterize. The important ones, fronts,

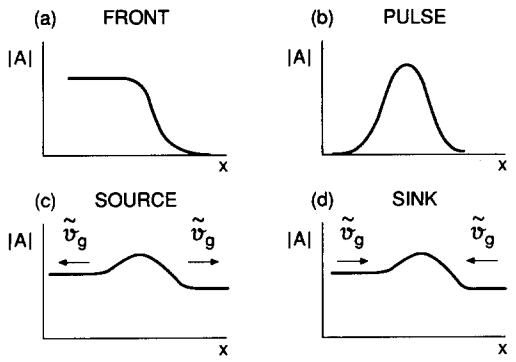

Fig. 1. Schematic sketch of various coherent structures: (a) front; (b) pulse; (c) source; (d) sink. The quantity $\tilde{v}_g$, defined in eq. (2.50) is the group velocity of the nonlinear state in the frame moving with the structure.

pulses, sources and sinks are schematically indicated in fig. 1. By studying the stability properties of the fixed points with the dynamics of eq. (1.3) we can find the *multiplicity* of solutions of eq. (1.3) of a given type. In some cases we find a discrete set and in others a one- or two-parameter family, parametrized by v and/or ω. The physically relevant front solutions are a two-parameter family plus a discrete set for $\varepsilon > 0$, and a discrete set for $\varepsilon < 0$. Furthermore, there is in general a discrete set of pulses which by symmetry includes stationary ($v = 0$) ones, a discrete set of sources, and a one-parameter family of sinks.

It should be noted that in the absence of additional symmetries these counting arguments generally yield an *upper bound* for the multiplicity of coherent structures, since they only take into account the restrictions on the orbits of eq. (1.3) resulting from the stability properties of the fixed points. Further restrictions may arise from the behavior of the orbits between the fixed points. This is illustrated by consideration of a special case of eq. (1.1), the nonlinear diffusion equation [22, 23]

$$\partial_t u = \partial_x^2 u + f(u), \tag{1.4}$$

where u and f are real functions. In this limit a mechanical analogy can be found, from which exact results are easily obtained for the multiplicity of fronts and pulses. From a comparison with the counting arguments we can show that in general[#1] the latter overestimate the multiplicity of solutions, i.e they allow for orbits that are not found as actual solutions of the system (1.3).

Besides studying the multiplicity of coherent structures we can also find a number of exact front, pulse, source and sink solutions of eq. (1.3), some of which have been obtained by previous authors [20, 24–26]. A particularly important one is an exact front solution with velocity $v^\dagger$ and spatial decay rate $\kappa_L^\dagger$ which we call the "nonlinear front". It can be obtained analytically when it exists, and it turns out to play an essential role in the selection of patterns.

Apart from the trivial symmetries of space and time translation, parity and multiplication by a constant phase, we know of no symmetries of the cubic or quintic complex Ginzburg–Landau equation (1.1) with general parameters. We therefore expect our analysis to yield an upper bound on the multiplicity of coherent structures. For special parameter values new symmetries do appear, e.g. Galilian or dilatation

[#1] For the real equation (1.4) there are also finite front solutions that correspond to singular orbits of the dynamical system (1.3) for which $\kappa \to \pm\infty$. For these the counting argument may be reformulated in terms of different variables (see section 2.3.3).

invariance, and these typically lead to continuous families of solutions. Surprisingly, Bekki and Nozaki [26] have presented a family of exact solutions of the cubic Ginzburg–Landau equation which we show to be *sources*, whereas on the basis of the stability of the fixed points of the dynamical system (1.3) only a discrete set of sources is in general expected. As we will discuss, we conjecture that this discrepancy is due to the existence of a "hidden symmetry" of the Bekki–Nozaki solution.

Front selection has been discussed in the literature primarily in terms of what has come to be known as "linear marginal stability" [9–11]. This involves a "linear front" with velocity v^* and decay rate κ_L^*, which are simply obtained by use of a stationary phase argument [10, 13, 23] from the dispersion relation of the starting equations linearized about the $A = 0$ state. Our selection conjectures [8] are a generalization of previous selection hypotheses [9–13], and reduce to these in cases where the latter are known [27] to apply. They can be stated as follows: Let us start from an initial localized disturbance embedded in the $A = 0$ state. Then for $\varepsilon > 0$, the linear front v^*, κ_L^* is selected from the family, unless there exists a nonlinear front with $v^\dagger > v^*$ *and* $|\kappa_L^\dagger| > |\kappa_L^*|$. For $\varepsilon < 0$, if a nonlinear front with $v^\dagger > 0$ exists it is selected. If $v^\dagger < 0$, or if no nonlinear front exists, then the results depend more sensitively on initial conditions. Typically, there is an interval $\varepsilon_2 < \varepsilon < \varepsilon_3 \leq 0$ in which pulses are selected, with either periodic or chaotic time dependence depending on the shape of the initial disturbance. For $\varepsilon < \varepsilon_2$ the disturbance decays back to $A = 0$, and if $\varepsilon_3 < 0$ then the interval $\varepsilon_3 < \varepsilon \leq 0$ is the one mentioned above where $v^\dagger > 0$, and the nonlinear front is selected. Since ε_3 is defined by the relation $v^\dagger = 0$ (unless $v^\dagger = 0$ for some $\varepsilon > 0$, in which case $\varepsilon_3 = 0$), we can find ε_3 analytically for given parameters (ε, c_i) in eq. (1.1). The value of ε_2, on the other hand, is not in general obtainable analytically.

A caveat for these predictions concerns the stability of the created front. From the wavevector $q_N^\dagger$ or q_N^* of the wave state left behind the front, we can predict whether this state is stable to modulational (Benjamin–Feir) [28] instabilities. If it is, we expect the front to be a stable solution, but if not, the front will be unstable, i.e. its velocity will depend on time. In that case we expect the time-averaged velocity $\bar{v}$ to be close to the predicted value, either $v^\dagger$ or v^*. More generally, for $\varepsilon > 0$, all results known to us are consistent with the conjecture that v^* represents a strict lower bound, i.e. $\bar{v} \geq v^*$ for all cases.

All of the above results and conjectures have been tested by numerical calculations of the PDE (1.1). As shown in what follows, our calculations provide confirmation of the conjectures, i.e. we have found no counterexamples. In view of the large parameter space involved in these tests (parameters ε, c_i, and arbitrary initial conditions) we cannot say we have definitely *confirmed* the conjectures, only that we have found consistency. There may well be parameter ranges and/or initial conditions where the behavior is different.

Another way to approach the selection problem is by perturbing about known solutions in special parameter regimes [15–18, 29–31]. We have chosen to start from a system we call the generalized derivative Schrödinger equation

$$\partial_t A = ic_1 \partial_x^2 A + ic_3 |A|^2 A + ic_5 |A|^4 A + \partial_x \left[\left(s_0 + s_2 |A|^2 \right) A \right], \tag{1.5}$$

and to perturb with a dissipative term on the rhs of eq. (1.5) of the form

$$b_1 B = b_1 \left(\partial_x^2 A + |A|^2 A - |A|^4 A \right). \tag{1.6}$$

It turns out that the unperturbed system (1.5) leads to an *integrable* [21] dynamical system (1.3) whose

orbits can be calculated analytically. In particular, we find a two-parameter family of pulses indexed by v and ω, whose existence is connected to the Hamiltonian property of the dynamical system (1.3) resulting from eq. (1.5), which the general case does not possess. We also have a one-parameter family of fronts indexed by v, having fixed frequency $\omega(v)$. The dissipative perturbation (1.6) then has the effect of *selecting* from the members of the families particular values of v and ω. Mathematically the selection is achieved [15–18, 29–31] by introducing a slow time variable $T = b_1 t$, and finding nonlinear differential equations for $v(T)$ and $\omega(T)$, whose fixed-point solutions are the values selected by the perturbation. In the absence of the s_0 and s_2 terms in eq. (1.5), only stationary ($v = 0$) pulses are selected, as already noted by Elphick and Meron [17] and by Malomed [16]. However, for $s_0, s_2 \neq 0$ the velocity is a complicated function of all the parameters, which is $\mathcal{O}(b_1^0)$, i.e. not small when $0 < b_1 \ll 1$. An interesting feature of the dynamics of v and ω in the slow time variable T is that it has direct relevance for the PDE, unlike the dynamical system (1.3). Indeed, stability in the slow dynamics is a necessary condition for the stability of the corresponding pulse in the PDE, though of course it is not sufficient in view of the restricted class of disturbances considered in the perturbative calculation. Nevertheless, we obtain expressions for the domain of stability of pulses $\varepsilon_2 < \varepsilon < \varepsilon_3$, and for the domain $\varepsilon_3 < \varepsilon$ where the nonlinear front is selected. We can compare the values of ε_3 and of the nonlinear velocity $v^\dagger(\varepsilon)$ with our general expressions, and we find detailed agreement to lowest order in the perturbation b_1.

Elphick and Meron [17] have previously carried out a similar perturbation theory, expanding about the nonlinear Schrödinger limit, (1.5) with $c_5 = s_0 = s_2 = 0$. As pointed out by the authors, this equation possesses dilatation and Galilean symmetries, both of which are broken by the dissipative perturbation that selects a particular pulse. It is clear from our calculation, however, that this example is misleading since the dissipationless terms in eq. (1.5) proportional to c_5 and s_2 already break these symmetries, but the double family of pulses remains. As mentioned above, the important effect of the dissipative perturbation is to destroy the Hamiltonian property of the dynamical system (1.3), and thereby select discrete pulses.

Besides the exact nonlinear front, we have examined a number of other exact solutions of eq. (1.1) proposed by previous authors and have found some additional ones. We show, for example, that the front found by Nozaki and Bekki [25a] is part of the family that contains the linear front v^*, κ_L^*, and is therefore not in general selected since it does not coincide with the linear front. The family of "hole" solutions proposed in ref. [26] is shown by us to be a family of sources. We have generalized the pulse ansatz of Hocking and Stewartson [24] to the quintic case (1.1), but we find that the ensuing pulse is confined to a subspace of the parameter space (c_1, c_3, c_5), and moreover that it is never in the stable domain $\varepsilon_2 < \varepsilon < \varepsilon_3$.

Although we have made definite progress in elucidating the selection problem we posed above, our main results are conjectures rather than proofs, and even if the conjectures are accepted as true, there remain gaps in our understanding. First of all, for large sectors of the parameter space there is no nonlinear front $v^\dagger$, $\kappa_L^\dagger$, and our conjectures do not provide unambiguous information. In some of these regions the system no doubt has only chaotic attractors and their study requires quite different methods. For example, in numerical calculations we have observed the invasion of the stable $A = 0$ state by an expanding chaotic domain for $\varepsilon < 0$. Such strongly chaotic fronts are not covered by our methods and conjectures, even though they do not contradict them. In fact stable pulse solutions were also found in the same parameter range for different initial conditions. Analogously, there are cases for $\varepsilon < 0$ where uniform amplitude states are stable but no nonlinear fronts exist. According to our rules stable pulse solutions are also expected to exist in these parameter ranges, and to be attracting for sufficiently localized initial conditions. On the other hand there must exist other initial conditions which will lead to

the stable uniform amplitude states, but we have not determined whether these states can be created via front propagation.

The above limitations arise because our formulation is strongly tied to the 3-mode dynamical system (1.3), whose form depends on the *second-order* spatial derivatives in eq. (1.1). We know, however, that both linear [9–11] and nonlinear [11] marginal stability are applicable more generally, for example to the fourth-order Swift–Hohenberg model [32]

$$\partial_t u = \varepsilon u - \left(\partial_x^2 + q_0^2\right)^2 u - u^3, \tag{1.7}$$

and its extension to the subcritical case [11]. Fourth-order models, moreover, may have stable pulses even for the real equation [33], and one might ask whether the selection problem and front/pulse competition can be understood in this more general context. Moreover, from the study of (1.7) and other models with higher space derivatives it is clear that linear marginal stability is valid even if the front it creates is not uniformly translating in time [34, 35]. For the complex Ginzburg–Landau equation (1.1), we may predict analytically whether the linear front is uniformly translating, i.e. whether it connects to an appropriate nonlinear state via an orbit of eq. (1.3). In one example where it does not, we have found numerically that the velocity v had nontrivial time dependence due to the generation of space–time defects behind the front (see section 6 and ref. [36]). A similar effect was observed by Dee [34] for fronts propagating into linearly unstable nonlinear states a_N. Whether a uniformly translating solution is created or not, all results known to us are consistent with the conjecture that for $\varepsilon > 0$, v^* is a lower bound for the time averaged velocity $\bar{v}$ at long times. Moreover, unless a nonlinear front intervenes, this bound is actually reached in the leading edge, i.e. $\bar{v} = v^*$.

Finally, we may mention a limitation of our perturbative treatment, revealed by comparing the results to the exact solutions we have found, in the limit of small values of the parameter b_1. From this comparison we see that whole classes of nonperturbative solutions exist, i.e. the perturbation theory only picks up a subset of the relevant solutions, those that are continuously tied to solutions of the unperturbed problem.

In section 2 the dynamical system consisting of 3 coupled ODE's is defined, its fixed points are identified and their stability is studied for the complex Ginzburg–Landau equation (1.1). This allows an analysis of the multiplicity of coherent structure solutions, i.e. fronts, pulses, sources and sinks. Section 3 identifies those cases possessing symmetries and/or conservation laws, where a more complete analysis of the dynamical system is possible. In particular, for the generalized derivative Schrödinger equation the dynamical system is *integrable* and all pulse and front solutions are obtained analytically. For the general nonintegrable case, certain "integrable orbits" of the dynamical system provide particular exact solutions. The basic selection conjectures for the complex Ginzburg–Landau equation are presented in section 4, and their relation to the modulational (Benjamin–Feir) instability is discussed. Section 5 is devoted to the perturbation expansion about the generalized derivative Schrödinger limit mentioned above. This calculation provides an analytic confirmation of the selection conjectures for certain sectors of parameter space, as well as a calculation of the limits ε_2 and ε_3 of pulse stability. In section 6 various numerical simulations are carried out, to test the results and conjectures of the previous sections. Excellent agreement is obtained with the basic front/pulse selection hypotheses; in particular, the dependence of the results on initial conditions in the domain $\varepsilon_2 < \varepsilon < \varepsilon_3$ is illustrated. Section 7 concludes with a brief summary, a discussion of the experimental relevance of our work, and a list of open theoretical problems.

2. The generalized complex Ginzburg–Landau equations and the three-mode dynamical system

2.1. Definition of the PDE's and ODE's

2.1.1. General case

We start with the generalized Ginzburg–Landau equation (first-order in time and second-order in space) for the complex function $A(x,t)$ in one space dimension[#2],

$$\partial_t A = (b_1 + \mathrm{i}c_1)\partial_x^2 A + f_1(|A|^2)\,A + \partial_x\big[f_2(|A|^2)A\big] + \big[\partial_x f_3(|A|^2)\big]A, \tag{2.1}$$

where the f_l are general complex functions of the real argument $|A|^2$ with

$$f_l = f_{l\mathrm{r}} + \mathrm{i}f_{l\mathrm{i}} \quad (l = 1,2,3), \tag{2.2}$$

and b_1 and c_1 are real constants (the coefficient of $\partial_t A$ can always be made unity by dividing through).

We will primarily study a particular class of solutions of eq. (2.1), namely *uniformly translating solutions*, that have the form

$$A(x,t) = \mathrm{e}^{-\mathrm{i}\omega t}\hat{A}(x - vt), \tag{2.3}$$

where ω and v are real parameters. For this class of solutions the partial differential equation (PDE) (2.1) reduces to a set of *ordinary* differential equations (ODE's) for the amplitude and phase of $\hat{A}$. Indeed, setting[#3]

$$\hat{A}(\xi) = a(\xi)\,\mathrm{e}^{\mathrm{i}\phi(\xi)}, \tag{2.4a}$$

$$\xi = x - vt, \tag{2.4b}$$

$$q(\xi) = \partial_\xi \phi, \qquad \kappa(\xi) = a^{-1}\partial_\xi a, \tag{2.4c}$$

and inserting (2.4) into (2.1), we find after some algebra

$$\begin{aligned} \partial_\xi a &= \kappa a, \\ \partial_\xi q &= \mathscr{Q}(a,q,\kappa), \\ \partial_\xi \kappa &= \mathscr{K}(a,q,\kappa), \end{aligned} \tag{2.5}$$

where

$$\begin{aligned} \mathscr{Q} = {} & -\tilde{b}_1\omega + \tilde{c}_1 v\kappa - \tilde{b}_1 vq - 2\kappa q + \tilde{c}_1\big[f_{1\mathrm{r}} + 2(f'_{2\mathrm{r}} + f'_{3\mathrm{r}})\kappa a^2 + f_{2\mathrm{r}}\kappa - f_{2\mathrm{i}}q\big] \\ & - \tilde{b}_1\big[f_{1\mathrm{i}} + 2(f'_{2\mathrm{i}} + f'_{3\mathrm{i}})\kappa a^2 + f_{2\mathrm{i}}\kappa + f_{2\mathrm{r}}q\big], \end{aligned} \tag{2.6a}$$

$$\begin{aligned} \mathscr{K} = {} & -\tilde{c}_1\omega - \tilde{b}_1 v\kappa - \tilde{c}_1 vq - \kappa^2 + q^2 - \tilde{b}_1\big[f_{1\mathrm{r}} + 2(f'_{2\mathrm{r}} + f'_{3\mathrm{r}})\kappa a^2 + f_{2\mathrm{r}}\kappa - f_{2\mathrm{i}}q\big] \\ & - \tilde{c}_1\big[f_{1\mathrm{i}} + 2(f'_{2\mathrm{i}} + f'_{3\mathrm{i}})\kappa a^2 + f_{2\mathrm{i}}\kappa + f_{2\mathrm{r}}q\big], \end{aligned} \tag{2.6b}$$

[#2] We use the notation $\partial_t A$ for partial derivatives and, when no confusion can arise, for total derivatives as well (e.g. $\partial_\xi a = \mathrm{d}a/\mathrm{d}\xi$). Occasionally we will use a prime to indicate a derivative with respect to the argument.

[#3] The representation of the dynamics of eq. (2.1) in terms of the 3 variables a, κ, q becomes singular when $a(\xi)$ has zeroes. In such cases a better representation is in terms of the 4 variables $a(\xi)$, $\partial_\xi a$, $\phi(\xi)$ and $\partial_\xi \phi$ (see Landman [20] and section 2.3.3).

where

$$\tilde{b}_1 = b_1\left(b_1^2 + c_1^2\right)^{-1}, \quad \tilde{c}_1 = c_1\left(b_1^2 + c_1^2\right)^{-1}, \tag{2.7}$$

and the f_l are functions of a^2, so $f'_{1r} = \mathrm{d}f_{1r}/\mathrm{d}a^2$, etc.

2.1.2. The complex Ginzburg–Landau equation

Many of our results will be confined to a special case of eq. (2.1), which we call the complex Ginzburg–Landau equation, for which

$$f_1 = \varepsilon - (b_3 - \mathrm{i}c_3)a^2 - (b_5 - \mathrm{i}c_5)a^4, \tag{2.8}$$

where the coefficients ε, b_i, c_i are real. Note that imaginary constant terms $\mathrm{i}c_{00}$ in f_1 and $\mathrm{i}c_{01}$ in f_2 [i.e. linear terms $\mathrm{i}c_{00}A + \mathrm{i}c_{01}\partial_x A$ in eq. (2.1)] can be removed by the transformation $A \to A\mathrm{e}^{\mathrm{i}(c_{00}t - c_{01}x/2b_1)}$. Moreover, a constant real term in f_2 can be eliminated by a Galilean transformation (see below). Apart from such constant terms in f_2 we define the Ginzburg–Landau equation by the choices

$$f_2 = f_3 = 0, \tag{2.9}$$

so eq. (2.1) becomes

$$\partial_t A = \varepsilon A + (b_1 + \mathrm{i}c_1)\partial_x^2 A - (b_3 - \mathrm{i}c_3)|A|^2 A - (b_5 - \mathrm{i}c_5)|A|^4 A. \tag{2.10}$$

We now still have the freedom to set any three of the coefficients (no two of which are in the same term) to unity in absolute magnitude, by appropriate choices of scaling of time, space and A. When $b_3 > 0$, the equation has a *supercritical bifurcation* at $\varepsilon = 0$, and one often takes $b_5 = c_5 = 0$ (b_5 is not needed for stability) and $b_1 = b_3 = |\varepsilon| = 1$, so the equation has two parameters, c_1 and c_3. When $b_3 < 0$, we have a *subcritical bifurcation*, and we must retain $b_5 > 0$ (or some higher-order term) for stability (see fig. 2). It is then usual to take $b_1 = -b_3 = b_5 = 1$, and the equation has the four parameters ε, c_1, c_3 and c_5. We shall retain the form (2.10) for later convenience in analyzing the dynamical system (2.6) [corresponding to the f_l given by eq. (2.8)], but unless otherwise noted we assume the subcritical case $b_3 < 0$.

2.1.3. Other special cases

A special cases of eq. (2.10) is the "nonlinear Schrödinger" equation ($\varepsilon = b_1 = b_2 = b_3 = b_5 = c_5 = 0$, $c_1 = 1$)

$$\partial_t A = \mathrm{i}\partial_x^2 A + \mathrm{i}c_3|A|^2 A \quad \text{(NLS)}, \tag{2.11}$$

which is both Hamiltonian and integrable. Its extension, the "quintic-cubic Schrödinger" equation ($\varepsilon = b_1 = b_3 = b_5 = 0$, $c_1 = 1$),

$$\partial_t A = \mathrm{i}\partial_x^2 A + \mathrm{i}c_3|A|^2 A + \mathrm{i}c_5|A|^4 A \quad \text{(QCS)}, \tag{2.12}$$

is Hamiltonian but not integrable. Other interesting cases are the "derivative nonlinear Schrödinger"

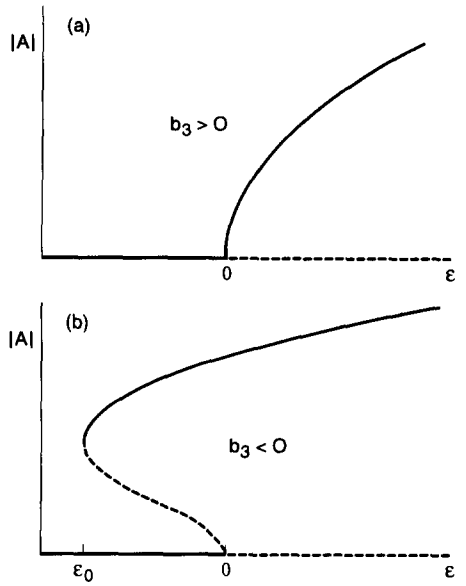

Fig. 2. Bifurcation diagram for the complex Ginzburg–Landau equation (2.10) showing (a) a supercritical and (b) a subcritical bifurcation. Solid lines denote stable states and dashed lines unstable states. Only solutions with wavevector $q_N = 0$ are represented. For $q_N \neq 0$ the solution is obtained by the transformation $\varepsilon \to \varepsilon - b_1 q_N^2$, but the stability properties are more complicated.

equation [37] ($b_1 = f_1 = 0$, $f_{2r} = s_0 + s_2|A|^2$, $c_1 = 1$)

$$\partial_t A = i\partial_x^2 A + s_0 \partial_x A + s_2 \partial_x(|A|^2 A), \quad \text{(DNS)}, \tag{2.13}$$

and the combination of eqs. (2.12) and (2.13) which we will call the "quintic derivative Schrödinger" equation,

$$\partial_t A = i\partial_x^2 A + s_0 \partial_x A + s_2 \partial_x(|A|^2 A) + ic_3|A|^2 A + ic_5|A|^4 A \quad \text{(QDS)}. \tag{2.14}$$

The special case $c_5 = 0$ of eq. (2.14) has been referred to as the modified nonlinear Schrödinger equation (MNS, see Ohkuma et al. [37]). Like the NLS or DNS, the MNS is integrable (see Wadati et al. [37]) but the general case (2.14) is not.

Equation (2.14) is invariant under the transformation $x \to -x$, $t \to -t$, $A \to A^*$. Such a transformation yielding the identity when applied twice, is called an involution. Equations like (2.14) for which an involution exists are termed "reversible" by Roberts and Quispel [38], who discuss some general implications of such reversibility. We shall study these special cases, as well as other variants of the basic system (2.1), in what follows.

2.2. *Fixed points and their stability for the complex Ginzburg–Landau equation*

2.2.1. *Fixed points*

For the complex Ginzburg–Landau equation (2.10) the functions $\mathscr{R}$ and $\mathscr{I}$ of (2.5) reduce to

$$\mathscr{R} = -\tilde{b}_1(\omega + vq) + \tilde{c}_1(\varepsilon + v\kappa) - 2\kappa q - \left(\tilde{b}_1 c_3 + \tilde{c}_1 b_3\right)a^2 - \left(\tilde{b}_1 c_5 + \tilde{c}_1 b_5\right)a^4, \tag{2.15a}$$

$$\mathscr{I} = -\tilde{c}_1(\omega + vq) - \tilde{b}_1(\varepsilon + v\kappa) + q^2 - \kappa^2 + \left(\tilde{b}_1 b_3 - \tilde{c}_1 c_3\right)a^2 + \left(\tilde{b}_1 b_5 - \tilde{c}_1 c_5\right)a^4, \tag{2.15b}$$

with $\tilde{b}_1, \tilde{c}_1$ given by eq. (2.7). The set of coupled ODE's (2.5) may be considered as a *dynamical system* [19, 20] in the pseudotime variable $\xi = x - vt$, and orbits in the three-dimensional phase space of eq. (2.5) will correspond to uniformly translating solutions of eq. (2.10). The simplest "orbits" are fixed points, which satisfy

$$\partial_\xi a = \partial_\xi q = \partial_\xi \kappa = 0, \tag{2.16}$$

and by eq. (2.15) we can distinguish two types:

- The "nonlinear" (N) fixed points with

$$a_N \neq 0, \qquad \kappa_N = 0, \tag{2.17}$$

with q_N in general nonzero, and

- The "linear" (L) fixed points with

$$a_L = 0, \qquad \kappa_L \neq 0, \tag{2.18}$$

and q_L again nonzero in general. The nonlinear fixed points correspond to traveling-wave solutions of the PDE,

$$A(x,t) = a_N \, e^{-i\omega_N t + iq_N x}, \tag{2.19a}$$

with

$$\varepsilon = b_1 q_N^2 + b_3 a_N^2 + b_5 a_N^4, \tag{2.19b}$$

$$\omega_N = \omega + v q_N = c_1 q_N^2 - c_3 a_N^2 - c_5 a_N^4. \tag{2.19c}$$

In the supercritical case ($b_3 > 0$, $b_5 = 0$) the band of allowed wavevectors is

$$0 \leq b_1 q_N^2 \leq \varepsilon. \tag{2.20}$$

For $b_3 < 0$ and $b_5 > 0$, there is a subcritical bifurcation at $\varepsilon = 0$ and a saddle-node bifurcation at

$$\varepsilon_{SN} = \varepsilon_0 = -b_3^2/4b_5. \tag{2.21}$$

For $\varepsilon \geq \varepsilon_0$ the branch of a_N solutions that is stable to amplitude perturbations (see below) has

$$2b_5 a_N^2 + b_3 > 0, \tag{2.22}$$

(see fig. 2). The band of allowed wavevectors in this case is

$$0 \leq b_1 q_N^2 \leq \varepsilon + b_3^2/4b_5. \tag{2.23}$$

Thus for given values of the parameters (ε, b_i, c_i) the solutions (2.17) corresponding to N fixed points form a two-parameter family indexed by v and ω or by v and q_N[#4].

At the linear fixed point (2.18) we have

$$\omega = -vq_L - 2b_1\kappa_L q_L + c_1(q_L^2 - \kappa_L^2), \tag{2.24a}$$

$$\varepsilon = -v\kappa_L + 2c_1\kappa_L q_L + b_1(q_L^2 - \kappa_L^2), \tag{2.24b}$$

which may also be rewritten as the complex linear dispersion relation

$$\omega = -vQ_L + i\varepsilon - i(b_1 + ic_1)Q_L^2, \tag{2.25}$$

where

$$Q_L = q_L - i\kappa_L. \tag{2.26}$$

From eqs. (2.19) and (2.25) it is clear that for fixed ω and v there are always two L fixed points, whereas the multiplicity of the N fixed points on the upper branch (2.22) depends strongly on parameters; the number of fixed points can vary from zero to four.

2.2.2. Stability in the PDE dynamics

The linear stability of the plane-wave states (2.17) in the original (PDE) dynamics of eq. (2.10) can be obtained by the standard linearization. Let

$$A(x,t) = \tilde{a}(x,t)\, e^{i\tilde{\phi}(x,t)}. \tag{2.27}$$

Then the amplitude and phase satisfy the PDE's

$$\partial_t \tilde{a} = b_1\left[\partial_x^2\tilde{a} - a(\partial_x\tilde{\phi})^2\right] - c_1\left[2(\partial_x\tilde{a})(\partial_x\tilde{\phi}) + a\partial_x^2\tilde{\phi}\right] + \varepsilon\tilde{a} - b_3\tilde{a}^3 - b_5\tilde{a}^5, \tag{2.28a}$$

$$\partial_t\tilde{\phi} = b_1\left[2\tilde{a}^{-1}(\partial_x\tilde{a})(\partial_x\tilde{\phi}) + \partial_x^2\tilde{\phi}\right] + c_1\left[\tilde{a}^{-1}\partial_x^2\tilde{a} - (\partial_x\tilde{\phi})^2\right] + c_3\tilde{a}^2 + c_5\tilde{a}^4. \tag{2.28b}$$

Let us write

$$\begin{aligned}
&\tilde{a}(x,t) = a_N + \tilde{a}_1,\\
&\tilde{\phi}(x,t) = q_N x - \omega_N t + \tilde{\phi}_1,\\
&\tilde{a}_1 = \tilde{a}_{01}\exp[iQx + \lambda t],\\
&\tilde{\phi}_1 = \tilde{\phi}_{01}\exp[iQx + \lambda t],
\end{aligned} \tag{2.29}$$

[#4]A uniformly translating solution can be written in the form (2.3) (with $\hat{A}$ a function of only one variable) in only one frame of reference, so there is a one-to-one correspondence between states of the PDE (2.1) and orbits of the dynamical system (2.5), (2.6). Since the traveling wave solutions (2.19a), which are represented by N fixed points, can be written in the form (2.3) with *any* v, the two-parameter family of fixed points of the dynamical system indexed by v and ω corresponds to a one-parameter family of traveling waves indexed by $\omega_N = \omega + vq_N$.

and linearize eq. (2.28) about $\tilde{a}_{01}, \tilde{\phi}_{01}$. The ensuing characteristic equation for λ is

$$\tilde{\lambda}^2 + \tilde{\lambda}\beta_{BF} + \gamma_{BF} = 0, \tag{2.30}$$

with

$$\tilde{\lambda} = \lambda + 2ic_1 q_N Q, \tag{2.31a}$$

$$\beta_{BF}(Q) = 2b_1 Q^2 + 2a_N^2(2b_5 a_N^2 + b_3), \tag{2.31b}$$

$$\gamma_{BF}(Q) = (c_1 Q^2 - 2ib_1 q_N Q)^2 + b_1 Q^2(b_1 Q^2 + 2b_3 a_N^2 + 4b_5 a_N^4) - 2a_N^2(c_3 + 2c_5 a_N^2)(c_1 Q^2 - 2ib_1 q_N Q). \tag{2.31c}$$

For stability we require that the solutions $\lambda(Q)$ of eq. (2.30) satisfy

$$\mathrm{Re}\,\lambda(Q) < 0, \quad \text{for all } Q. \tag{2.32}$$

Applying this condition for $Q \to 0$ we require $\beta_{BF}(0) > 0$ which is the condition (2.22) mentioned earlier. In general, the vanishing of $\mathrm{Re}\,\lambda(Q)$ signals a modulational (or "Benjamin–Feir") instability [28, 39]. The set of q_N for which condition (2.32) holds is called the Benjamin–Feir stable band. It is easy to evaluate $\lambda(Q)$ numerically and to check the stability of any particular solution a_N, q_N of (2.19), for given values of the parameters ε, b_i, c_i.

In the limit $Q \to 0$ we have $\gamma_{BF} \ll \beta_{BF}^2$. The condition (2.32) for stability is then obtained by examining the terms of order Q^4 of one of the roots. We thus must retain terms to second order in γ_{BF} and the condition becomes

$$\mathrm{Re}\left[\gamma_{BF}/\beta_{BF} + \gamma_{BF}^2/\beta_{BF}^3\right] > 0, \tag{2.33a}$$

or

$$(b_3 + 2b_5 a_N^2)^2\left[2a_N^4(b_1 b_5 - c_1 c_5) + a_N^2(b_1 b_3 - c_1 c_3) - 2b_1^2 q_N^2\right] - 2b_1^2 q_N^2(c_3 + 2c_5 a_N^2)^2 > 0. \tag{2.33b}$$

For the cubic equation ($b_5 = c_5 = 0$, $b_3 = b_1 = 1$) this becomes, using eq. (2.19),

$$q_N^2 < \varepsilon(1 - c_1 c_3)/(3 - c_1 c_3 + 2c_3^2), \tag{2.34}$$

in agreement with eq. (10) of Malomed [39a]. Thus a necessary condition for stability in the cubic case is the well-known relation

$$1 - c_1 c_3 > 0. \tag{2.35}$$

In the general case if eq. (2.33) is satisfied one can test for the stability with respect to higher Q by writing the relation $\mathrm{Re}\,\lambda(Q) = 0$ as

$$\mathrm{Re}\,\gamma_{BF} = \mathrm{Im}\,\gamma_{BF}/4\beta_{BF}^2, \tag{2.36}$$

which leads to a cubic equation in Q^2. One then requires for stability that this equation should have no positive roots. Alternatively one can simply evaluate $\mathrm{Re}\,\lambda(Q)$ numerically as a function of Q and check, for given values of the parameters $\{\varepsilon, b_i, c_i\}$, whether it remains negative for all Q.

2.2.3. Stability in the ODE dynamics

For later reference, we also wish to know the stability properties of the N and L fixed points, within the dynamical system (2.5), (2.15). We therefore linearize those equations about the fixed point solutions (2.17) and (2.18). At the linear fixed point L the three eigenvalues are

$$\lambda_{\mathrm{L}}^{0} = \kappa_{\mathrm{L}}, \tag{2.37a}$$

$$\lambda_{\mathrm{L}}^{(\pm)} = -\left(\tilde{b}_1 v + 2\kappa_{\mathrm{L}}\right) \pm \mathrm{i}|\tilde{c}_1 v - 2q_{\mathrm{L}}|. \tag{2.37b}$$

We shall denote the L fixed points by $\mathrm{L}_{\pm}$ depending on the sign of κ_{L}, i.e. L_{-} represents a state that is evanescent for $\xi \to +\infty$,

$$\mathrm{L}_{-}: \kappa_{\mathrm{L}} < 0, \quad A(x,t) \sim \mathrm{e}^{\kappa_{\mathrm{L}}\xi} = \mathrm{e}^{-|\kappa_{\mathrm{L}}|(x-vt)}, \tag{2.38}$$

and L_{+} a state evanescent for $\xi \to -\infty$,

$$\mathrm{L}_{+}: \kappa_{\mathrm{L}} > 0, \quad A(x,t) \sim \mathrm{e}^{\kappa_{\mathrm{L}}\xi} = \mathrm{e}^{|\kappa_{\mathrm{L}}|(x-vt)}. \tag{2.39}$$

In discussing the stability properties of the fixed points we assume $v > 0$, since the case $v < 0$ can be obtained from the following symmetry of the dynamical system (2.5), (2.15):

$$v \to -v, \quad \xi \to -\xi, \quad \kappa \to -\kappa, \quad q \to -q, \quad a \to a. \tag{2.40}$$

To determine the stability properties of the two L fixed points labelled L_1 and L_2 from eqs. (2.37) we must know the signs and magnitudes of the κ_{L}. From eq. (2.25) it follows that the two roots $Q_{\mathrm{L}1}$ and $Q_{\mathrm{L}2}$ satisfy

$$Q_{\mathrm{L}1} + Q_{\mathrm{L}2} = \mathrm{i}v\left(\tilde{b}_1 - \mathrm{i}\tilde{c}_1\right). \tag{2.41}$$

For $\kappa_{\mathrm{L}} = -\mathrm{Im}\, Q_{\mathrm{L}}$ this implies

$$\mathrm{Re}\,\lambda_{\mathrm{L}1}^{(\pm)} = -\left(\tilde{b}_1 v + 2\kappa_{\mathrm{L}1}\right) = -\mathrm{Re}\,\lambda_{\mathrm{L}2}^{(\pm)} = \left(\tilde{b}_1 v + 2\kappa_{\mathrm{L}2}\right), \tag{2.42}$$

for all v. For $\varepsilon < 0$ there is one fixed point[#5] with $\kappa_{\mathrm{L}} < 0$ ($\mathrm{L}_{-1}, \kappa_{\mathrm{L}1} < 0$) and one with $\kappa_{\mathrm{L}} > 0$ ($\mathrm{L}_{-2}, \kappa_{\mathrm{L}2} > 0$), and eq. (2.42) then implies that in this case $\mathrm{Re}\,\lambda_{\mathrm{L}1}^{(\pm)} > 0$ while $\mathrm{Re}\,\lambda_{\mathrm{L}2}^{(\pm)} < 0$. For $\varepsilon > 0$, on the other hand, the signs of κ_{L} depend on v: for $v < v_{\mathrm{cL}}$, with

$$v_{\mathrm{cL}} = |c_1\varepsilon - \omega b_1|/(b_1\varepsilon)^{1/2}, \tag{2.43}$$

we have $\kappa_{\mathrm{L}1} < 0$ (L_{-1}) and $\kappa_{\mathrm{L}2} > 0$ (L_{+2}). As before this entails $\mathrm{Re}\,\lambda_{\mathrm{L}1}^{(\pm)} > 0$, and $\mathrm{Re}\,\lambda_{\mathrm{L}2}^{(\pm)} < 0$ in this regime. For $v > v_{\mathrm{cL}}$ we have two L_{-} fixed points L_{-1} and L_{-2}. Although $\mathrm{Re}\,\lambda_{\mathrm{L}}^{(\pm)}$ may go through zero at some $v > v_{\mathrm{cL}}$, it is clear that even if this happens there is always one fixed point with three attractive

[#5] From eq. (2.25) we have for $v \to 0$, $Q_{\mathrm{L}}^2 \sim (q_0 + \mathrm{i}\kappa_0)^2$, so we can define $\kappa_{\mathrm{L}1} = -\kappa_0 < 0$, $\kappa_{\mathrm{L}2} = \kappa_0 > 0$ at small v, and for $v \to \infty$ we have $\kappa_{\mathrm{L}1} \sim -vb_1, \kappa_{\mathrm{L}2} \sim -\varepsilon/v$. Furthermore, from eq. (2.24b) it follows that κ_{L} (viewed as a function of v) can only go through zero for $\varepsilon > 0$, and since $\mathrm{d}\kappa_{\mathrm{L}}/\mathrm{d}v = -2b_1[(v/q_{\mathrm{L}} - 2c_1)^2 + 4b_1^2]^{-1} < 0$ when $\kappa_{\mathrm{L}} = 0$, each root can only go through zero once. These results together imply that $\kappa_{\mathrm{L}1} < 0$ for any ε, and that $\kappa_{\mathrm{L}2}$ goes through zero once as a function of v for $\varepsilon > 0$. This zero occurs at $v = v_{\mathrm{cL}} = |c_1\varepsilon - \omega b_1|/(b_1\varepsilon)^{1/2}$, so for $\varepsilon > 0$ we have $\kappa_{\mathrm{L}2} > 0$ for $v < v_{\mathrm{cL}}$ and $\kappa_{\mathrm{L}2} < 0$ for $v > v_{\mathrm{cL}}$ as stated in eq. (2.43).

eigendirections and one with a single attractive eigendirection. If we denote the latter by L_{-1}, we finally have the following stability properties for the two linear fixed points:

$$\varepsilon < 0: \quad L_{-1}(++-), \quad L_{+2}(+--), \quad \text{for all } v, \tag{2.44a}$$

$$\varepsilon > 0: \quad L_{-1}(++-), \quad L_{+2}(+--), \quad \text{for } 0 < v < v_{cL}, \tag{2.44b}$$

$$L_{-1}(++-), \quad L_{-2}(---), \quad \text{with } |\kappa_{L1}| > |\kappa_{L2}|, \quad \text{for } v > v_{cL}, \tag{2.44c}$$

with v_{cL} given in eq. (2.43).

The stability of the nonlinear fixed point is determined by the secular equation

$$\lambda^3 + \alpha_N \lambda^2 + + \beta_N \lambda + \gamma_N = 0, \tag{2.45}$$

with

$$\alpha_N = 2\tilde{b}_1 v, \tag{2.46}$$

$$\beta_N = \tilde{b}_1^2 v^2 + (\tilde{c}_1 v - 2q_N)^2 - 2a_N^2\left[\left(\tilde{b}_1 b_3 - \tilde{c}_1 c_3\right) + 2\left(\tilde{b}_1 b_5 - \tilde{c}_1 c_5\right)a_N^2\right], \tag{2.47}$$

$$\gamma_N = 2a_N^2\left\{-v\tilde{b}_1 b_1^{-1}\left(b_3 + 2b_5 a_N^2\right) + 2q_N\left[\left(\tilde{b}_1 c_3 + \tilde{c}_1 b_3\right) + 2\left(\tilde{b}_1 c_5 + \tilde{c}_1 b_5\right)a_N^2\right]\right\}, \tag{2.48a}$$

$$= 2a_N^2\left\{-(\tilde{c}_1 v - 2q_N)\left[\left(\tilde{b}_1 c_3 + \tilde{c}_1 b_3\right) + 2\left(\tilde{b}_1 c_5 + \tilde{c}_1 b_5\right)a_N^2\right]\right.$$
$$\left. -\tilde{b}_1 v\left[\left(\tilde{b}_1 b_3 - \tilde{c}_1 c_3\right) + 2\left(\tilde{b}_1 b_5 - \tilde{c}_1 c_5\right)a_N^2\right]\right\}. \tag{2.48b}$$

The signs of the real parts of the roots of eq. (2.45) are obtained quite generally from the formulas given in the appendix. We will denote N fixed points as N_+ or N_- depending on the sign of γ_N. Since $\alpha_N > 0$, according to (A.2d) an N_- fixed point always has $+--$, whereas according to (A.2a, b) an N_+ fixed point can have $---$ or $++-$ depending on v and q_N, which determine the sign of $(\alpha_N\beta_N - \gamma_N)$. From eq. (2.48a) it is clear that γ_N is always a decreasing function of v on the upper branch where eq. (2.22) holds, so that for large enough v we have $\gamma_N < 0$, and there are only N_- fixed points. For $v \to 0$ on the other hand there is one N_+ and one N_- fixed point, since by eq. (2.19) there are two fixed points with q_N of opposite sign, and the coefficient of q_N in eq. (2.48a) has a definite sign. In order to describe the fixed-point structure it is simplest to follow their evolution from $v = 0$ at fixed q_N, considering ω to be a function of q_N and v, given by eq. (2.19). The fixed point with $\gamma_N < 0$ at $v = 0$ retains $\gamma_N < 0$ and we denote it as $N_{-1}(+--)$. The other fixed point is $N_{-2}(+--)$ for sufficiently large v, and $N_+(++-)$ for $v = 0$. For intermediate v the structure is either $N_+(++-)$ or $N_+(---)$, depending on parameters. In summary, we thus have

$$v < v_{cN1}: \qquad N_-(+--) \quad \text{and} \quad N_+(++-), \tag{2.49a}$$

$$v_{cN1} < v < v_{cN2}: \qquad N_{-1}(+--) \quad \text{and} \quad N_+(---), \tag{2.49b}$$

$$v > v_{cN2}: \qquad N_{-1}(+--) \quad \text{and} \quad N_{-2}(+--). \tag{2.49c}$$

The precise values of v_{cN1} and v_{cN2} depend on parameters and will not be needed in what follows.

Another property of the N states is the group velocity v_g of the waves obtained from eq. (2.19),

$$v_g = d\omega_N/dq_N = \tilde{v}_g + v, \tag{2.50a}$$

$$\tilde{v}_g = d\omega/dq_N = -v + 2c_1 q_N - (c_3 + 2c_5 a_N^2)(da_N^2/dq_N), \tag{2.50b}$$

$$q_N = -(2b_1)^{-1}(b_3 + 2b_5 a_N^2)(da_N^2/dq_N). \tag{2.50c}$$

The quantity $\tilde{v}_g$ is the group velocity in the frame moving with velocity v. Use of eq. (2.19b) to evaluate da_N^2/dq_N and comparison with eq. (2.48) yields

$$\tilde{v}_g = \gamma_N(b_1^2 + c_1^2)\left[2a_N^2(b_3 + 2b_5 a_N^2)\right]^{-1}, \tag{2.51}$$

so that eq. (2.51) implies for the physically relevant upper branch (2.22)

$$\operatorname{sgn} \tilde{v}_g = \operatorname{sgn} \gamma_N. \tag{2.52}$$

The implications of eq. (2.52) for the stability of fronts are discussed in section 4.

2.3. *Coherent structures*

2.3.1. *Definitions of fronts, pulses, sources and sinks*

Besides the N and L fixed points, we can define other solutions of the PDE (2.10) by finding *heteroclinic trajectories* of the dynamical system (2.5), (2.15), joining different L and N fixed points [20]. These represent coherent structures, of which we can define the three different classes[#6] mentioned in the introduction and illustrated in fig. 1:

- pulses, going[#7] from an L_+ to an L_- fixed point;
- fronts, going from an N fixed point to an L_- fixed point, or from an L_+ fixed point to an N fixed point;
- domain boundaries, joining two N fixed points.

Necessary conditions for the existence of such orbits are obtained by requiring that the orbit be orthogonal to any unstable direction at an incoming fixed point[#7]. For example a pulse orbit coming into an L_- $(++-)$ fixed point must be adjusted to be orthogonal to both of its unstable $(+)$ directions. This is achieved by adjusting the parameters in the system, typically v or ω, at fixed ε, b_i, c_i.

A front will be called *positive* if it represents a situation where the N state invades the L state, i.e. if $v > 0$ under our convention that N is on the left and L on the right. Domain boundaries whose N states have group velocities $\tilde{v}_g$, eq (2.50), of opposite sign are defined as *sinks* if they have incoming waves ($\tilde{v}_g > 0$ for $\xi \to -\infty$, $\tilde{v}_g < 0$ for $\xi \to \infty$) or *sources* if they have outgoing waves ($\tilde{v}_g < 0$ for $\xi \to -\infty$, $\tilde{v}_g > 0$ for $\xi \to +\infty$).

[#6] The nomenclature for coherent structures is not uniform in the literature: pulses are also referred to as solitons or s-waves, fronts are known as kinks or shocks, sinks are called shocks, sources are called targets, and domain boundaries are sometimes referred to as holes, pulses or fronts.

[#7] We define the orbits as going from $\xi = -\infty$ to $\xi = +\infty$.

2.3.2. Counting arguments for the existence of coherent structures

The results we have obtained in section 2.3.1 for the stability of the fixed points, together with symmetry considerations, allow us to find necessary conditions for the existence of the various coherent structures. Consider e.g. a trajectory flowing from an N fixed point to an L fixed point. If the N fixed point has n_N unstable directions, there are $n_N - 1$ free parameters characterizing the flow on the n_N-dimensional subspace spanned by the unstable eigenvectors. Together with the parameter v and ω, this yields $n_N + 1$ free parameters. If the L fixed point that the trajectory needs to flow into has n_L unstable directions, the requirement that the trajectory should come in orthogonal to these yields n_L conditions. The multiplicity of this type of trajectory will therefore be $n = n_N - n_L + 1$, and, depending on n, we will say we are left with either an n-parameter family ($n \geq 1$), or a discrete set of structures ($n = 0$), or no structure at all ($n < 0$). These arguments, based as they are on *necessary* conditions, yield an upper limit[#8] for the multiplicity of a particular class of structures, i.e. the likelihood of finding nearby structures *if* one is known to exist. We shall typically consider the parameters ε, b_i and c_i to be fixed, and find multiplicities as v and ω are varied. In cases where an N state is involved we can eliminate ω in favor of q_N via eq. (2.19), and it is usually more convenient to consider v and q_N as the parameters to be varied.

Clearly, the counting arguments are based on the assumption that the various conditions for flow into and out of the fixed points are independent. When the dynamical system has *symmetries*, it can happen that fewer parameter adjustments are needed in order to satisfy the constraints, thus leading to *larger* multiplicities of solutions. In the discussion below we will first consider the cubic-quintic complex Ginzburg–Landau equation in the general case with no special symmetries. We will then consider particular choices of the $\{\varepsilon, b_i, c_i\}$ where the multiplicities change as a result of additional symmetries (see section 3.2.3).

2.3.2.1. Fronts. A positive front is an orbit from N to L_-, and a negative front an orbit from L_+ to N. (We are only considering $v > 0$, since $v < 0$ is equivalent by the transformation (2.40).) For $\varepsilon > 0$, according to (2.44b, c) there are two L_- fixed points $L_{-1}(+\,+\,-)$ and $L_{-2}(-\,-\,-)$, and either one or two $N_-(+\,-\,-)$ fixed points[#9] depending on v. When there is one N_- fixed point, the other fixed point is $N_+(+\,+\,-)$ or $N_+(-\,-\,-)$. An orbit from $N_-(+\,-\,-)$ to $L_-(+\,+\,-)$ has a unique outgoing direction, and in order to arrive at $L_-(+\,+\,-)$, the incoming direction must be made orthogonal to both unstable eigenvectors, requiring adjustment of two parameters, v and q_N. Thus we expect in general a discrete set of such fronts, with velocities v_f and ω_f. For a front going from $N_-(+\,-\,-)$ to $L_-(-\,-\,-)$, on the other hand, all incoming directions are stable at L_-, so we expect a two-parameter family of such fronts, indexed by v and q_N. The $N_+(+\,+\,-)$ fixed point has a one-parameter continuum of outgoing directions, so fronts represented by $N_+(+\,+\,-) \to L_-(+\,+\,-)$ therefore exist as a one-parameter family, whereas $N_+(+\,+\,-) \to L_-(-\,-\,-)$ yields a three-parameter family.

The results we have obtained in section 2.2.3 for the stability of the fixed points, coupled with the above arguments, lead to the following multiplicities for positive fronts ($N_- \to L_-$ or $N_+ \to L_-$):

- For $\varepsilon > 0$: There is always at least one discrete set of $N_- \to L_-$ fronts. For $v > v_{cL}$ there is in addition a two-parameter family of $N_- \to L_-$ fronts. There are also families of $N_+ \to L_-$ fronts whose

[#8] Strictly speaking the counting arguments yield an upper limit for the multiplicity of orbits of the dynamical system (2.5). There might be other solutions of the PDE (2.1) not of the form (2.3), which one may wish to refer to as coherent structures, but we do not consider these here.

[#9] Recall that we define $L_\pm$ according to the sign of κ_L (eq. (2.38)), and $N_\pm$ according to the sign of γ_N (see after eq. (2.48)), or in view of eq. (2.52), according to the sign of the group velocity $\tilde{v}_g$.

multiplicities can be readily established once the v_{cNi} and v_{cL} are known. We shall not work these out in detail since we will see that fronts coming from N_+ are dynamically unstable.

• For $\varepsilon < 0$: There is a discrete set of $N_- \to L_-$ fronts, plus families of $N_+ \to L_-$ fronts which again depend on v.

Similarly, negative fronts ($L_+ \to N_+$ or $L_+ \to N_-$) can be shown to have the following multiplicities:

• For $\varepsilon > 0$: Negative fronts ($L_+ \to N$) exist only for $v < v_{cL}$. There is a one-parameter family of $L_+ \to N_-$ fronts, plus either a discrete set or a two-parameter family of $L_+ \to N_+$ fronts, depending on the relative magnitudes of v_{cL} and the v_{cNi}.

• $\varepsilon < 0$: There is always a one-parameter family of $L_+ \to N_-$ fronts, plus a discrete set or a two-parameter family of $L_+ \to N_+$ fronts for $v_{cN1} < v < v_{cN2}$.

2.3.2.2. Pulses. Pulses correspond to $L_+ \to L_-$ orbits so the counting is quite simple. From the results in eq. (2.44) we expect a discrete set to exist for $\varepsilon < 0$ and for $\varepsilon > 0$, with $v < v_{cL}$. According to this argument, the condition that the discrete pulse be stationary

$$v_p = 0, \tag{2.53}$$

would seem to require an additional adjustment, i.e. would only be satisfied in a codimension-one subspace of the $\{\varepsilon, b_i, c_i\}$ parameter space. It turns out, however, that for stationary pulses there is an additional symmetry of eqs. (2.5) and (2.15),

$$\xi \to -\xi, \qquad q \to -q, \qquad \kappa \to -\kappa, \qquad a \to a, \tag{2.54}$$

which eliminates one of the necessary parameter adjustments. Indeed, starting from the L_+ fixed point ($a_L = 0$, $q_L \neq 0$, $\kappa_L \neq 0$) an arbitrary orbit intersects the $\kappa = 0$ plane at some point a_0, q_0, and we can use the parameter ω to fix $q_0 = 0$. The pulse orbit is then completed by symmetry from $(a_0, 0, 0)$ to the point L_- whose coordinates are $(0, -q_L, -\kappa_L)$. Thus stationary pulses are generically contained in the discrete set $\{v_p, \omega_p\}$.

2.3.2.3. Sources and sinks. From eq. (2.52) we see that sources can be defined as $N_- \to N_+$ orbits, and sinks as $N_+ \to N_-$ orbits, since the subscript on N can refer either to the sign[#9] of γ_N or $\tilde{v}_g$. For $v = 0$ the N_+ fixed point of eq. (2.15) always has according to the discussion following eq. (2.48) the stability properties $N_+(++-)$. A source (target) corresponds to an $N_-(+--) \to N_+(++-)$ orbit and in general requires adjusting two parameters, but once again we can use the symmetry (2.54) to eliminate one adjustment for $v = 0$: a trajectory leaving $N_-(a_N \neq 0, q_N \neq 0, \kappa_N = 0)$ in general hits the $q = 0$ plane at the point $(a_0, 0, \kappa_0)$, and we can use ω (or q_N) to set $\kappa_0 = 0$ or $a_0 = 0$. This means that there is in general a discrete set of $v = 0$ sources. The source orbit going to $N_+(a_N, -q_N, 0)$ is then completed by symmetry. A sink (shock) corresponds to an $N_+(++-) \to N_-(+--)$ orbit, and it has the additional freedom of a one-parameter family of departing directions from $N_+(++-)$, so we are left with a family of $v = 0$ sinks, indexed by q_N.

For $v \neq 0$, the above arguments yield a discrete set of sources for small v, but a possible two-parameter family of $N_-(+--) \to N_+(---)$ sources in the range $v_{cN1} < v < v_{cN2}$ where an $N_+(---)$ fixed point exists. Sinks, represented by $N_+(++-) \to N_-(+--)$ orbits, form a two-parameter family in the range $v < v_{cN1}$ where the $N_+(++-)$ fixed point exists.

For sources and sinks we may make general quantitative statements about the velocity, knowing only the properties of the two fixed points [39b]. Let us consider the general form (2.1) with $f_2 = f_3 = 0$

$$\partial_t A + (b_1 + ic_1)\partial_x^2 A + f_1(|A|^2)A, \tag{2.55}$$

with

$$f_1 = f_{1r} + if_{1i}. \tag{2.56}$$

Then the N fixed-point conditions analogous to (2.19b, c) imply

$$b_1 q_N^2 = f_{1r}(a_N^2), \tag{2.57}$$

which we assume to be invertible (i.e. we consider only the stable branch defined by a generalization of eq. (2.22)],

$$a_N^2 = f_{1r}^{-1}(b_1 q_N^2), \tag{2.58}$$

and

$$\omega + vq_N - c_1 q_N^2 = -f_{1i}(a_N^2). \tag{2.59}$$

The group velocity is[#2]

$$\tilde{v}_g = (d\omega/dq_N) = -v + 2c_1 q_N - 2b_1 q_N f'_{1i}/f'_{1r}. \tag{2.60}$$

For an $N_1 \to N_2$ domain boundary we have, assuming $q_{N1} \neq q_{N2}$,

$$v = c_1(q_{N1} + q_{N2}) + \left(\frac{f_{1i}(a_{N1}^2) - f_{1i}(a_{N2}^2)}{q_{N1} - q_{N2}}\right), \tag{2.61}$$

$$\tilde{v}_{g1} + \tilde{v}_{g2} = 2\left(\frac{f_{1i}(a_{N1}^2) - f_{1i}(a_{N2}^2)}{q_{N1} - q_{N2}}\right) - 2b_1\left(\frac{f'_{1i}(a_{N1}^2)\,q_{N1}}{f'_{1r}(a_{N1}^2)} + \frac{f'_{1i}(a_{N2}^2)\,q_{N2}}{f'_{1r}(a_{N2}^2)}\right). \tag{2.62}$$

These relations, together with eq. (2.58) express v and $\tilde{v}_{g1} + \tilde{v}_{g2}$ in terms of q_{N1} and q_{N2} alone. For the cubic case

$$f_1 = \varepsilon - (b_3 - ic_3)a^2, \tag{2.63}$$

eqs. (2.61) and (2.62) become

$$v = (c_1 + b_1 c_3/b_3)(q_{N1} + q_{N2}), \tag{2.64}$$

$$\tilde{v}_{g1} = (c_1 + b_1 c_3/b_3)(q_{N1} - q_{N2}) = -\tilde{v}_{g2}. \tag{2.65}$$

Thus in this case any domain boundary is either a source ($\tilde{v}_{g1} > 0 \leftarrow \rightarrow$) or a sink ($\tilde{v}_{g1} < 0 \rightarrow \leftarrow$), or a homoclinic trajectory $N_1 \to N_1$ for which $\tilde{v}_{g1} = \tilde{v}_{g2}$ and $q_{N1} = q_{N2}$($\rightarrow \rightarrow$ or $\leftarrow \leftarrow$), in which case eq. (2.65)

does not hold. For the quintic or higher-order equations more general domain boundaries can exist, with arbitrary relation between $\tilde{v}_{g1}$ and $\tilde{v}_{g2}$.

2.3.2.4. Summary of counting arguments. We summarize the above arguments by singling out the structures that will turn out to be dynamically significant in the general case with no additional symmetries.

(i) There exists a discrete set of ($N_- \to L_-$) fronts for all ε, and a two-parameter family of such fronts for $\varepsilon > 0$.

(ii) There is a discrete set of pulses. Since for every pulse with velocity v there is one with velocity $-v$ the discrete set will in general include stationary pulses ($v_p = 0$).

(iii) There is a discrete set of sources (targets), and a one-parameter family of sinks (shocks) at low velocities. At higher velocities one can have one-parameter families of sources and two-parameter families of sinks.

(iv) For the cubic equation ($f_2 = f_3 = 0$, $f_1 = \varepsilon - (b_3 - ic_3)a^2$, Bekki and Nozaki [26] have found a family of moving sources (see section 3.3.3), in contradiction to the counting argument. We conjecture that this is due to a hidden symmetry of their solution. A similar situation may well obtain for moving pulses.

2.3.3. The nonlinear diffusion equation

The arguments given up to now provide (in the absence of additional symmetries) an upper limit to the multiplicity of coherent structures, since they only involve the stability of the phase space orbits at their end points. In certain cases more detailed information can be obtained by studying the full orbit. The simplest example is the nonlinear diffusion equation [9, 11, 22, 23], obtained by setting $f_{1i} = f_2 = f_3 = 0$ in the starting equation (2.1), and confining oneself to real solutions, i.e. writing

$$\partial_t A_r = \partial_x^2 A_r + f(A_r), \tag{2.66}$$

where for the Ginzburg–Landau case $f(A_r) = f_{1r}(A_r^2) A_r$, but more generally f need not be an odd function. The dynamical system (2.5) for uniformly translating solutions $A_r(x,t) = u(x - vt)$ then becomes

$$\partial_\xi^2 u + v\partial_\xi u + f(u) = 0, \tag{2.67}$$

where the function u, in contrast to $a = |u|$, can now be both positive and negative. The above equation describes a classical particle of unit mass with damping constant v (either positive or negative) moving in the potential

$$V(u) = \int^u f(y)\,\mathrm{d}y. \tag{2.68}$$

Let us consider a function $f(u)$ with three zeros as in fig. 3a, corresponding to the case $\varepsilon > 0$. Then the points $u_\pm$ that are stable equilibria of eq. (2.67) are maxima of the potential V, and the unstable equilibrium $u = 0$ is a minimum of V. A front is represented by an orbit that begins at a maximum of V ($u = u_+$, say) and ends up at $u = 0$. For large v the particle leaving $u = u_+$ will come to rest at $u = 0$ without overshoot, but below some critical damping $v = v_s$ there will be an overshoot and damped oscillations about $u = 0$. For some value $v = v_{min}$ the particle will precisely reach the other maximum at $u = u_-$ and this orbit represents a stationary kink solution between the two stable fixed points $u = u_\pm$,

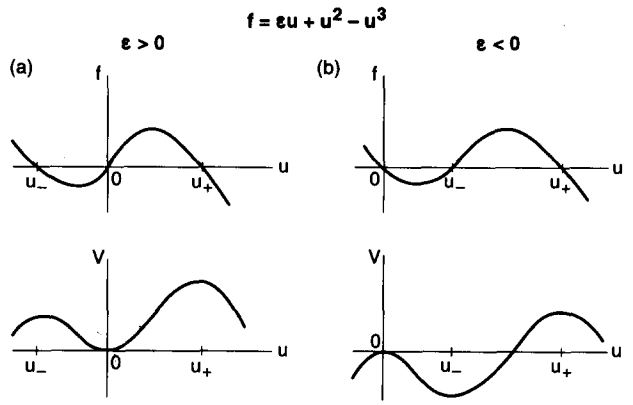

Fig. 3. Illustration of the behavior of the functions f and V of the nonlinear diffusion equation given in eqs. (2.66) and (2.68), for the particular case $f = \varepsilon u + u^2 - u^3$. (a) $\varepsilon > 0$; (b) $\varepsilon < 0$.

i.e. a domain boundary in our classification. For $v < v_{\min}$ the orbit goes off to $u = -\infty$, so it does not represent a finite solution of eq. (2.67). We thus have a one-parameter family of fronts with velocities $v_{\min} < v < \infty$ for $\varepsilon > 0$. In the Ginzburg–Landau model we have $f(u) = f_{1r}(u^2)u = \varepsilon u + u^3 - u^5$, leading to a symmetric potential and $v_{\min} = 0$. For the asymmetric case $f(u) = \varepsilon u + u^2 - u^3$ the results of Ben-Jacob et al. [9] imply that $v_{\min} = 1/\sqrt{2}$. Note that although for any velocity in the range $v > v_{\min}$ a unique front exists, the decay rate $\kappa_L(v)$ associated with these fronts is a *discontinuous* function of v. In particular, for the velocity at which the orbit first overshoots the point $u = 0$ upon decreasing the velocity v, either $\kappa_L(v)$ or $d\kappa_L(v)/dv$ has a discontinuity. (See section 4.2.)

A pulse solution is an orbit beginning and ending at $u = 0$ and it is clear that for $\varepsilon > 0$ none exists, since $u = 0$ is at a minimum of the potential $V(u)$.

Turning now to $\varepsilon < 0$, fig. 3b, a front is represented by an orbit from the maximum of the potential at u_+ to the maximum at $u = 0$. It is clear that there is no longer a family, but rather a unique velocity for such an orbit. Similarly, there is a unique pulse orbit and it has $v = 0$, since the trajectory leaving $u = 0$ must return to $u = 0$. Moreover it exists only for $\varepsilon > \varepsilon_1$, where ε_1 is the value such that $V(u = 0) = V(u = u_+)$.

The foregoing results allow us to compare the actual multiplicity of solutions with the predictions obtained from the arguments of section 2.3.2, based on an analysis of the orbits of the dynamical system (2.5), (2.15) in the vicinity of the fixed points. As stated earlier, the counting arguments give an upper bound for the number of orbits of the dynamical system. For example, when specialized to the case $c_i = 0$, the calculation of section 2.3.2.2 yields stationary pulses for arbitrary ε, though we know that pulses only exist for $\varepsilon_1 < \varepsilon < 0$. On the other hand, for $\varepsilon > 0$, eq. (2.67) has oscillatory front solutions in the range $v_{\min} < v < v^* = 2\varepsilon^{1/2}$ that do not correspond to finite orbits of the dynamical system (2.5), (2.15) for $c_i = 0$, since $|\kappa| \to \infty$ every time $u = 0$. These solutions are of course not predicted by the counting arguments based on the dynamical system (2.5) either. However, for the dynamical system (2.67) the counting argument can be formulated directly using the variables u and $\partial_\xi u$. In these variables, the oscillatory front solutions do correspond to finite orbits and are consistent with the counting arguments.

Likewise, in the general case (2.5), (2.15) we can circumvent the problem associated with the divergence of orbits when $a \to 0$ with $\partial_\xi a$ finite as follows. We allow a to take on negative values as well, and in the region where a goes through zero with finite slope, we use the dynamical system $(a, q, \partial_\xi a)$ instead of (a, q, κ). Since the trajectories remain unique in this set of first-order ODE's, we can connect

them to the trajectories in the (a, q, κ) phase space in a unique way. Hence, the counting arguments based on the stability properties of the fixed points remain unchanged, and they will therefore represent an upper bound for the multiplicity of uniformly translating coherent structures of the PDE. The perturbative calculations of section 5 confirm this expectation.

3. Analytic results

In this section we discuss a number of exact results concerning the generalized complex Ginzburg–Landau equation (2.1) that can be obtained analytically. These are either in the form of symmetries, conservation laws, or exact solutions of the dynamical system (2.5), (2.6) for special cases.

3.1. Symmetries and conservation laws

Suppose eq. (2.1) has a continuous symmetry [21], i.e. it is invariant under a one-parameter family of transformations $A \to \mathcal{T}_\mu(A) = A_\mu$. Then if a coherent structure exists for some value of the parameter ($\mu = 0$, say), we generate a family by applying $\mathcal{T}_\mu$. We shall see that families also arise in systems with conservation laws. We therefore consider special cases of eq. (2.1) for which conservation laws and continuous symmetries can be found.

3.1.1. Conservation laws

We define the normalization integral

$$\mathcal{N}(t) = \int_{-\infty}^{\infty} |A(x,t)|^2 \, dx, \tag{3.1}$$

and note that in the case

$$b_1 = f_{1r} = f_{2i} = f_{3i} = 0, \tag{3.2}$$

this quantity is conserved, i.e.

$$\partial_t \mathcal{N} = 0, \tag{3.3}$$

for solutions that decay sufficiently fast at $x = \pm\infty$. Similarly, we define a momentum

$$\mathcal{P} = -ic_1 \int_{-\infty}^{\infty} [(\partial_x A^*)A - (\partial_x A)A^*] \, dx + \int_{-\infty}^{\infty} dx f_{4r}(|A|^2), \tag{3.4}$$

with f_{4r} to be determined. A calculation using eq. (2.1) shows that

$$\partial_t \mathcal{P} = 0, \quad \text{for} \quad b_1 = f_{1r} = f_{2i} = f_3 = 0, \tag{3.5}$$

if f_{4r} is given by[#2]

$$f'_{4r}(a^2) = 2f_{2r}(a^2). \tag{3.6}$$

(Note that we have not found a momentum operator for $f_{3r} \neq 0$, though one may exist.)

3.1.2. Continuous symmetries

Apart from space and time translations which are continuous symmetries of the full equation (2.1), we can find special cases where other symmetries exist. The first is space–time dilatation invariance,

$$x' = \lambda x, \qquad t' = \lambda^2 t, \qquad A' = \lambda^{-1} A, \tag{3.7}$$

which holds for

$$f_2 = f_3 = 0, \qquad f_{1r} = -b_3 a^2, \qquad f_{1i} = c_3 a^2, \tag{3.8}$$

a special case of which is the nonlinear Schrödinger equation (3.19) ($b_1 = b_3 = 0$, see below). Another continuous symmetry is Galilean invariance

$$x' = x + vt, \qquad t' = t, \qquad A'(x', t') = \exp\left[\left(\tfrac{1}{2}\mathrm{i}v\right)\left(x + \tfrac{1}{2}vt\right)\right] A(x, t), \tag{3.9}$$

which holds for eq. (2.1) when

$$b_1 = 0 \quad \text{and} \quad f_2 = 0 \tag{3.10}$$

(in eq. (3.9) we have set $c_1 = 1$).

These examples show that the standard connection between symmetries and conservation laws expressed by Noether's theorem (see Hill [38]) does not hold for eq. (2.1) and various special cases we consider, due to the lack of a variational principle. For example $f_2 \neq 0$ breaks Galilean invariance even though there is a conserved momentum for $f_{2r} \neq 0$, and conversely (complex) $f_1 \neq 0$, $f_3 \neq 0$ do *not* break Galilean invariance, even though we have not found a conserved momentum or any other conservation law for this case.

3.2. Integrability of the ODE's

3.2.1. General integrability conditions

Even in the absence of conservation laws or continuous symmetries, there are conditions under which the dynamical system (2.5), (2.6) is integrable, i.e. its solutions can be written down in closed form. Such conditions have been obtained by Florjanczyk and Gagnon [21] who also discuss the connection with Painlevé theory (see Cariello and Tabor [21]). We will obtain similar though less general results by direct inspection of the ODE's. Indeed, if

$$b_1 = f_{1r} = f_{2i} = 0, \qquad c_1 = 1, \tag{3.11}$$

eq. (2.6a) can be put into the form

$$\partial_\xi q = \kappa\left[v - 2q + 2(f'_{2r} + f'_{3r})a^2 + f_{2r}\right], \tag{3.12}$$

whose general solution, in view of eq. (2.4c), is

$$q(a^2) = \frac{1}{2a^2}\int^{a^2} \mathrm{d}y\,\left[v + 2y(f'_{2r} + f'_{3r}) + f_{2r}\right]. \tag{3.13}$$

Then eq. (2.6b) becomes

$$\partial_\xi \kappa + \kappa^2 + \phi_0(a^2) + \phi_1(a^2)\,\kappa = 0, \tag{3.14a}$$

$$\phi_0(a^2) = \omega + vq - q^2 + f_{1i} + f_{2r}q, \tag{3.14b}$$

$$\phi_1(a^2) = 2f'_{3i}a^2, \tag{3.14c}$$

or equivalently,

$$\partial_\xi^2 a + a\phi_0(a^2) + \phi_1(a^2)\partial_\xi a = 0. \tag{3.15}$$

This equation represents the motion of a classical particle in the potential

$$V_0(a^2) = \tfrac{1}{2}\int^{a^2} \phi_0(y)\,\mathrm{d}y, \tag{3.16}$$

with damping $\phi_1(a^2)$. In the undamped case,

$$f'_{3i} = 0, \tag{3.17}$$

the equation of motion can be integrated by quadrature

$$\kappa^2(a^2) = -2a^{-2}V_0(a^2) + 2a_0^{-2}V_0(a_0^2), \tag{3.18a}$$

$$a(\xi) = \int^{\xi} \mathrm{d}\eta \left\{-2V_0(a^2(\eta)) + 2\left[a^2(\eta)/a_0^2\right]V_0(a_0^2)\right\}^{1/2}, \tag{3.18b}$$

where a_0 is the value of a where $\kappa(a_0) = 0$.

From the mechanical analogy for eq. (3.15) with $\phi_1 = 0$, it is clear that if the potential (3.16) is finite at $a = 0$ and has the correct shape, then any orbit leaving $a = 0$ must return to $a = 0$ by conservation of energy. In contrast to the situation in eq. (2.67) where v is a damping constant, a pulse orbit here requires no special adjustment of the potential, i.e. it occurs over a range in the parameters v and ω, thus assuring a double family of pulses. Specifically, if $q(a = 0)$ given by eq. (3.13) remains finite, the potential (3.16) will have a finite extremum at $a = 0$, and for sufficiently large $|\omega|$ this extremum will be a maximum. The only condition for the existence of a double family of pulses is then that the nonlinear terms f_{1i} and f_{2r} should be such that $V_0(a^2)$ increases to a value larger than $V_0(0)$. Similarly, the requirement that $V_0(a^2)$ have another maximum for $a \neq 0$ such that $V_0(0) = V_0(a^2)$, imposes one condition, so we expect to find one-parameter families of fronts. Note that the above arguments depend on the integrability of (2.5), (2.6) and the Hamiltonian nature of eq. (3.15) which follows from eqs. (3.11) and (3.17), and are satisfied even when $f_{2r} \neq 0$ and/or $f'_{3r} \neq 0$. The condition $f_{2r} \neq 0$ implies breaking of Galilean symmetry (3.9), and $f'_{3r} \neq 0$ apparently invalidates momentum conservation (3.5), but neither of these prevent the existence of a double family of pulses.

3.2.2. Solitons in the nonlinear Schrödinger equation

The nonlinear Schrödinger equation

$$\partial_t A = \mathrm{i}\partial_x^2 A + \mathrm{i}c_3|A|^2 A, \tag{3.19}$$

with $c_3 = \pm 1$ is not only Hamiltonian, but also completely integrable [15]. For $c_3 > 0$ an important class of solutions are the solitons of which an example is

$$A(x,t) = e^{it}(2/c_3)^{1/2}\operatorname{sech} x, \tag{3.20}$$

corresponding to $v = 0$, $\omega = -1$. Then a double family of solitons indexed by v and ω can be generated by applying the Galilean and dilatation transformations (3.7) and (3.9). We shall not dwell on the special dynamical significance of the solitons for this integrable case.

For $c_3 < 0$, we have the so-called "dark solitons" [6]

$$a^2(x) = a_0^2 + (a_N^2 - a_0^2)\tanh^2\left[\sqrt{\tfrac{1}{2}(a_N^2 - a_0^2)|c_3|}\, x\right], \tag{3.21a}$$

$$q(x) = d_1 a^{-2}(x), \tag{3.21b}$$

for arbitrary $\omega > 0$ and $d_1 \leq 4\omega^3/(27c_3^2)$, where a_N and a_0 are the solutions of

$$(|c_3|a_N^2 - \omega)a_N^4 - d_1^2 = 0, \tag{3.21c}$$

$$a_0^2 = 2(\omega/|c_3| - a_N^2). \tag{3.21d}$$

We therefore have a *three-parameter* family of such structures at nonzero v. For $d_1 \to 0$, eqs. (3.21c, d) imply that $a_0 \to 0$. These solitons are often referred to as "fundamental" dark solitons [6]. For nonzero v, they form a *two-parameter* family.

The nonlinear Schrödinger equation and its extensions also admit spatially periodic nonlinear solutions (see e.g. ref. [21]), but these will not be discussed here.

3.2.3. *Pulses and fronts in the quintic-cubic and generalized derivative Schrödinger equations*

3.2.3.1. Generalized derivative Schrödinger equation. Let us consider the dynamical system (2.5), (2.6) with

$$f_{1r} = f_{2i} = b_1 = f_3 = 0, \tag{3.22}$$

already considered in section 3.2.1 (the condition $f_{3r} = 0$ is not necessary, but it is taken for simplicity). For this integrable system we have the general solutions written down in eqs. (3.18). Let us choose $c_1 = 1$ and

$$f_{1i} = c_3 a^2 + c_5 a^4, \tag{3.23a}$$

$$f_{2r} = s_0 + s_2 a^2, \tag{3.23b}$$

i.e. we have *combined* the quintic-cubic and derivative Schrödinger equations (2.12) and (2.13), to form the quintic derivative Schrödinger equation (2.14). From eq. (3.13) the wavevector q takes the form

$$q = d_1 a^{-2} + q_0 + q_2 a^2. \tag{3.24}$$

For pulse solutions we must pick $d_1 = 0$, so eqs. (3.13) and (3.18) become

$$q = \tfrac{1}{2}(v + s_0) + \tfrac{3}{4}s_2 a^2 \equiv q_0 + q_2 a^2, \tag{3.25a}$$

$$\kappa^2 = d_0 + d_2 a^2 + d_4 a^4, \tag{3.25b}$$

$$d_0 = -\omega - \tfrac{1}{4}(v + s_0)^2, \tag{3.26a}$$

$$d_2 = -\tfrac{1}{2}c_3 - \tfrac{1}{4}s_2(v + s_0), \tag{3.26b}$$

$$d_4 = -\tfrac{1}{3}(c_5 + 3s_2^2/16). \tag{3.26c}$$

The solution $a(\xi)$, given by eq. (3.18b) can be put into the form

$$a^2(\xi) = (d_3 + d_5 \cosh d_6 \xi)^{-1}, \tag{3.27}$$

where the relation $\kappa = \partial_\xi a/a$ implies

$$d_3 = -(d_2/2d_0), \quad d_5^2 = (d_2^2 - 4d_0 d_4)/4d_0^2, \quad d_6^2 = 4d_0. \tag{3.28}$$

This pulse solution generalizes the so-called "Alfvén solitons" of the derivative nonlinear Schrödinger equation [37], and reduces to those when $c_3 = c_5 = s_0 = 0$. It also reduces to the $\omega = -4$ member of the nonlinear Schrödinger pulse family (3.20) when $c_5 = v = s_2 = s_0 = 0$. As anticipated, the pulses (3.27) form a two-parameter family of solutions indexed by v and ω, but since the equation is neither Galilean nor dilatation invariant the dependence of the coefficients on v and ω is nontrivial.

If we retain $d_1 \neq 0$ in eq. (3.24) we find other types of solutions (e.g. domain boundaries) but we shall not explore these further here.

3.2.3.2. The quintic-cubic equation. For $f_{2r} = 0$ we have the quintic-cubic Schrödinger equation (2.12) studied earlier by Gagnon [40], and for $v = 0$ eqs. (3.25a) and (3.26) reduce to

$$q = 0, \tag{3.29}$$

and

$$d_3 = -c_3/4\omega, \quad d_5 = \left[(-c_5/3\omega) + (c_3^2/16\omega^2)\right]^{1/2}, \quad d_6 = 2(-\omega)^{1/2}, \tag{3.30}$$

implying

$$\omega < 0. \tag{3.31}$$

For $v \neq 0$ we replace ω by $\omega + \frac{1}{4}v^2$ and q by $\frac{1}{2}v$, as implied by the Galilean invariance of eq. (2.12), or as can be seen directly from eqs. (3.25a) and (3.26). Now the dependence on v is trivial, but in contrast to the nonlinear Schrödinger equation (2.11) to which eq. (2.12) reduces for $c_5 = 0$, the dependence on ω is nontrivial.

In order to study the pulse solutions in more detail we must distinguish four different cases, depending on the signs of c_3 and c_5, i.e. on the quadrant in the (c_3, c_5) plane. (We assume $v = 0$ as in eqs. (3.29) and (3.30).)

In quadrant I, $c_3 > 0$, $c_5 > 0$, for $|\omega| \to 0$ we have $d_3, d_5 > 0$ and $d_3 \approx d_5$, so the pulse (3.27) resembles the soliton of the nonlinear Schrödinger equation and has amplitude proportional to $|\omega|^{1/2}$. For $|\omega| \gg$

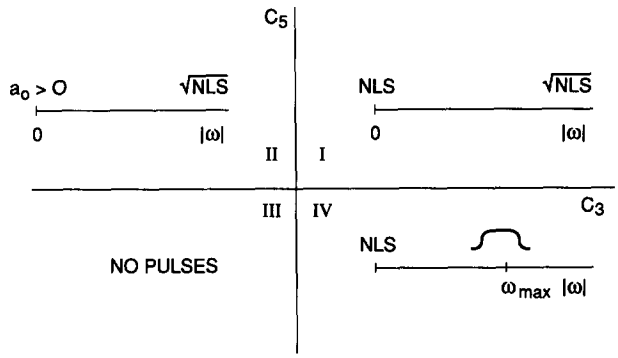

Fig. 4. Illustration of the range of existence of pulse solutions in the quintic-cubic Schrödinger equation (2.12) in the four quadrants of the (c_3, c_5) plane. The notations NLS, $\sqrt{\text{NLS}}$, etc. are explained in the text.

$3c_3^2/16c_5$, on the other hand, we have $d_5 \gg d_3$ and

$$a \approx (3|\omega|/c_5)^{1/4}\left[\cosh\left(\sqrt{2|\omega|}\,\xi\right)\right]^{-1/2}, \tag{3.32}$$

so it is a^2 rather than a which has the form of the soliton (3.20). We indicate this in fig. 4 by the notation $\sqrt{\text{NLS}}$.

In quadrant II ($c_3 < 0$, $c_5 > 0$) pulses exist once again for all $\omega < 0$, but since this is the dark soliton regime (3.21) when $c_5 = 0$, the pulses do not reduce to NLS solitons for $|\omega| \to 0$. Instead they have *finite* amplitude

$$\lim_{|\omega|\to 0} a(\xi = 0) = [3|c_3|/2c_5]^{1/2}. \tag{3.33}$$

In quadrant III ($c_3 < 0$, $c_5 < 0$) we have $d_5 < -d_3, d_3 < 0$ and the solutions have a square-root singularity at some finite ξ, so they are not normalizable and we will ignore this case.

In quadrant IV ($c_3 > 0$, $c_5 < 0$), the small-$|\omega|$ behavior is as in quadrant I, but there is now a *maximum* value of $|\omega|$,

$$\omega_{max} = 3c_3^2/16|c_5|. \tag{3.34}$$

When $|\omega| \to \omega_{max}$ (i.e. $d_5 \to 0$ in eq. (3.30)) the width of the pulse diverges logarithmically, and the amplitude approaches

$$a_{max}^2 = a_N^2 = 3c_3/4|c_5|. \tag{3.35}$$

This corresponds to a pair of *fronts*, each one of which has the form

$$a_f^2(\xi) = a_N^2[1 + \exp(-2\kappa_L \xi)]^{-1}, \tag{3.36a}$$

$$\kappa_L = \pm(-3c_3^2/16c_5)^{1/2} = \pm(\omega_{max})^{1/2}, \tag{3.36b}$$

(we have displaced the edge to $\xi = 0$). Thus fronts exist for a particular ω, but of course there is still a family indexed by v. Note that when $|\omega| = \omega_{max}$ we have

$$\kappa(a^2) = (-c_5/3)^{1/2}(a^2 + 3c_3/4c_5), \tag{3.37}$$

i.e. κ is a linear function of a^2. The properties of the pulse solution (3.30) in the quintic-cubic Schrödinger equation are summarized in fig. 4.

3.3. Exact solutions of the complex Ginzburg–Landau equation

Even if there are no conservation laws or symmetries, and if the integrability conditions are not satisfied, as is the case for the complex Ginzburg–Landau equations (2.1) or (2.10), it is still possible to find particular exact solutions[#10] for certain parameter values.

3.3.1. Nonlinear front

Guided by the form (3.37) and by heuristic stability arguments [see ref. [11] and section 4], we make the following ansatz [8] for a front solution of the full complex Ginzburg–Landau equation[#11] (2.10), which we shall refer to as the "nonlinear front"[#12],

$$q(a^2) = q_N + e_0(a^2 - a_N^2), \tag{3.38a}$$

$$\kappa(a^2) = e_1(a^2 - a_N^2), \tag{3.38b}$$

with constants q_N, a_N, e_0, e_1 to be determined. A similar solution was found independently by Klyachkin [42], but he did not investigate its dynamical significance (see also Cariello and Tabor [42] and Powell et al. [43]). Insertion of the ansatz (3.38) into the ODE's (2.5), (2.15) leads to two quadratic polynomial equations in the variable $a^2(\xi)$. Requiring that these relations be satisfied identically, we find six relations (for the coefficients of a^0, a^2 and a^4 in the two equations) which after some rewriting become

$$\omega = -vq_N + c_1 q_N^2 - c_3 a_N^2 - c_5 a_N^4, \tag{3.39a}$$

$$\varepsilon = b_1 q_N^2 + b_3 a_N^2 + b_5 a_N^4, \tag{3.39b}$$

$$3e_1^2 - e_0^2 = \tilde{b}_1 b_5 - \tilde{c}_1 c_5, \tag{3.39c}$$

$$4e_1 e_0 = -(\tilde{c}_1 b_5 + \tilde{b}_1 c_5), \tag{3.39d}$$

$$\tilde{c}_1 c_3 - \tilde{b}_1 b_3 + (\tilde{b}_1 e_1 + \tilde{c}_1 e_0)v - 2q_N e_0 + (2e_0^2 - 4e_1^2)a_N^2 = 0, \tag{3.39e}$$

$$\tilde{b}_1 c_3 + \tilde{c}_1 b_3 - (\tilde{c}_1 e_1 - \tilde{b}_1 e_0)v + 2q_N e_1 - 6e_0 e_1 a_N^2 = 0, \tag{3.39f}$$

where according to eq. (2.7) $\tilde{b}_1 = b_1(c_1^2 + b_1^2)^{-1}$, $\tilde{c}_1 = c_1(c_1^2 + b_1^2)^{-1}$. For $b_1 \neq 0$ the solution of the system (3.39) may be written in the form

$$q_N = q_N^\dagger = e_2 + e_3 a_N^2, \tag{3.40a}$$

$$v = v^\dagger = e_4 + e_5 a_N^2, \tag{3.40b}$$

$$a_N^4 + e_6 a_N^2 + e_7 = 0, \tag{3.40c}$$

$$\kappa_L = \kappa_L^\dagger = -e_1 a_N^2, \tag{3.40d}$$

[#10] There is considerable literature on exact solutions of real equations such as (2.66), some of which can be found in ref. [41].

[#11] As explained below, the ansatz also works in the more general case in which the functions f_2 and f_3 of eq. (2.1) are linear in a^2.

[#12] In ref. [8] we used the term "selected front" for eq. (3.38), but we prefer "nonlinear front" since it is only selected when the conditions (4.14) are met.

with

$$e_2 = -\left[(\tilde{c}_1 e_1 - \tilde{b}_1 e_0)(\tilde{c}_1 c_3 - \tilde{b}_1 b_3) + (\tilde{b}_1 e_1 + \tilde{c}_1 e_0)(\tilde{b}_1 c_3 + \tilde{c}_1 b_3)\right] \Big/ \left[2\tilde{b}_1 (e_0^2 + e_1^2)\right], \tag{3.41a}$$

$$e_3 = \left(2\tilde{c}_1 e_0^2 e_1 + \tilde{b}_1 e_0 e_1^2 + 2\tilde{c}_1 e_1^3 + \tilde{b}_1 e_0^3\right) \Big/ \tilde{b}_1 (e_0^2 + e_1^2), \tag{3.41b}$$

$$e_4 = -\left[e_1(\tilde{c}_1 c_3 - \tilde{b}_1 b_3) + e_0(\tilde{b}_1 c_3 + \tilde{c}_1 b_3)\right] \Big/ \tilde{b}_1 (e_0^2 + e_1^2), \tag{3.41c}$$

$$e_5 = 4e_1/\tilde{b}_1, \tag{3.41d}$$

$$e_6 = (2e_2 e_3 - b_3/b_1)/(e_3^2 + b_5/b_1), \tag{3.41e}$$

$$e_7 = (e_2^2 - \varepsilon/b_1)/(e_3^2 + b_5/b_1). \tag{3.41f}$$

An examination of the above equations shows that they provide explicit expressions for the front parameters $v^\dagger, q_N^\dagger, \omega^\dagger, (a_N^2)^\dagger$ in terms of the original parameters of eq. (2.10), since eqs. (3.41) express all quantities in terms of $\{b_i, c_i, \varepsilon\}$ and the pair (e_0, e_1) which itself can be reexpressed in terms of $\{b_i, c_i, \varepsilon\}$ by solving the quadratic equations (3.39c, d).

The multiplicity of solutions can be found as follows: First note that given $\{b_i, c_i, \varepsilon\}$, the pair (e_0, e_1) is uniquely determined by (3.39c, d) up to a sign change of both variables, since for $e_1 \neq 0$ the equation

$$3e_1^4 - (\tilde{b}_1 b_5 - \tilde{c}_1 c_5) e_1^2 - \tfrac{1}{16}(\tilde{b}_1 c_5 + \tilde{c}_1 b_5)^2 = 0 \tag{3.42}$$

has a single positive root $e_1^2 > 0$, and a change of sign of both e_0 and e_1 leads to an equivalent front (3.38) by the symmetry (2.40). Thus e_2 through e_7 are uniquely determined, and a solution that is stable to amplitude perturbations will be found if a_N^2 satisfies (2.22),

$$a_N^2 \geq -b_3/2b_5. \tag{3.43}$$

This condition implies the following multiplicities:

$$b_3/b_5 < e_6: \begin{cases} \text{1 solution if:} & \begin{cases} 4e_7 \leq 2e_6 b_3/b_5 - b_3^2/b_5^2, & (3.44a) \\ \text{and} \\ 4e_7 \leq e_6^2, & (3.44b) \end{cases} \\ \text{no solution otherwise.} \end{cases}$$

$$e_6 < b_3/b_5: \begin{cases} \text{2 solutions if:} & (2b_3/b_5)e_6 - b_3^2/b_5^2 < 4e_7 < e_6^2, & (3.44c) \\ \text{1 solution if:} & 4e_7 \leq (2b_3/b_5)e_6 - b_3^2/b_5^2, & (3.44d) \\ \text{no solution if:} & e_6^2 < 4e_7. & (3.44e) \end{cases}$$

From the above equations we may show analytically that

$$\partial_\varepsilon v^\dagger = e_5 \partial_\varepsilon a_N^2 = \left[e_5 \left(b_1 e_3^2 + b_5 \right) \left(2a_N^2 + e_6 \right) \right]^{-1}, \tag{3.45a}$$

so for $e_1 > 0$ (the proper choice for a front from an N to an L fixed point as in fig. 1a) and $b_1 > 0$, $b_5 > 0$ (necessary for stability) we have

$$\operatorname{sgn}\left(\partial_\varepsilon v^\dagger \right) = \operatorname{sgn}\left(2a_N^2 + e_6 \right) > 0, \tag{3.45b}$$

where we have used the stability condition (2.22).

Another general property of the solution (3.40), (3.41) is the group velocity $\tilde{v}_g^\dagger$, given according to eq. (2.60) by the expression

$$\tilde{v}_g^\dagger = -v^\dagger + 2c_1 q_N^\dagger + 2b_1 q_N^\dagger \left(\frac{c_3 + 2c_5 a_N^2}{b_3 + 2b_5 a_N^2} \right). \tag{3.46}$$

As noted in section 4.2, for stability we require $\tilde{v}_g^\dagger < 0$ and although we have not succeeded in showing that this condition is always satisfied, in all the parameter ranges where we have solved eq. (3.40) for $v^\dagger$ numerically, $\tilde{v}_g^\dagger$ was found to be negative.

The sign of $\tilde{v}_g$ is also related to the following point: The ansatz (3.38b) corresponds to a first order ODE for $a(\xi)$ [11]. In phase space, this means that the nonlinear front trajectory flows out of the N fixed point along a single unstable direction. Suppose, however, that it flows out of an N_+ fixed point with $++-$ structure along one of the two unstable eigendirections. In this case the counting argument implies that the nonlinear front is a member of a one-parameter family. Although we have not been able to rule out this possibility in general, the stability arguments of section 4 as well as the numerical simulations of section 6 are consistent with the hypothesis that whenever it is selected, the nonlinear front flows out of an N_- fixed point with $+--$ structure. In view of (2.52), it then also has $\tilde{v}_g^\dagger < 0$.

We also note that the nonlinear front flows into an L fixed point along a stable eigendirection. As we will see later, for very large ε this fixed point is of type L_{-2} which by eq. (2.44) has three stable directions. In this case, the nonlinear front therefore is a member of a (two-parameter) family of fronts, but as we shall see, it is then not the selected front.

For the cubic Ginzburg–Landau equations ($b_5 = c_5 = 0$, $\varepsilon = b = b_3 = 1$) Nozaki and Bekki [25a] have obtained an exact front solution that can be defined by the ansatz

$$q = q_N + e_8 \kappa_L (1 - a/a_N), \tag{3.47a}$$

$$\kappa = \kappa_L (1 - a/a_N), \tag{3.47b}$$

which yields

$$a^2 = a_N^2 \left[1 + \exp(-\kappa_L \xi) \right]^{-2}, \quad \kappa_L < 0, \tag{3.48}$$

where a_N, κ_L, q_N and e_8 can easily be calculated in terms of c_1 and c_3. It turns out, however, that this solution is a member of the family of $N_- \rightarrow L_{-2}$ fronts obtained in section 2, and as discussed in sections 4 and 6, these fronts are not selected by the dynamics starting from localized initial conditions.

Let us now consider the Galilean invariant limit $b_1 = 0$, for which eqs. (3.40) and (3.41) yield (setting $c_1 = -b_3 = b_5 = 1$)

$$a_N^2 = a_{N0}^2(c_3, c_5), \tag{3.49a}$$

$$\varepsilon = \varepsilon_0(c_3, c_5) = -a_{N0}^2 + a_{N0}^4, \tag{3.49b}$$

$$q_N^\dagger - \tfrac{1}{2}v^\dagger = q_0(c_3, c_5), \tag{3.49c}$$

where a_{N0}^2, ε_0 and q_0 are $\mathcal{O}(1)$ functions of the parameters c_3, c_5, easily calculated from eq. (3.41). Thus the ansatz (3.38) defines a one-parameter family of fronts (as it must from the Galilean symmetry) but *only* for the special value $\varepsilon = \varepsilon_0$. For $\varepsilon \neq \varepsilon_0$ there is no solution of the form (3.38). When $0 < b_1 \ll 1$, the family collapses to a particular solution (choosing the one with $v^\dagger > 0$) of the form

$$v^\dagger = 2b_1^{-1/2}(\varepsilon - \varepsilon_0)^{1/2} + v_1^\dagger, \tag{3.50a}$$

$$q_N^\dagger = b_1^{-1/2}(\varepsilon - \varepsilon_0)^{1/2} + q_{N1}^\dagger, \tag{3.50b}$$

where $v_1^\dagger$ and $q_{N1}^\dagger$ are $\mathcal{O}(1)$ functions of c_3 and c_5. Thus $v^\dagger(b_1, \varepsilon)$ is singular for $b_1 \to 0$, $\varepsilon \to \varepsilon_0$ and a perturbation expansion of (3.40) and (3.41) in b_1 is rather delicate.

Note also that eq. (3.39d) shows that in the case $b_1c_5 + b_5c_1 = 0$ one has $e_0 = 0$ (since $e_1 \neq 0$), so that the wavenumber q is a constant. The other expressions also simplify considerably in this case.

3.3.2. Exact pulse solution

For the complex Ginzburg–Landau equation (2.10) we make the following pulse ansatz ([8], see also ref. [42]) which generalizes the exact solution of Hocking and Stewartson [24] to the quintic case,

$$\kappa^2 = d_0 + d_2a^2 + d_4a^4, \tag{3.51a}$$

$$q = d_7 + d_8\kappa. \tag{3.51b}$$

This ansatz leads to the equations

$$\tilde{c}_1 v - 2d_7 = \tilde{b}_1 v = 0, \tag{3.52a}$$

$$\tilde{c}_1\varepsilon - \tilde{b}_1\omega - \tilde{b}_1 v d_7 = 2d_8d_0, \tag{3.52b}$$

$$\tilde{b}_1\varepsilon + \tilde{c}_1\omega + \tilde{c}_1 v d_7 - d_7^2 = d_0(d_8^2 - 1), \tag{3.52c}$$

$$\tilde{b}_1c_3 + \tilde{c}_1b_3 = -3d_2d_8, \tag{3.52d}$$

$$\tilde{b}_1b_3 - \tilde{c}_1c_3 = -d_2(d_8^2 - 2), \tag{3.52e}$$

$$\tilde{b}_1c_5 + \tilde{c}_1b_5 = -4d_4d_8, \tag{3.52f}$$

$$\tilde{b}_1b_5 - \tilde{c}_1c_5 = -d_4(d_8^2 - 3). \tag{3.52g}$$

For $b_1 = 0$ (the Galilean invariant case) we find a family of solutions with arbitrary v. When $b_1 \neq 0$, we must have $v = d_7 = 0$ by eq. (3.52a), and we are left with 6 equations in the 5 unknowns d_0, d_2, d_4, d_8 and ω. This overdetermined set is only soluble in a codimension-one subspace of the set $(\varepsilon, c_1, c_3, c_5)$,

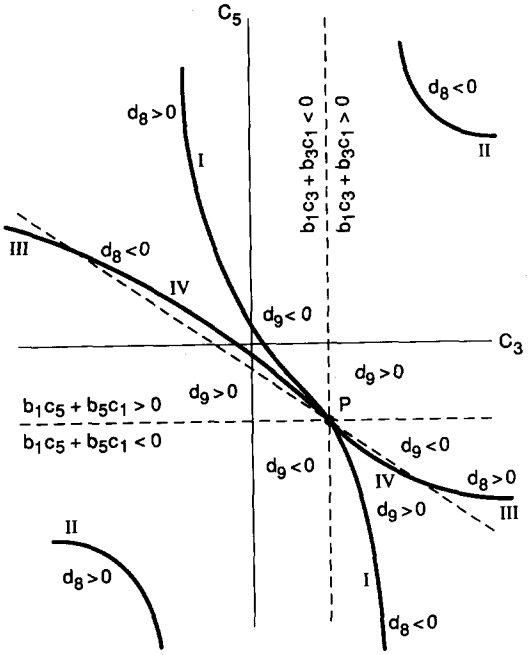

Fig. 5. Subspace of the (c_3, c_5) plane where exact pulse solutions of the form (3.51) exist, in the subcritical case $(b_3/b_1 < 0)$ for fixed $c_1 > 0$. The subspace is indicated by the thick solid lines. The plane is divided into sectors by the dashed lines $b_1c_5 + b_5c_1 = 0$ (horizontal), $b_1c_3 + b_3c_1 = 0$ (vertical) and $c_5(b_1/2b_5) - c_3(b_1/3b_3) + \frac{1}{6}c_1 = 0$ (diagonal), meeting at P. The subspace is traced out along the segments I → IV marked $d_8 < 0$ as d_8 goes from $-\infty$ to 0, and along the segments I → IV marked $d_8 > 0$ when d_8 goes from 0 to $+\infty$. The signs of the terms of eqs. (3.55) and (3.54c) in the different sectors are indicated on the figure.

which we parametrize as follows:

$$c_3 = \frac{6b_1b_3d_8 - 2c_1b_3(d_8^2 - 2)}{6c_1d_8 + 2b_1(d_8^2 - 2)}, \tag{3.53a}$$

$$c_5 = \frac{4b_1b_5d_8 - c_1b_5(d_8^2 - 3)}{4c_1d_8 + b_1(d_8^2 - 3)}. \tag{3.53b}$$

Elimination of d_8 from eqs. (3.53a) and (3.53b) yields a relation between c_1, c_3 and c_5 (which does not involve ε). For fixed $c_1 > 0$, this subspace is indicated by the thick solid lines in fig. 5 for the subcritical case $b_3 < 0$. The curves are obtained by tracing c_3 and c_5 according to eqs. (3.53) upon varying d_8 from $-\infty$ to 0 (segments, I, II, III, IV marked $d_8 < 0$) and from 0 to $+\infty$ (segments I, II, III, IV marked $d_8 > 0$). Within the subspace the solution is

$$v = 0, \tag{3.54a}$$

$$\omega = -\frac{\varepsilon}{b_1}\frac{c_3c_5b_1 + c_1(3c_3b_5 - 2c_5b_3)}{c_1b_3b_5 + (3b_3c_5 - 2c_3b_5)}, \tag{3.54b}$$

$$d_0 = \kappa_L^2 = -\varepsilon/2d_8d_9, \tag{3.54c}$$

$$d_9 = -\frac{3b_3}{\tilde{c}_1b_3 + c_3\tilde{b}_1} + \frac{2b_5}{\tilde{c}_1b_5 + c_5\tilde{b}_1}, \tag{3.54d}$$

the maximum amplitude a_0 being the smallest root of

$$a_0^4 + \frac{4}{3}\left(\frac{c_1b_3 + b_1c_3}{c_1b_5 + b_1c_5}\right)a_0^2 + \frac{2\varepsilon}{(\tilde{c}_1b_5 + \tilde{b}_1c_5)d_9} = 0. \tag{3.55}$$

According to these equations, exact pulse solutions exist in the subspace whenever (i) $d_0 = \kappa_L^2$ is, according to eq. (3.54c), positive, and (ii) eq. (3.55) has a positive real root. Clearly, eq. (3.54c) shows that for given b_i and c_i pulses exist either for $\varepsilon > 0$ or for $\varepsilon < 0$ but not for both. Whether pulses do indeed exist for given sign of ε, and if so, over what range, is determined by eq. (3.55). Consider again fig. 5 corresponding to the case $b_3/b_1 < 0$ and $c_1 > 0$ fixed. The signs of the various terms entering eqs. (3.55) and (3.54c) are indicated in the different sectors of the plane. For the existence of pulse solutions on the various line segments, these results imply

- I: pulses exist for all $\varepsilon > 0$;
- II: no pulses exist;
- III: pulses exist for $0 < \varepsilon < \varepsilon_{max}$;
- IV: pulses exist for $\varepsilon_{min} < \varepsilon < 0$; (3.56)

where ε_{max} and ε_{min} can be calculated in terms of the b_i and c_i. Note that for $\varepsilon = \varepsilon_{min}$ and $\varepsilon = \varepsilon_{max}$ the quadratic equation (3.55) for a_0^2 has a double root, so the pulse ansatz (3.51) reduces to the one for the nonlinear front, eq. (3.38). Hence at ε_{min} and ε_{max} there exists a nonlinear front solution (3.38) with $v^\dagger = 0$. Since by eq. (3.45) $\partial_\varepsilon v^\dagger > 0$, the pulses of segment IV always coexist with a positive nonlinear front $v^\dagger > 0$. As shown in section 4.2, this means that these pulses are always *unstable* to the formation of a front. The pulses in segments I and III only exist for $\varepsilon > 0$, when the $A = 0$ state (L fixed point) is linearly unstable.

For the case $b_3/b_1 > 0$ shown in fig. 6 (supercritical bifurcation) the phase diagram follows from the previous one by applying the symmetry $c_3 \to -c_3$, $c_5 \to c_5$, $d_0 \to d_0$, $\omega \to \omega$, $d_9 \to d_9$ within the subspace (3.53). Pulse solutions are then only found in segments I and II of fig. 6, and only for $\varepsilon > 0$. The above results imply that the pulses obtained from the ansatz (3.51) are *never* expected to be stable in an ideal infinite system. From the ansatz (3.51) it is easy to find the functions $a(\xi)$ and $q(\xi)$ (the former turns out to be given by eq. (3.27)). Niemela et al. [2] have found that the resulting expressions fit their experimentally observed pulse shapes rather well, but the coefficients d_i were fitted and not related to any starting model. Moreover, in view of the abovementioned instability in an infinite system the significance of the fit is obscure. In section 7 we shall comment briefly on the possible stability of pulses in a finite system for $\varepsilon > 0$.

3.3.3. *Sources and sinks*

For the cubic Ginzburg–Landau equation ($b_5 = c_5 = 0$, $\varepsilon = b_1 = b_3 = 1$) a simple source solution has been written down by Nozaki and Bekki [25b] (they call it a hole) in the form

$$q^2 = q_N^2 a^2 / a_N^2, \tag{3.57a}$$

$$a\kappa = a_N \kappa_0 \left(1 - a^2/a_N^2\right), \tag{3.57b}$$

leading to a solution with $v = 0$ and

$$a^2(x) = a_N^2 \tanh^2(\kappa_0 x), \tag{3.58a}$$

$$q(x) = q_N \tanh \kappa_0 x + \pi\delta(x), \tag{3.58b}$$

$$\kappa_0^2 = \tfrac{1}{2}(1 + c_1\omega)/\left(1 + c_1^2\right), \tag{3.58c}$$

$$q_N = \left(\tfrac{2}{3}\kappa_0\right)(c_1 - \omega)/(1 + c_1\omega), \tag{3.58d}$$

$$a_N^2 = (c_1 - \omega)/(c_1 + c_3), \tag{3.58e}$$

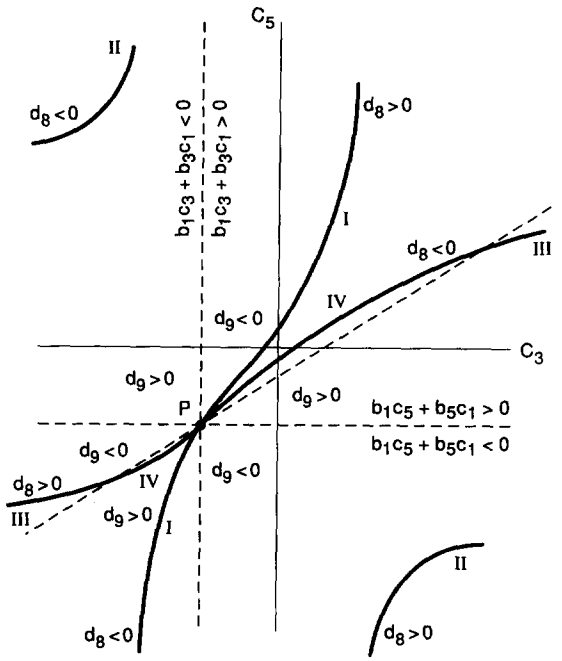

Fig. 6. As fig. 5, but for the supercritical case $b_3 > 0$.

where ω is the solution of the equation

$$\omega^2(1 - e_0 c_1) - (2c_1 + e_0 c_1 c_3 + e_0)\omega + c_1^2 - e_0 c_3 = 0, \tag{3.58f}$$

with $e_0 = \frac{9}{2}(1 + c_1^2)/(c_1 + c_3)$. Using eq. (2.65) we indeed verify that this solution is a source, since we have

$$q_+ = \lim_{x \to \infty} q(x) = q_N \operatorname{sgn} \kappa_0, \tag{3.59a}$$

$$\tilde{v}_{g+} = 2(c_1 + c_3) q_N \operatorname{sgn} \kappa_0 = \frac{2 \operatorname{sgn} \kappa_0 (c_1 - \omega)^2}{3\kappa_0 a_N^2 (1 + c_1^2)} > 0, \tag{3.59b}$$

the condition for a source. We shall test the stability of this solution in section 6.

For $c_1, c_3 \to \infty$, one of the roots of eq. (3.58f) becomes $\omega \approx -c_3$, which to leading order implies $\kappa_0^2 = \omega/2c_1$, $q_N \approx 0$ and $a_N^2 \approx 1$. After a rescaling of time it is easily seen that eq. (3.51) reduces to the fundamental dark soliton (3.21) of the nonlinear Schrödinger equation in this limit.

A more complicated domain boundary ($N_1 \to N_2$ orbit) for the cubic equation was also found by Bekki and Nozaki [26]. Contrary to our previous examples this solution is not simply expressed in terms of polynomials $q(a^2)$ and $\kappa(a^2)$, but rather in the explicit form

$$\hat{A}(\xi) = a_2 \left(\frac{1 + z\, e^{-2\kappa_0 \xi}}{1 + e^{-2\kappa_0 \xi}} \right) \exp\left(i \int^{\xi} \tilde{q}(\xi')\, d\xi' \right), \tag{3.60a}$$

$$\tilde{q}(\xi) = \tfrac{1}{2}[q_+ + q_- \tanh \kappa_0 \xi], \tag{3.60b}$$

where a_2, κ_0, q_+ and q_- are real and z is complex. Insertion of eq. (3.60) into the ODE for $\hat{A}(\xi)$,

$$(1+\mathrm{i}\omega)\hat{A} + v\partial_\xi \hat{A} + (1+\mathrm{i}c_1)\partial_\xi^2 \hat{A} - (1-\mathrm{i}c_3)|\hat{A}|^2\hat{A} = 0, \tag{3.61}$$

leads to an algebraic equation with terms of order 1, $\mathrm{e}^{-2\kappa_0\xi}$, $\mathrm{e}^{-4\kappa_0\xi}$ and $\mathrm{e}^{-6\kappa_0\xi}$ (and a common denominator $(1+\mathrm{e}^{-2\kappa_0\xi})^3$). Equating the 4 coefficients to zero we find 4 complex equations in the 8 real coefficients a_2, κ_0, q_+, q_-, Re z, Im z, ω and v, thus a priori a discrete solution. The equations found in this manner are not in a convenient form for analytic evaluation, but a numerical solution reveals that they in fact lead to a *continuous family* parametrized by v.

Bekki and Nozaki [26], in a clever application of Hirota's method of factorization [25b], have succeeded in finding the analytic solution by parametrizing the ansatz (3.60) as

$$\hat{A}(\xi) = \mathrm{e}^{\mathrm{i}q_+/2} GF^{-(1+\mathrm{i}\alpha)}, \tag{3.62a}$$

$$G = a_2(\mathrm{e}^{\kappa_0\xi_0} + z\,\mathrm{e}^{-\kappa_0\xi}), \tag{3.62b}$$

$$F = \mathrm{e}^{\kappa_0\xi} + \mathrm{e}^{-\kappa_0\xi}, \tag{3.62c}$$

with the real parameter α replacing q_-. Inserting the form (3.62) into the differential equation (3.61) and using the relations

$$F\partial_\xi G = G\partial_\xi F + 2\kappa_0 a_2(1-z), \tag{3.63a}$$

$$(\partial_\xi F)(\partial_\xi G) = \kappa_0^2 GF - 2\kappa_0^2 a_2(1+z), \tag{3.63b}$$

we arrive at the relation

$$\begin{aligned}&\left[1+\mathrm{i}\omega + \tfrac{1}{2}\mathrm{i}vq_+ - \tfrac{1}{4}(1+\mathrm{i}c_1)\left(q_+^2 + 4\kappa_0^2\alpha^2\right)\right]F^2 - \mathrm{i}\alpha\left[v + \mathrm{i}(1+\mathrm{i}c_1)q_+\right]F\partial_\xi F \\ &\quad -(1-\mathrm{i}c_3)|G|^2 - 4\kappa_0^2(1+\mathrm{i}c_1)(2+\mathrm{i}\alpha)(1+\mathrm{i}\alpha) \\ &\quad +2\kappa_0 a_2\left\{\left[v + \mathrm{i}(1+\mathrm{i}c_1)q_+\right](1-z) + 2\kappa_0(1+\mathrm{i}c_1)(1+\mathrm{i}\alpha)(1+z)\right\}F/G = 0.\end{aligned} \tag{3.64}$$

Letting $\xi \to \pm\infty$ we equate the coefficients of $\mathrm{e}^{\pm 2\kappa_0\xi}$ to zero to find the fixed point conditions,

$$1 + \mathrm{i}\omega + \mathrm{i}vq_2 - (1+\mathrm{i}c_1)q_2^2 - (1-\mathrm{i}c_3)a_2^2 = 0, \tag{3.65a}$$

$$1 + \mathrm{i}\omega + \mathrm{i}vq_1 - (1+\mathrm{i}c_1)q_1^2 - (1-\mathrm{i}c_3)a_2^2|z|^2 = 0, \tag{3.65b}$$

where

$$q_1 = \tfrac{1}{2}(q_+ - q_-), \quad q_2 = \tfrac{1}{2}(q_+ + q_-), \tag{3.66}$$

are the fixed-point wavevectors, and

$$q_- = -2\kappa_0\alpha. \tag{3.67}$$

We are then left with an expression of the form

$$C_1 + C_2 F/G = 0, \tag{3.68}$$

where $C_{1,2}$ are complex constants, independent of ξ. The only solution of eq. (3.68) is $C_1 = C_2 = 0$, i.e.

$$a_2^2(1+|z|^2+z+z^*) - \alpha^{-2}(q_1-q_2)^2(1+ic_1)(2+i\alpha)(1+i\alpha)/(1-ic_3) = 0, \tag{3.69}$$

$$[v + i(1+ic_1)(q_1+q_2)](1-z) - \alpha^{-1}(q_2-q_1)(1+ic_1)(1+i\alpha)(1-ic_3)^{-1}(1+z) = 0. \tag{3.70}$$

We thus have again 4 complex equations (3.65a, b), (3.69) and (3.70) in 8 real unknowns, i.e. in general a discrete solution. However, the imaginary part of eq. (3.69) yields

$$\alpha = d_2 = -d_4 \pm (2+d_4^2)^{1/2}, \tag{3.71}$$

$$d_4 = \tfrac{3}{2}(c_1c_3 - 1)/(c_1 + c_3), \tag{3.72}$$

and from eq. (3.65) we have the general fixed-point relations

$$a_1^2 = |z|^2 a_2^2 = 1 - q_1^2, \quad a_2^2 = 1 - q_2^2, \tag{3.73a}$$

$$\omega = c_1 - v(1 + q_1q_2)/(q_1+q_2), \tag{3.73b}$$

$$v = (c_1 + c_3)(q_1 + q_2). \tag{3.73c}$$

Using eq. (3.73c) we solve eq. (3.70) for z to find

$$z = \frac{q_1+q_2-\eta(q_1-q_2)}{q_1+q_2+\eta(q_1-q_2)} = |z|e^{i\theta}, \tag{3.74}$$

$$\eta = -(1 - i\alpha^{-1})(1+ic_1)/(1-ic_3) = \eta_r + i\eta_i, \tag{3.75}$$

and note that the imaginary part of eq. (3.69) together with eq. (3.75) yield the relation $\mathrm{Re}\,\eta(2+i\alpha) = 0$, which implies

$$\alpha = 2\eta_r/\eta_i. \tag{3.76}$$

Equation (3.74) can be transformed to

$$(q_1+q_2)^2 d_0^2 + (q_1-q_2)^2 d_1^2 = 1, \tag{3.77}$$

$$\tan\theta = \frac{2\eta_i(q_2^2 - q_1^2)}{(q_2+q_1)^2 - |\eta|^2(q_2-q_1)^2}, \tag{3.78}$$

$$d_0^2 = (1+\eta_r)/4\eta_r, \tag{3.79}$$

$$d_1^2 = (|\eta|^2 + \eta_r)/4\eta_r, \tag{3.80}$$

where the sign in eq. (3.71) may always be chosen such that $\eta_r > 0$, thus assuring that (3.79) and (3.80) are positive. We are now left with the real part of eq. (3.69), which turns out to be *satisfied identically*, when eqs. (3.73)–(3.80) hold, thus completing the analytic solution of Bekki and Nozaki [26], which corresponds to a one-parameter family of solutions. (It turns out that their version of eq. (3.78) is

incorrect. The numerical values provided in their fig. 1b agree with eq. (3.78) above). To summarize, the solution (3.62) is found for any $|v| < v_{\max} = |(c_1 + c_3)/d_0|$ by calculating α from eq. (3.71), η from eq. (3.75), q_1 and q_2 from eqs. (3.73c), (3.77), (3.79) and (3.80), ω and a_2 from eqs. (3.73), κ_0 from eq. (3.67), and θ from eq. (3.78).

We may now verify that the family (3.64), parametrized by v, represents sources. Indeed, assuming $\kappa_0 > 0$ we have for $\xi \to +\infty$, $q_N = q_2$, and we note that $\eta_r > 0$ implies the condition $\alpha(c_1 + c_3) < 0$. Then eqs. (2.65) and (3.67) lead to

$$\operatorname{sgn} \tilde{v}_{g2} = \operatorname{sgn}[(c_1 + c_3)(q_2 - q_1)] = -\operatorname{sgn}[\alpha\kappa_0(c_1 + c_3)] = \operatorname{sgn} \kappa_0 > 0, \tag{3.81a}$$

which is the condition for a source. For $\kappa_0 < 0$ and $\xi \to +\infty$ we have $q_N = q_1$ and

$$\operatorname{sgn} \tilde{v}_{g1} = \operatorname{sgn}[(c_1 + c_3)(q_1 - q_2)] = \operatorname{sgn}[\alpha\kappa_0(c_1 + c_3)] = -\operatorname{sgn} \kappa_0 > 0, \tag{3.81b}$$

once again the condition for a source.

The existence of a family of sources for general values of the parameters c_1 and c_3 of the cubic equation violates the counting arguments presented in section 2.3.2.3, and in our view presents a serious challenge to our understanding of phase space methods as applied to coherent structures. We believe that it is the special symmetries of the ansatz (3.60) that allow an escape from the counting arguments, which assume "generic" intersections of manifolds in phase space.

In fact, the existence of a family of solutions of the form (3.60) would be equally surprising if they turned out to be sinks: the counting argument of section 2.3.2.3 for the existence of a family of sinks is based on the extra degree of freedom provided by the *two* unstable directions of the outgoing fixed point $N_+(++-)$. However, since the solution (3.60) can be expanded in powers of $e^{\pm 2\kappa_0\xi}$, the corresponding trajectory approaches each fixed point along a *fixed* eigendirection. From naive counting, one expects such solutions to form a discrete set irrespective of whether they are sources or sinks.

Let us discuss the symmetry of eq. (3.60) in more detail. Besides the usual parity symmetry (2.40) of the dynamical system (2.5), which translates to

$$\text{P:} \quad v \to -v, \quad q_1 \to -q_1, \quad q_2 \to -q_2, \quad \kappa_0 \to -\kappa_0, \tag{3.82}$$

the ansatz (3.60) has a "relabelling" symmetry,

$$\text{R:} \quad q_1 \to q_2, \quad a_1^2 \to a_2^2, \quad \kappa_0 \to -\kappa_0, \quad z \to z^{-1}. \tag{3.83}$$

Moreover, from the form of eq. (3.60) it follows that the unstable eigenvalue at the $N_+(--+)$ fixed point $\lambda_0^{(+)} = 2\kappa_0$ is equal and opposite to the stable eigenvalue $\lambda_0^{(-)} = -2\kappa_0$ at the $N_-(++-)$ fixed point[#13]. Surprisingly, the relation $\lambda_0^{(+)} = -\lambda_0^{(-)}$ turns out to be sufficient to determine the orbit completely. Indeed, for a given v and ω, the dynamical system (2.5) for the cubic equation has two N fixed points. Now consider v fixed with $|v| \le v_{\max} = |(c_1 + c_3)/d_0|$. For arbitrary ω, the eigenvalues at the two fixed points are different; now adjust ω so as to satisfy the symmetry $\lambda_0^{(+)} = -\lambda_0^{(-)}$. The flow out of and into the two fixed points along the two corresponding eigendirections is thereby determined, but we see no a priori reason why these two one-dimensional manifolds should intersect. Nevertheless, the existence of the family of solution (3.60) shows that they do intersect for arbitrary c_1 and c_3, and for

[#13] It follows from the discussion of section 2.2.3 that the N_- fixed point has a $(++-)$ structure for small v. For larger v, in particular close to the maximum v of the family (3.60), the N_- fixed point is often found to have a $(---)$ structure. In these cases, the naive counting allows for the existence of a two-parameter family of source solutions.

arbitrary $|v| \leq v_{\max}$. Apparently imposing a symmetry at the fixed points guarantees that it will be maintained all along the trajectory in this case!

While we have noted these symmetries, and we believe that they are related to the existence of a family of sources, we have been unable to find an argument showing directly how the symmetry leads to a breakdown of genericity in phase space. Presumably this breakdown is limited to the cubic equation, but it could also lead to a family of moving *pulses* generalizing the solution of Hocking and Stewartson [24].

4. Marginal stability conjectures and selection criteria

Having described a large class of exact solutions of our basic system (2.10), and having provided explicit expressions for some of these, we wish to investigate their dynamical properties, i.e. their stability and the likelihood that they will be reached from typical initial conditions. Our major hypothesis is that in certain cases to be specified the exact front solution $v^\dagger, \omega^\dagger$, eq. (3.40), controls the dynamics of the PDE (2.10) for a large class of initial conditions. Since this hypothesis is related to earlier marginal stability conjectures we first summarize these.

4.1. Linear marginal stability

The linear marginal stability hypothesis has been applied quite generally to fronts advancing into unstable states ($\varepsilon > 0$) about which the dynamical equation can be linearized. Let us introduce the complex dispersion relation, analogous to eq. (2.25) for the dynamical equation linearized about the unstable state

$$\Omega(Q) = \Omega_r + i\Omega_i, \quad Q = q_L - i\kappa_L. \tag{4.1}$$

Then the linear marginal stability hypothesis [9–14] states that the selected velocity v^* has the property that in a frame moving with that velocity a disturbance will neither grow nor decay. As shown in ref. [11] its value can be obtained from the function $\Omega(Q) = \Omega(q_L, \kappa_L)$ by first using the relation

$$\left.\frac{\partial \Omega_i}{\partial q_L}\right|_{\kappa_L} = 0, \tag{4.2}$$

to define the functions $q_L(\kappa_L), \Omega_i(\kappa_L) = \Omega_i(q_L(\kappa_L), \kappa_L)$, and a family of "stable" fronts with velocities

$$v(\kappa_L) = -\Omega_i(\kappa_L)/\kappa_L. \tag{4.3}$$

Then the chosen front v^*, κ_L^*, q_L^* is obtained from the marginal stability condition

$$\frac{dv}{d\kappa_L} = 0, \tag{4.4}$$

as the minimum of the curve $v(\kappa_L)$.

For the complex Ginzburg–Landau equation the linear dispersion relation is given by eq. (2.25) with

$$\Omega = \omega + Qv = \omega + (q_L - i\kappa_L)v. \tag{4.5}$$

The q_L obtained from eq. (4.2) is given by

$$q_L = -c_1\kappa_L/b_1, \tag{4.6}$$

and the branch of solutions (4.3) is

$$v(\kappa_L) = -\kappa_L/\tilde{b}_1 - \varepsilon\kappa_L^{-1}, \quad \varepsilon > 0. \tag{4.7}$$

Thus the marginal stability values obtained from eq. (4.4) are

$$v^* = 2\left(\varepsilon/\tilde{b}_1\right)^{1/2}, \tag{4.8a}$$

$$\kappa_L^* = -\left(\tilde{b}_1\varepsilon\right)^{1/2}, \tag{4.8b}$$

$$\omega^* = -c_1\varepsilon/b_1, \tag{4.8c}$$

and a solution only exists for $\varepsilon > 0$, i.e. when the $A = 0$ state is unstable.

It is well known [9–14] that the linear marginal stability mechanism also applies to models which do not admit uniformly translating front profiles, such as the Swift–Hohenberg equation (1.7). The new feature of the complex Ginzburg–Landau equation is, however, that this property of the linear front (i.e. whether it is uniformly translating or not) depends on parameters. To see this, note that with v^* and ω^* given by eqs. (4.8), eqs. (2.19) become

$$\varepsilon = b_1 q_N^{*2} + b_3 a_N^{*2} + b_5 a_N^{*4}, \tag{4.9a}$$

$$-c_1\varepsilon/b_1 + 2\left(\varepsilon/\tilde{b}_1\right)^{1/2} q_N^* = c_1 q_N^{*2} - c_3 a_N^{*2} - c_5 a_N^{*4}. \tag{4.9b}$$

A necessary condition for the existence of a uniformly translating solution is that these two equations for a_N^* and q_N^* should have a solution. It should be stressed that these conditions are *different* from the "conservation of nodes" argument [11] first used by Dee and Langer [9], to relate the parameters in the leading edge of the front to the wavelength λ_N of the nonlinear state behind the front, which yields $2\pi\lambda_N^{-1} = \mathrm{Re}\,\omega^*/v^* - q_L^*$. The latter relation only holds for nonuniformly translating fronts; for profiles of the uniformly translating type (2.4), conservation of nodes is trivially satisfied in the frame moving with the front. From eq. (2.43) we find

$$v_{cL} = 2c_1(\varepsilon/b_1)^{1/2} < v^*, \tag{4.10}$$

so that if eq. (4.9) has a solution, the results of section 2.3.2 imply the existence of a two-parameter family of uniformly translating fronts containing the linear front v^* as a member. For the cubic equation, (2.10) with $b_1 = b_3 = 1$ and $c_5 = b_5 = 0$, the solution of eq. (4.9) is

$$q_N^* = \frac{\left(1 + c_1^2\right)^{1/2} - \left(1 + c_3^2\right)^{1/2}}{c_1 + c_3}, \tag{4.11a}$$

$$\left(a_N^*\right)^2 = 2\frac{(c_1c_3 - 1) + \left(1 + c_1^2\right)^{1/2}\left(1 + c_3^2\right)^{1/2}}{\left(c_1 + c_3\right)^2}. \tag{4.11b}$$

Since a solution of eqs. (4.11) exists for any value of c_1 and c_3, we generally expect that there will exist a

corresponding uniformly translating solution of the cubic Ginzburg–Landau equation. Whether this solution will actually be observed depends also on the Benjamin–Feir stability of the nonlinear state (4.11) (see e.g. ref. [25a]).

To analyze the implications of eq. (4.9) in the case of a subcritical bifurcation, let us choose the scaling $b_1 = -b_3 = b_5 = 1$ and first consider the behavior in the two limits $\varepsilon \to 0$ and $\varepsilon \to \infty$. For $\varepsilon \to \infty$ we can solve for a_N^* as a function of q_N^* on the upper branch (2.22), provided $-\sqrt{\varepsilon - \frac{1}{4}} < q_N^* < \sqrt{\varepsilon - \frac{1}{4}}$. By investigating the left-hand and right-hand sides of eq. (4.9b) as a function of q_N^* in this interval, it is easy to see that eq. (4.9) always has a solution in this limit. This is analogous to what was found in the cubic case. For $\varepsilon = 0$, on the other hand, we find by eliminating q_N^* that the equations only have roots with $\frac{1}{2} \le a_N^{*2} \le 1$ in the parameter ranges

$$-2c_3 + c_1 < c_5 < -c_3,$$
$$-c_3 < c_5 < -2c_3 + c_1. \tag{4.12}$$

It follows that there are large sectors of parameter space where fronts propagating with the linear marginal stability speed v^* are not uniformly translating for $\varepsilon \to 0$ (the size of these sectors shrinks with increasing ε). We shall return to this question in section 4.2 below and in section 6 where we show some numerical examples of nonuniformly translating fronts. In the examples that we discuss phase slips occur in the front region, and we have found no way to express the wavenumber q_N of the nonlinear state behind the front in terms of v^*, κ_L^* and q_L^*.

As noted by previous authors [9–11], the linear marginal stability criterion only applies for fronts with localized initial conditions, e.g. $A(x,0) = 0$, $x > x_0$. For a front decaying sufficiently slowly as $x \to +\infty$, e.g. for

$$A(x,0) \sim e^{-|\bar{\kappa}|x}, \quad |\bar{\kappa}| < |\kappa^*|, \tag{4.13a}$$

the selected front velocity will be

$$v(\bar{\kappa}) = -\bar{\kappa}/\tilde{b}_1 - \varepsilon/\bar{\kappa} > v^*. \tag{4.13b}$$

This is an example of a violation of the linear marginal stability criterion caused by a particular initial condition, and also an illustration of the stability of the fronts on the branch $v(\kappa_L)$. On the other hand, this branch is only accessible from a restricted (and somewhat artificial) set of initial conditions, and it has been termed "irrelevant" by Powell et al. [43]. These authors point out that in a number of cases (e.g. the real Ginzburg–Landau equation, $c_i = 0$, with oscillatory initial conditions) the *approach* of the velocity to the selected value v^* is via a set of unstable fronts with $v < v^*$, rather than along the stable set $v(\kappa_L)$. Moreover, it has been shown by one of us [11, 14] that for the real Ginzburg–Landau equation with Im $A = 0$, nonnegative initial conditions also lead to fronts whose velocity approaches v^* from below.

4.2. Nonlinear selection

Another violation of the linear marginal stability criterion which we term "nonlinear selection" occurs when there exists a discrete front, with a velocity $v^\dagger$ and a spatial decay rate $|\kappa_L^\dagger|$ satisfying

$$v^\dagger > v^* \quad \text{and} \quad |\kappa_L^\dagger| > |\kappa_L^*|. \tag{4.14}$$

It was noticed earlier for a number of models [9, 11], and proved rigorously [27] for the nonlinear diffusion equation (2.66), that when the conditions (4.14) are satisfied it is indeed the front $v^\dagger, \kappa_L^\dagger$ that is selected over the linear front v^*, κ_L^*. Moreover, this is consistent with an extended (nonlinear) marginal stability hypothesis [11] since in that case the front $v^\dagger, \kappa_L^\dagger$ is still the stable one with the minimum velocity, i.e. fronts with $v > v^\dagger$ are linearly stable, while those with $v < v^\dagger$ are unstable. Our conjecture [8] is that this result applies quite generally, and moreover, that for the complex Ginzburg–Landau equation (2.10) the relevant discrete front is the one obtained from the ansatz (3.38), which we termed the "nonlinear front"[#12].

In particular, recalling the L fixed-point structure (2.44) we see that if for $\varepsilon > 0$ and $v > v^* > v_{cL}$ we choose the orbit going to L_{-1} rather than L_{-2}, i.e. the discrete orbit rather than a member of the family, we may satisfy eq. (4.14) since $|\kappa_{L1}| > |\kappa_{L2}|$. Furthermore, as will be discussed in section 6, for large ε the nonlinear front (3.40) satisfies $v^\dagger > v^*$ but *not* $|\kappa^\dagger| > |\kappa^*|$, so it is not selected. When this occurs the nonlinear front flows into L_{-2}, and is therefore a member of a two-parameter family.

For $\varepsilon < 0$, on the other hand, there is no family of fronts emanating from N_-, i.e. no linear front v^*, and our conjecture is that $v^\dagger$ will be selected whenever such a front has $v^\dagger > 0$. When $v^\dagger < 0$, or when the ansatz (3.38) does not lead to a solution with real v and ω, we conjecture that pulse solutions will in general exist, at least for large enough $\varepsilon < 0$, though their stability depends on initial conditions. When ε becomes sufficiently negative, i.e. $\varepsilon < \varepsilon_2$ for some $\varepsilon_2 < 0$, the pulses no longer exist or are always unstable, and an initial condition with $A \neq 0$ decays to $A = 0$.

Let us briefly discuss fronts emanating from an N_+ fixed point. Since these are constructed from N states with the group velocity $\tilde{v}_g$ (in the frame moving with velocity v) positive (see eq. (2.52) and footnote 9), we argue that a small disturbance will overtake the front and will therefore destabilize it. We thus conjecture that fronts emanating from N_+ are never stable. This is why we did not study their multiplicity in great detail in section 3.3.1.

In summary, our conjectures on the evolution of a localized initial condition can be stated as follows (see fig. 7):

• For $\varepsilon > 0$, we calculate the linear front v^*, κ_L^* from eq. (4.8) and the nonlinear front $v^\dagger, \kappa_L^\dagger$ from eq. (3.40). The linear front will be selected unless there exists a nonlinear front with

$$v^\dagger > v^* \quad \text{and} \quad |\kappa_L^\dagger| > |\kappa_L^*|, \tag{4.15}$$

in which case the nonlinear front will be selected. In general we expect linear marginal stability at large ε and we define $\varepsilon^\dagger$ such that v^* is chosen for $\varepsilon > \varepsilon^\dagger$ and $v^\dagger$ is chosen for $\varepsilon < \varepsilon^\dagger$. If no solution of eqs. (3.38) is found satisfying (4.14) we have $\varepsilon^\dagger = 0$.

• For $\varepsilon < 0$, if there is a solution of eqs. (3.38) with $v^\dagger > 0$ near $\varepsilon = 0$, and if ε_3 is the value of ε where $v^\dagger = 0$, then the front $v^\dagger$ will be selected for $\varepsilon_3 < \varepsilon < 0$. When $v^\dagger < 0$ (i.e., in view of (3.45), for $\varepsilon < \varepsilon_3$) or if eqs. (3.38) yield no solution with real v, then the situation is more complicated. The solutions depend more sensitively on initial conditions, but in general we expect to find stable pulses over some range $\varepsilon_2 < \varepsilon < \varepsilon_3$, while for $\varepsilon < \varepsilon_2$ an initial disturbance $A(x, 0) \neq 0$ will decay to zero. Note that in general pulses only exist as a discrete set, and this set is expected to contain *stationary* pulses ($v = 0$). Since we can calculate $v^\dagger$ analytically from our ansatz via eq. (3.40) we can predict the value of ε_3 for given $\{b_i, c_i\}$, but we have no such general prediction for ε_2.

A useful way to illustrate the implications of these rules and conjectures is to plot the regions where $v^\dagger(\varepsilon = 0) > 0$ in the $\{c_1, c_3, c_5\}$ parameter space. This is shown in fig. 8 for the three cases $c_1 = 0$, $c_1 = 2$

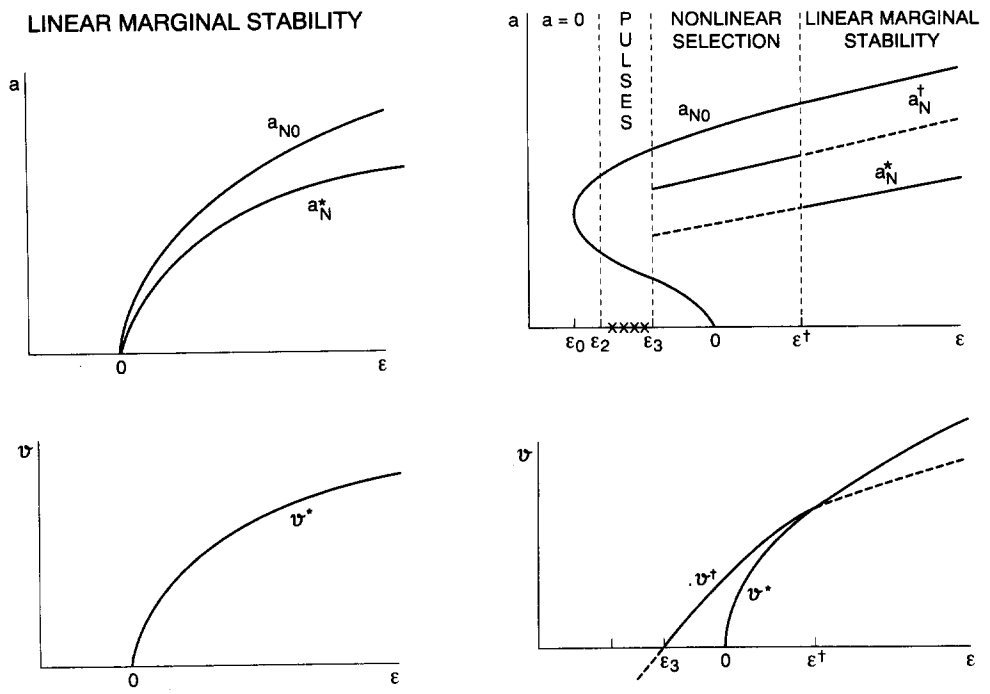

Fig. 7. Illustration of front and pulse selection on a schematic bifurcation diagram and plot of front velocity vs. ε for (a) the supercritical and (b) the subcritical case. The uniform amplitude nonlinear state has amplitude a_{N0} and wavevector $q_N = 0$. In the supercritical case (a), linear marginal stability is expected to hold in general, with a velocity v^* which vanishes at $\varepsilon = 0$. As explained in the text, the nonlinear state created behind this front has amplitude a_N^* and wavevector q_N^*. In the subcritical case (b) the nonlinear front, when it exists, has velocity $v^\dagger$ and leaves behind a state with amplitude $a_N^\dagger$, while the linear marginal stability front has velocity v^* and in simple cases an amplitude a_N^*. In each region of ε the selected front is indicated by a solid line, while the other one is drawn as a dashed line. Stable pulse solutions are found in the range $\varepsilon_2 < \varepsilon < \varepsilon_3$ indicated by crosses, where ε_3 is defined by $v^\dagger(\varepsilon_3) = 0$. For $\varepsilon < \varepsilon_2$ a disturbance typically decays back to the $a = 0$ state.

and $c_1 = 10$, where these regions are contained between the solid lines in the (c_3, c_5) plane. Since according to eq. (3.45) $\partial_\varepsilon v^\dagger > 0$, the upper range of stability of pulses in these areas is $\varepsilon_3 < 0$. Outside these regions, there are no nonlinear fronts with positive speed $v^\dagger$ for any $\varepsilon < 0$, and hence stable pulses may exist up to $\varepsilon_3 = 0$, and for $\varepsilon > 0$ fronts will propagate with speed v^*. According to eq. (4.12), however, linear marginal stability fronts can only by *uniformly translating* for $\varepsilon \downarrow 0$, in the area between the dashed lines of fig. 8. For $c_1 = 0$, fig. 8a shows that this area falls inside the range where $v^\dagger$ $(\varepsilon = 0) > 0$. Thus, depending on c_3 and c_5, either uniformly translating nonlinear fronts or nonuniformly translating linear fronts can arise for $\varepsilon \downarrow 0$. As fig. 8 illustrates, for increasing values of c_1 the regions of parameter space where one may observe uniformly translating linear fronts, will expand. Note also that as mentioned earlier, for increasing ε the parameter ranges where $v^\dagger(\varepsilon) > v^*(\varepsilon)$, will shrink.

According to fig. 8, uniformly translating fronts typically only exist in a band near the diagonal $c_5 = -c_3$. Apparently, in the subcritical case smooth front propagation for $\varepsilon \simeq 0$ is only possible if the nonlinear dispersive terms roughly cancel each other. Furthermore, according to the rules formulated above, pulses will remain stable up to $\varepsilon_3 = 0$ outside the solid lines. Hence a strong effective nonlinear dispersion promotes the stability of pulses.

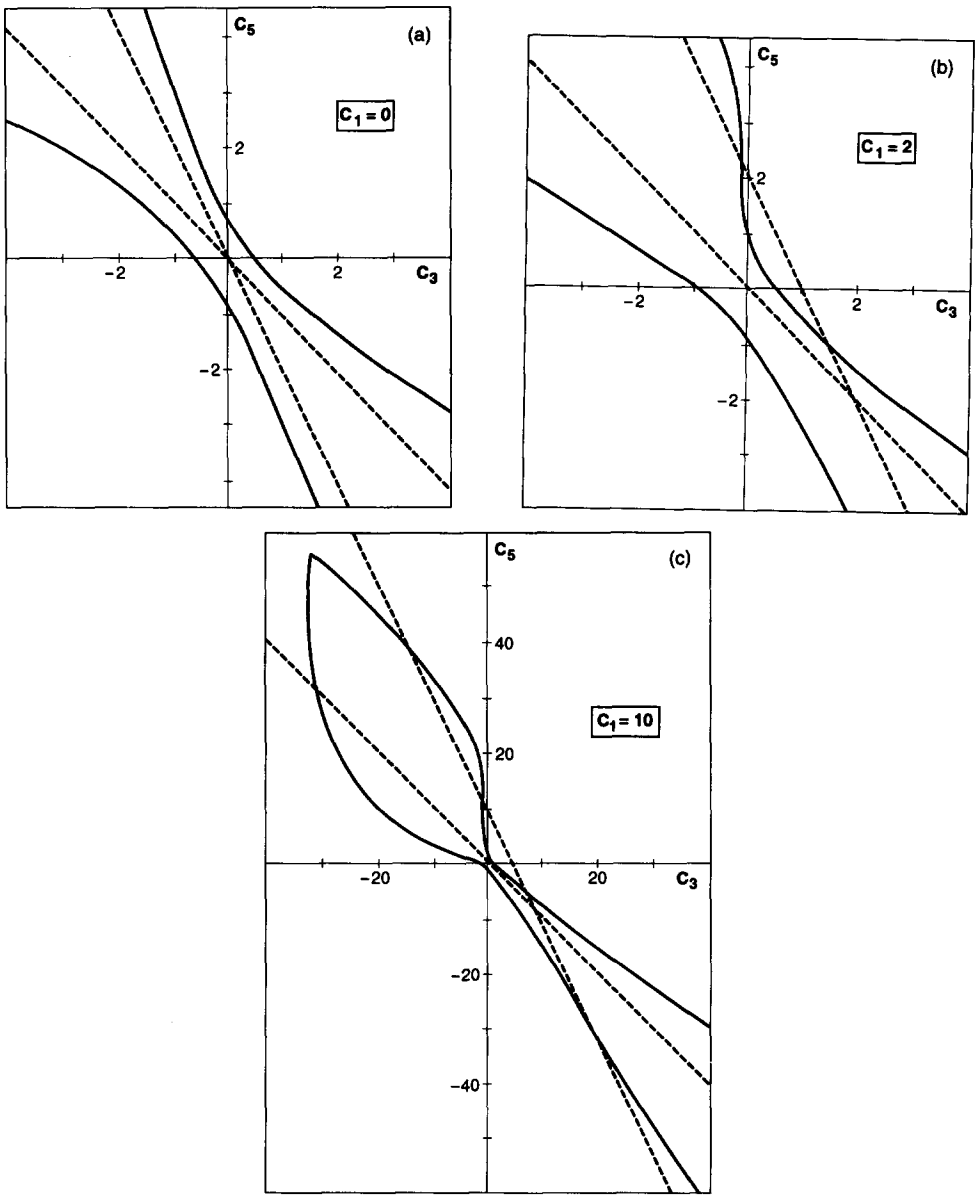

Fig. 8. Illustration of the range of existence of nonlinear fronts with $v^{\dagger} > 0$ in the (c_3, c_5) plane for $\varepsilon = 0$ and constant c_1. The region where $v^{\dagger}(\varepsilon = 0) > 0$, and hence $\varepsilon_3 < 0$, is bounded by the two solid lines. Outside this region, our rules predict $\varepsilon_3 = 0$. The dashed lines bound the region where according to eq. (4.12) uniformly translating linear front solutions can exist. Thus outside the areas bounded by the solid and dashed lines, linear marginal stability fronts will be selected but they will be nonuniformly translating in the limit $\varepsilon \downarrow 0$. (a) $c_1 = 0$; (b) $c_1 = 2$; (c) $c_1 = 10$.

4.3. Effect of Benjamin–Feir instability

We have already excluded from consideration fronts emanating from N_+ fixed points, because we argued in section 4.2 that they would be unstable. It is still possible, however, even with $N_- \to L_-$ fronts, to have the wavevector q_N of the N state be outside the band of Benjamin–Feir stability determined by (2.32). In contrast to the "nonlinear instability" associated with the positive group velocity $\tilde{v}_g$ of fronts emanating from N_+ states, the Benjamin–Feir instability is "linear", and so does not eliminate the corresponding $N_- \to L_-$ front completely. Indeed, since we have found $\tilde{v}_g$ to be always negative (see after eq. (3.46)), the instability in the region behind the front is only convective in the frame moving with the front. As in the case of spiral waves in two dimensions, where the range of stability extends into the Eckhaus unstable regime because the instability is only convective [45], the emergence of a convectively unstable state behind the front need not necessarily destroy the propagating front. Nevertheless, we are no longer dealing with a uniformly translating solution, so we must add to our selection criteria the proviso that the N_- state be in the stable band. It will turn out that if q_N is outside the stable band, but not too far outside, then the calculated $v^\dagger$ is often still a good approximation for the *average* velocity of the chaotic front produced. Since we have an analytic expression for the Benjamin–Feir stability band, eq. (2.32), we can make precise predictions concerning this aspect of front stability, and verify these predictions numerically.

Another difference between the linear Benjamin–Feir instability and the nonlinear instability associated with front–pulse competition, is that the former does not show the approximate symmetry along the diagonal $c_5 = -c_3$ displayed in fig. 8. In particular, since effects of the nonlinear dispersion terms are additive in linear stability considerations, we find (cf. eq. (2.35)) that for $c_1 > 0$ nonlinear amplitude states a_N in the first quadrant of the (c_3, c_5) plane tend to be unstable, while those in the third quadrant tend to be stable. As discussed in section 6 below, the resulting dynamical behavior is indeed quite different in these two quadrants.

4.4. Implications of the terms f_2 and f_3 in eq. (2.1)

In the analysis of the multiplicity of solutions in section 2.3.2 on the basis of counting arguments, we took $f_2(|A|^2) = f_3(|A|^2) = 0$ in eq. (2.1). Although it is straightforward to include these terms, the analysis becomes quite cumbersome, and we confine ourselves here to a qualitative discussion of the resulting change.

Since constant terms in f_2 and f_3 can be eliminated by a Galilean transformation, we will assume $f_2(0) = f_3(0) = 0$ in the present discussion, so that the L fixed points are unaffected by these terms. The counting argument will therefore once again lead to a discrete set of pulse solutions. However, the symmetry (2.54) which in the case $v = 0$, $f_2 = f_3 = 0$ gives rise to the stationary pulses, is absent if $f_2 \neq 0$ or $f_3 \neq 0$. Thus, as emphasized by Brand and Deissler [44], for $f_2 \neq 0$, $f_3 \neq 0$, pulse solutions will typically have a nonzero velocity; we show in section 5 that its value can be calculated perturbatively starting from the quintic derivative Schrödinger limit (2.15).

The N fixed points are of course affected by f_2 and f_3: although only f_2 enters the relation between a_N and q_N, both terms alter the stability of the N fixed points in the dynamical system (2.5). Nevertheless, for large v terms proportional to v still dominate the expression for α_N, β_N and γ_N in eq. (2.45), and in analogy with the results in section 2.2.2, we expect a discrete set of fronts for large v. For small v, however, the stability of the fixed points may be very different. In particular, since the symmetry (2.40) is now absent, and since the sign of α_N is no longer the same as the sign of v, it may be possible

for the N fixed point to have a $(+\ +\ +)$ structure for small v. This would imply the existence of a two-parameter family of fronts in the subcritical case for $\varepsilon < 0$.

In spite of these complications, it is easy to see that the nonlinear front ansatz (3.38) still solves the dynamical system (2.6) if f_2 and f_3 are of the form

$$f_2 = (s_2 + \mathrm{i}r_2)a^2, \qquad f_3 = (s_3 + \mathrm{i}r_3)a^2, \tag{4.16}$$

since upon substitution into eq. (2.6), these terms only generate terms of a form already present in eq. (2.6). Thus, the nonlinear front velocity $v^\dagger$ will be given by expressions similar to eq. (3.40). We have not analyzed these equations, but they are worth investigating further since, as will be discussed in section 7, the more general model is useful for understanding convection experiments.

5. Perturbation expansions

Perturbation expansions of pulse and front solutions about soluble cases have been carried out by many authors, either starting from the real equation ((2.10) with $f_{1\mathrm{i}} = f_2 = f_3 = 0$) for which there is a Lyapunov function [29–31] or starting from various Hamiltonian limits [15–19]. There is a large literature on perturbations of the integrable nonlinear Schrödinger equation, exploiting the inverse scattering method [15], or using more elementary techniques [17–19]. We wish to start from the cases considered in section 3.2 which are not integrable as PDE's but for which the dynamical system (2.5), (2.6) can be integrated. Specifically, we choose the generalized derivative Schrödinger equation, for which eq. (3.22) holds. As shown above, the system possesses a double family of pulses indexed by v and ω, and in some cases also a one-parameter family of fronts indexed by v. It also has two conserved quantities $\mathcal{N}$, eq. (3.1), and $\mathcal{P}$, eq. (3.4). The perturbations we consider break the conservation laws and pick out discrete members of the above families. A general way to calculate the effect of such perturbations is to consider the slow modes of the dynamical evolution operator, and to obtain solvability conditions from the equations of motion. As shown for example by Elphick and Meron [17] these conditions lead to nonlinear equations for the parameters v and ω (the constants of the unperturbed system) whose stable fixed points are the values selected by the perturbation. In our case we extend the approach of Fauve and Thual [18] who use a simpler method based on the conserved quantities $\mathcal{N}$ and $\mathcal{P}$, and arrive at equations for v and ω similar to those of Elphick and Meron [17]. Note that unlike the case considered by the latter authors, for our system the effect of the perturbation is not to break dilatation and Galilean symmetries, but to destroy the Hamiltonian nature of eq. (3.15) and to violate the conservation laws (3.3) and (3.5). As mentioned in the introduction, our example shows that breaking the symmetries is insufficient to pick out discrete v and ω. (Although the example of eq. (3.15) with $f'_{3\mathrm{i}} = 0$ but $f'_{3\mathrm{r}} \neq 0$ shows that violating the conservation laws does not necessarily destroy the double family of pulses, in the case treated below it does.)

5.1. *Perturbation about the quintic derivative Schrödinger limit*

Let us begin by considering the equation

$$\partial_t A = \mathrm{i}\partial_x^2 A + \mathrm{i}f_{1\mathrm{i}}(|A|^2)A + \partial_x\left[f_{2\mathrm{r}}(|A|^2)A\right] + bB, \tag{5.1a}$$

$$B = \partial_x^2 A + \hat{f}_{1\mathrm{r}}(|A|^2)A \equiv B_\mathrm{r} + \mathrm{i}B_\mathrm{i}, \tag{5.1b}$$

i.e. we take

$$c_1 = 1, \qquad b_1 = b \ll 1, \tag{5.2}$$

and for simplicity we have set $f_{2i} = f_3 = 0$ in the perturbation B (5.1b), which is considered to be $\mathcal{O}(1)$ [i.e. $\hat{f}_{1r} = b^{-1} f_{1r} = \mathcal{O}(1)$]. The unperturbed system has two conserved quantities, $\mathcal{N}$ and $\mathcal{P}$, eqs. (3.3), (3.5), but no nontrivial symmetries such as Galilean or dilatation invariance. We calculate the effects of the perturbation bB on *normalizable* solutions by calculating the time derivatives $\partial_t \mathcal{N}$ and $\partial_t \mathcal{P}$ which are of $\mathcal{O}(b)$. Indeed, using the equation of motion (5.1) and the definitions (3.1), (3.4), we find

$$\partial_t \mathcal{N} = b \int (BA^* + B^* A)\, \mathrm{d}x, \tag{5.3a}$$

$$\partial_t \mathcal{P} = 2b \int \left[\mathrm{i} B^* (\partial_x A) - \mathrm{i} B (\partial_x A^*) + f_{2r} (AB^* + BA^*) \right] \mathrm{d}x. \tag{5.3b}$$

We therefore introduce a slow time variable

$$T = bt, \tag{5.4}$$

and make the ansatz

$$A(x,t) = \mathrm{e}^{-\mathrm{i}\omega(T)t} \tilde{A}_0(\xi, v(T), \omega(T)) + bA_1, \tag{5.5}$$

where

$$\tilde{A}_0(\xi) = a(\xi)\, \mathrm{e}^{\mathrm{i}\phi(\xi)} \tag{5.6}$$

is the double family of pulse solutions, e.g. (3.25)–(3.28) indexed by v and ω, that exist for $b = 0$. The only dependence of the first term in eq. (5.5) on the perturbation b is via a slow time dependence $v(T), \omega(T)$. Inserting the ansatz (5.5) into eqs. (5.3) and neglecting the term bA_1, we find in lowest order in b,

$$\partial_T \mathcal{N} = 2 \int B_r a\, \mathrm{d}\xi, \tag{5.7a}$$

$$\partial_T \mathcal{P} = -4 \int \left[(q + f_{2r}) a B_r - a' B_i \right] \mathrm{d}\xi, \tag{5.7b}$$

$$B_r = a'' - q^2 a + \hat{f}_{1r} a, \tag{5.7c}$$

$$B_i = 2qa' + q'a. \tag{5.7d}$$

We now make the particular choices

$$\hat{f}_{1r} = \hat{\varepsilon} - \hat{b}_3 a^2 - \hat{b}_5 a^4, \tag{5.8a}$$

$$f_{2r} = s_0 + s_2 a^2, \tag{5.8b}$$

$$f_{1i} = c_3 a^2 + c_5 a^4, \tag{5.8c}$$

with

$$\hat{\varepsilon} = \varepsilon/b, \qquad \hat{b}_3 = b_3/b, \qquad \hat{b}_5 = b_5/b, \tag{5.9}$$

which, as mentioned earlier, are considered to be of order unity. Note that the Hamiltonian limit of the complex Ginzburg–Landau equation (2.10) corresponds to the case $f_{2r} = 0$, but we keep $f_{2r} \neq 0$ in the following analysis. The zeroth-order solution (5.6) has $a(\xi)$ given by (3.25a) and

$$q = \tfrac{1}{2}(s_0 + v) + \tfrac{3}{4}s_2 a^2 = q_0 + q_2 a^2. \tag{5.10}$$

Inserting these solutions into eqs. (5.7) we obtain

$$\partial_T \mathcal{N} = -2N_{02} + 2\big(\hat{\varepsilon} - q_0^2\big)N_{20} - 2\big(\hat{b}_3 + 2q_0 q_2\big)N_{40} - 2\big(\hat{b}_5 + q_2^2\big)N_{60}, \tag{5.11a}$$

$$\partial_T \mathcal{P} = -2(q_0 + s_0)\partial_T \mathcal{N} - \tfrac{28}{3}q_2\big[\big(\hat{\varepsilon} - q_0^2\big)N_{40} - \big(\hat{b}_3 + 2q_0 q_2\big)N_{60} - \big(\hat{b}_5 + q_2^2\big)N_{80}\big] + 8q_0 N_{02} + 44 q_2 N_{22}, \tag{5.11b}$$

where we have introduced the notation

$$N_{lm} = \int [a(\xi)]^l [a'(\xi)]^m \, \mathrm{d}\xi. \tag{5.12}$$

On the other hand from the definitions (3.1) and (3.4) we find, for $A(x,t)$ given by (5.5) and (5.6) the expressions[#14]

$$\mathcal{N} = N_{20}, \tag{5.13a}$$

$$\mathcal{P} = 2(q_0 - v)N_{20} - \tfrac{2}{3}q_2 N_{40}. \tag{5.13b}$$

Since the integrals N_{lm} are known functions of $v(T)$ and $\omega(T)$, we obtain from eq. (5.11) a system of coupled nonlinear first-order ODE's for $v(T)$ and $\omega(T)$. At the fixed point $\partial_T v = \partial_T \omega = 0$ we have

$$\partial_T \mathcal{P} = \partial_T \mathcal{N} = 0, \tag{5.14}$$

from which we obtain two relations determining v and ω.

For the quintic-cubic Schrödinger equation ($s_0 = s_2 = 0$, $q_0 = \frac{1}{2}v$, $q_2 = 0$) we find from eqs. (5.13) and (5.11)

$$\partial_T v = -4vN_{02}/N_{20}. \tag{5.15}$$

Now by Galilean invariance (3.9) of the unperturbed system we have

$$N_{lm}(\omega, v) = N_{lm}\big(\omega + \tfrac{1}{4}v^2, 0\big). \tag{5.16a}$$

[#14] We use the notation $\mathcal{N}$ and $\mathcal{P}$ to denote functionals of $A(x,t)$ and $A^*(x,t)$, and N_{lm} for their values when the particular ansatz (5.6) is used.

Moreover, it is easy to see that

$$N_{2l,2m}(\omega,0) > 0 \quad \text{for} \quad 0 < |\omega| < \omega_{\max}, \tag{5.16b}$$

so the only fixed point solution of eq. (5.14) with nonzero amplitude is $v = 0$, in accordance with the result of Elphick and Meron [17] for perturbations of the nonlinear Schrödinger equation. Our derivation generalizes their conclusion to the case of the quintic-cubic Schrödinger equation, and allows for general perturbations of the form (5.1b). The amplitude of the pulse will then be given by the fixed point of eq. (5.11a), which by (5.13a) may be written in the form

$$\partial_T \omega = 2(\partial_\omega N_{20})^{-1}\left[\hat{\varepsilon} N_{20} - \hat{b}_3 N_{40} - \hat{b}_5 N_{60} - N_{02}\right]. \tag{5.17}$$

We shall investigate this equation in more detail in the next subsection.

Turning to the quintic derivative Schrödinger equation in the simple case $s_2 = 0$, i.e. taking only $s_0 \neq 0$ in eq. (5.11), we find

$$N_{20}\partial_T v - 4 s_0 \partial_T N_{20} = -4(s_0 + v) N_{02}, \tag{5.18a}$$

$$\partial_T N_{20} = -2 N_{02} + 2\left[\hat{\varepsilon} - \tfrac{1}{4}(s_0 + v)^2\right] N_{20} - 2\hat{b}_3 N_{40} - 2\hat{b}_5 N_{60}. \tag{5.18b}$$

The fixed point values of v and ω are given by

$$v = -s_0, \tag{5.19a}$$

$$\omega = \omega_0, \tag{5.19b}$$

where ω_0 is the fixed point of eq. (5.17) valid for $v = s_0 = 0$, since the dependence of the N_{lm} on ω, s_0 and v is, according to eqs. (5.10) and (5.16a), via the variable $\omega + \frac{1}{4}(s_0 + v)^2$ for the Galilean invariant case $s_2 = 0$.

For the case $s_0 \neq 0$, $s_2 \neq 0$, eqs. (5.11) are coupled first-order nonlinear ODE's for $v(T)$ and $\omega(T)$ of the form

$$G_{11}\partial_T v + G_{12}\partial_T \omega = G_{10}, \tag{5.20a}$$

$$G_{21}\partial_T v + G_{22}\partial_T \omega = G_{20}, \tag{5.20b}$$

with

$$G_{11} = \partial_v N_{20}, \qquad G_{12} = \partial_\omega N_{20}, \tag{5.21a}$$

$$G_{10} = 2\left[\left(\hat{\varepsilon} - q_0^2\right) N_{20} - \left(\hat{b}_3 + 2 q_0 q_2\right) N_{40} - \left(\hat{b}_5 + q_2^2\right) N_{60} - N_{02}\right], \tag{5.21b}$$

$$G_{21} = 2(q_0 - v)\partial_v N_{20} - \tfrac{2}{3} q_2 \partial_v N_{40} - N_{20}, \tag{5.21c}$$

$$G_{22} = 2(q_0 - v)\partial_\omega N_{20} - \tfrac{2}{3} q_2 \partial_\omega N_{40}, \tag{5.21d}$$

$$\begin{aligned} G_{20} = {} & -4(3q_0 - v)\left(\hat{\varepsilon} - q_0^2\right) N_{20} + \left[4(3q_0 - v)\left(\hat{b}_3 + 2 q_0 q_2\right) - \tfrac{28}{3} q_2\left(\hat{\varepsilon} - q_0^2\right)\right] N_{40} \\ & + \left[4(3q_0 - v)\left(\hat{b}_5 + q_2^2\right) + \tfrac{28}{3} q_2\left(\hat{b}_3 + 2 q_0 q_2\right)\right] N_{60} \\ & + \tfrac{28}{3} q_2\left(\hat{b}_5 + q_2^2\right) N_{80} + 4(5q_0 - v) N_{02} + 44 q_2 N_{22}, \end{aligned} \tag{5.21e}$$

where according to eq. (5.10) $q_0 = \frac{1}{2}(s_0 + v)$ and $q_2 = \frac{3}{4}s_2$, and the N_{lm} are known functions of v and ω. This system will in general reach either a fixed point or a limit cycle, with a pulse velocity of order unity, which depends in general on all the parameters of the unperturbed starting equation (2.14). We have not analyzed eq. (5.20) in detail but we expect nontrivial results to emerge, analogous to those observed in reaction-diffusion systems [46].

5.2. *Pulses and fronts in the perturbed quintic-cubic Schrödinger equation*

Let us return to the analysis of eq. (5.17) appropriate to the quintic-cubic case where $s_0 = s_2 = 0$, and $v = 0$,

$$\partial_T \omega = 2[\partial_\omega N_{20}]^{-1}\left[\hat{\varepsilon} N_{20} - \hat{b}_3 N_{40} - \hat{b}_5 N_{60} - N_{02}\right]. \tag{5.22}$$

From the general formulas

$$N_{l0}(\omega) = \left(\frac{c_1}{2|\omega|}\right)^{1/2}\left(\frac{4g|\omega|}{c_3}\right)^{l/2}\left(\frac{1}{(l/2-1)!}\right)\left(-\frac{\mathrm{d}}{\mathrm{d}g}\right)^{l/2-1}\phi(g), \tag{5.23a}$$

$$N_{l2}(\omega) = \left(\frac{|\omega|}{2c_1}\right)\left[1 + \left(\frac{2g}{\frac{1}{2}l+1}\right)\frac{\mathrm{d}}{\mathrm{d}g} + \frac{g^2-1}{(\frac{1}{2}l+1)(\frac{1}{2}l+2)}\frac{\mathrm{d}^2}{\mathrm{d}g^2}\right]N_{(l+2)0}, \tag{5.23b}$$

for l even, where

$$g = (\operatorname{sgn} c_3)[1 + (\operatorname{sgn} c_5)\tilde{\omega}]^{-1/2}, \tag{5.24a}$$

$$\tilde{\omega} = 16|c_5\omega|/3c_3^2 = |\omega|/\omega_{\max}, \tag{5.24b}$$

$$\phi(g) = 2(1-g^2)^{-1/2}\arctan\left[(1-g^2)^{1/2}(1+g)^{-1}\right], \quad c_5 > 0, \tag{5.24c}$$

$$\phi(g) = (g^2-1)^{-1/2}\ln\left[\left(1+g+\sqrt{g^2-1}\right)/\left(1+g-\sqrt{g^2-1}\right)\right], \quad c_5 < 0, \tag{5.24d}$$

we obtain the limiting formulas

$$N_{l0} \sim |\omega|^{(l-1)/2}, \quad N_{l2} \sim |\omega|^{(l+3)/2}, \quad \tilde{\omega} \ll 1, \quad c_3 > 0, \tag{5.25a}$$

$$N_{l0} \sim |\omega|^{-1/2}, \quad N_{l2} \sim |\omega|^{1/2}, \quad \tilde{\omega} \ll 1, \quad c_3 < 0, \quad c_5 > 0, \tag{5.25b}$$

and

$$N_{l0} \sim |\omega|^{(l-2)/4}, \quad N_{l2} \sim |\omega|^{(l+4)/4}, \quad \tilde{\omega} \gg 1, \quad c_5 > 0, \tag{5.26a}$$

$$N_{l0} \sim \sqrt{2/c_3}\,(3c_3/4c_5)^{(l-1)/2}\ln(\omega_{\max} - |\omega|)^{-1/2},$$

$$N_{l2} \sim \text{constant}, \quad |\omega| \to \omega_{\max}, \quad c_5 < 0, \quad c_3 > 0. \tag{5.26b}$$

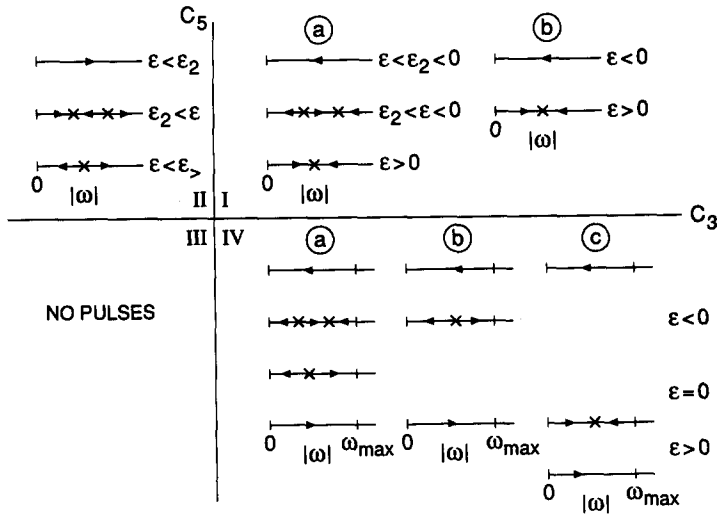

Fig. 9. Summary of possible scenarios for the existence and stability of pulses as determined by perturbing around the quintic-cubic Schrödinger equation (2.12). In each quadrant where pulses exist, a cross on the $|\omega|$ axis denotes a fixed point and an arrow the direction of the flow according to eq. (5.22).

Although it is straightforward to calculate the various terms in eq. (5.22) and obtain the dynamics of $\omega(T)$ in detail, this is not necessary to gain a qualitative understanding of the existence and stability of pulses in the various quadrants of the (c_3, c_5) plane discussed in section 3.3.3. Our aim is to describe the fixed-point structure of eq. (5.22) qualitatively as $\hat{\varepsilon} = \varepsilon/b_1$ varies, with $\hat{b}_3 = b_3/b_1 < 0$, $\hat{b}_5 = b_5/b_1 > 0$.

In quadrant I ($c_3 > 0$, $c_5 > 0$) we have $\partial_{|\omega|} N_{20} > 0$, so sgn $\partial_T|\omega| =$ sgn $\hat{\varepsilon}$ for $|\omega| \to 0$ and sgn $\partial_T|\omega| < 0$ for large $|\omega|$ when N_{60} dominates. This means that there is at least one fixed point for $\hat{\varepsilon} > 0$. For $\hat{\varepsilon} < 0$ there are either no fixed points (this is the case for large $|\hat{\varepsilon}|$) or a pair of fixed points[#15], one stable and one unstable, at $\hat{\varepsilon}_2 < \hat{\varepsilon} < 0$. The unstable fixed point goes to $\omega = 0$ at $\hat{\varepsilon} = 0$ and there is only the "stable" fixed point for $\hat{\varepsilon} > 0$. The two different scenarios are illustrated by a flow diagram in $|\omega|$ in fig. 9, and by a schematic bifurcation diagram for the pulse amplitude in fig. 10, where stable and unstable solutions are represented by solid and dashed lines, respectively. A similar analysis leads to the bifurcation diagrams shown in figs. 9 and 10 for quadrants II ($c_3 < 0$, $c_5 > 0$) and IV ($c_3 > 0$, $c_5 < 0$). (As shown in section 3.3.3 there are no unperturbed pulses in quadrant III.)

It should be clear from the above discussion that the stability we are establishing only refers to the particular class of perturbations compatible with the ansatz (5.5). Thus pulses are "stable" from this point of view for $\hat{\varepsilon} > 0$, even though it is clear that arbitrary perturbations about the $A = 0$ state will grow for $\hat{\varepsilon} > 0$ since this state is linearly unstable.

Let us ask whether we can draw any conclusions about front selection from the perturbation theory. We note first that since front solutions are not normalizable, a rigorous treatment must use the more general formalism mentioned above which involves solvability conditions. Furthermore, the analysis is complicated by the existence of at least two characteristic times in the evolution of $v(T)$, the relaxation time at the edge of the front and the diffusive time with which a perturbation changes the amplitude of the N state created by the front (see ref. [29]). We shall circumvent these difficulties by modifying the

[#15]Although we consider this unlikely, we have not been able to rule out the existence of more than one pair of fixed points.

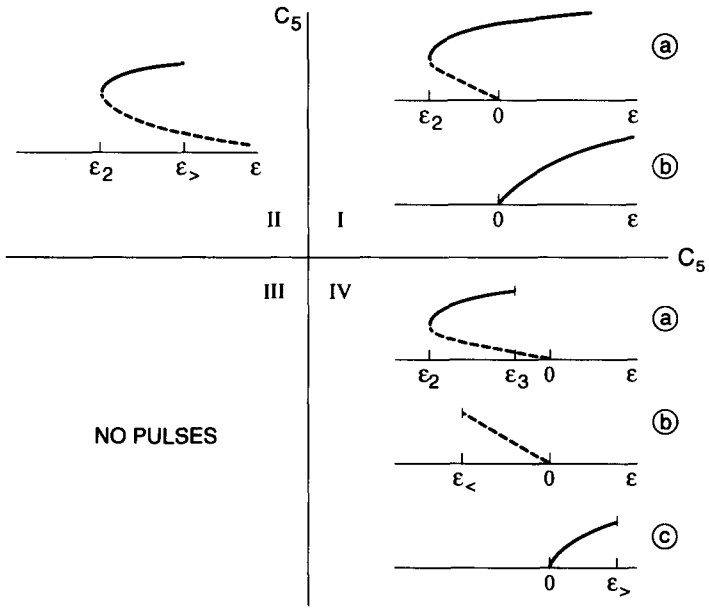

Fig. 10. Summary of the bifurcation structure of pulses as implied by the results of fig. 9. Dashed lines indicate unstable pulses within the dynamics of eq. (5.22), and solid lines stable pulses.

pulse perturbation theory to obtain a nonrigorous estimate of the front velocity in quadrant IV where a family of fronts (3.36) was found in the unperturbed system.

Let us take as our initial condition a pulse state made up of a positive and negative front (3.36) with velocities $\pm v_f$ (to be determined), the edges being placed at $x = \pm \frac{1}{2}L$, respectively (see fig. 11). This state is an approximate pulse solution with velocity $v_p = 0$, but with wavevectors $\pm q_N = \pm \frac{1}{2}v_f$ for $x \gtrless 0$, and a discontinuity in phase at $x = 0$. We now let this solution evolve according to eqs. (5.18), taking $\varepsilon_3 < \varepsilon < 0$ in scenario (a) of the fourth quadrant of figs. 9 and 10, with $\varepsilon \downarrow \varepsilon_3$. For $\varepsilon > \varepsilon_3$, the stable fixed point which exists for $\varepsilon < \varepsilon_3$, and for which $|\omega| \to \omega_{max}$ in the limit $\varepsilon \uparrow \varepsilon_3$, has just disappeared. Since for $\varepsilon \uparrow \varepsilon_3$ the shape of this pulse approaches that of two separate stationary fronts [see eq. (3.36)], for $\varepsilon > \varepsilon_3$ the pulse will develop into two fronts moving apart at a velocity which may be calculated as follows: We assume that the discontinuity at $x = 0$ remains localized, so for long times the frequency reaches ω_{max}, the amplitude reaches $a_N^2 = 3c_3/4|c_5|$ given in eq. (3.35), and the two fronts drift apart as the size $L(T)$ of the pulse grows. The evolution of this state can be estimated by calculating $\partial_T \mathcal{N}$ as in eq. (5.18b):

$$\tfrac{1}{2}\partial_T \mathcal{N} = \tfrac{1}{2}\partial_T N_{20} = -N_{02} + (\hat{\varepsilon} - q_f^2)N_{20} - \hat{b}_3 N_{40} - \hat{b}_5 N_{60}, \tag{5.27}$$

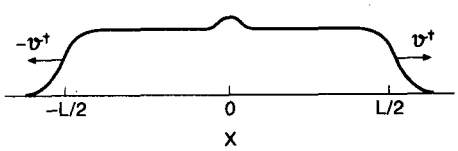

Fig. 11. Schematic sketch of the profile used to obtain the nonlinear front velocity $v^\dagger$ within the perturbation analysis.

where (for $c_3 = -c_5 = 1$)

$$N_{2l,0} = a_N^{2l} L(T) + \mathcal{O}(L^0), \tag{5.28a}$$

$$N_{02} = \mathcal{O}(L^0), \tag{5.28b}$$

$$q_f = \tfrac{1}{2} v_f, \qquad a_N^2 = \tfrac{3}{4}. \tag{5.28c}$$

For self-consistency we require a uniform growth of the pulse at the velocity $2v_f$, i.e.

$$\partial_T L(T) = 2v_f, \tag{5.29}$$

so eq. (5.27) yields

$$v_f = \left[\left(\hat{\varepsilon} - \tfrac{1}{4} v_f^2 \right) - \hat{b}_3 a_N^2 - \hat{b}_5 a_N^4 \right] L(T) + \mathcal{O}(L^0). \tag{5.30}$$

In order to cancel the term proportional to $L(T)$ we therefore determine the front velocity v_f to be given by

$$v_f^2 = 4\hat{\varepsilon} - 3\hat{b}_3 - \tfrac{9}{4}\hat{b}_5. \tag{5.31}$$

Let us now consider the nonlinear front (3.38) in this case ($c_1 = c_3 = -c_5 = 1$) expanded to lowest order in b_1. According to eq. (3.50) we find precisely

$$(v^\dagger)^2 = 4\hat{\varepsilon} - 3\hat{b}_3 - \tfrac{9}{4}\hat{b}_5 = v_f^2. \tag{5.32}$$

Thus for

$$\varepsilon > \varepsilon_3 = \tfrac{3}{4} b_3 + \tfrac{9}{16} b_5, \tag{5.33}$$

the perturbation theory leads to selection of a front with velocity v_f precisely equal to the velocity $v^\dagger$ of the nonlinear front given by the ansatz (3.38). In this way we have derived the nonlinear front selection of section 4.2 to lowest order in perturbation theory. A similar front selection phenomenon was found some years ago in the perturbed Sine–Gordon equation by McLaughlin and Scott [47].

Finally, let us comment briefly on the nearly real limit $|c_1| \ll 1$, where perturbation theory is also possible [29–31]. In particular, Malomed and Nepomnyashchy [30] have found a perturbative front solution (their "kink") near $\varepsilon = \varepsilon_1 = -3b_3^2/16b_5$, the point where the $a = 0$ and $a_{N0} = a_N(q_N = 0)$ solutions have the same "free energies" in the real case, and where $v^\dagger = 0$. For $0 < |c_1| \ll 1$, their velocity c (in their eq. (2.13)) agrees with $v^\dagger$, eq. (3.40b), (and with Klyachkin's [42] result) to $\mathcal{O}(c_i^2)$ and to lowest order in $\varepsilon - \varepsilon_1$. This calculation then gives ε_3 (where $v^\dagger = 0$) to $\mathcal{O}(c_i^2)$. For $0 < \varepsilon_3 - \varepsilon \ll 1$ they were able to construct a stable pulse solution whose width L diverges near ε_3. Specifically for the case $b_1 = -b_3 = 16b_5/3 = 1$, $c_1 = c_5 = 0$ they find

$$L \sim 4c_3^2 (\varepsilon_3 - \varepsilon)^{-1}.$$

These results are consistent with our conjectures and are qualitatively similar to those found in the Hamiltonian limit in scenario IV.a of fig. 10.

6. Numerical results

The rules formulated in section 4.2 as well as the results of the perturbation expansion in section 5 show that there is an intimate connection between the existence and stability of pulse solutions and the dynamics of fronts. A representative example for the complex equation (2.10) was already given in ref. [8], where with $b_1 = -b_3 = b_5 = 1$, $c_1 = -0.1$, $c_3 = 0.2$, $c_5 = 0.15$ the nonlinear front $v^\dagger$ exists, and its velocity $v^\dagger$ goes through zero at $\varepsilon_3 = -0.11$. Since, as discussed in section 3.3.1, $dv^\dagger/d\varepsilon > 0$, the front velocity $v^\dagger$ is positive for all $\varepsilon > \varepsilon_3$. In agreement with the rules formulated in section 4.2, it was found that localized or pulse-like initial conditions develop into two fronts that propagate out in opposite directions. For $\varepsilon_3 < \varepsilon < \varepsilon^\dagger$, the asymptotic front speed approached $v^\dagger$ given by eq. (3.40) with the predicted $q_N^\dagger$, while for $\varepsilon > \varepsilon^\dagger$ the front velocity approached the linear marginal stability velocity v^*. Moreover, stable pulse solutions were found in the finite interval $\varepsilon_2 < \varepsilon < \varepsilon_3$.

Equations (3.44) for the nonlinear front $v^\dagger$ show that the latter does not exist in all regions of parameter space. However, since ε only enters the expression for e_7, it is clear that if a nonlinear front exists for some $\varepsilon = \varepsilon'$, the equations can be solved for all $\varepsilon > \varepsilon'$. As a result, the existence of a nonlinear front in a certain region of parameter space is determined mainly by the c_i's and b_i's[#16], not so much by ε. We therefore plot in fig. 12 the behavior of $v^\dagger$ as a function of c_3 for two fixed values of ε. In both cases, the nonlinear front only exists over a finite range of c_3 values. Moreover, as illustrated in the figure, near the left edge of the range of existence, the nonlinear state $a_N^\dagger, q_N^\dagger$ is Benjamin–Feir unstable. This feature of the solution occurs frequently and it can be understood as follows: upon varying one of the c_i, the edge of the interval of existence is associated either with a point where two solutions of eq. (3.39) bifurcate [cf. eq. (3.44)] or where the solution on the upper branch ceases to exist. An example of the first mechanism occurs in fig. 12a and 12b on the right edge for $c_1 \approx 1.3$, and in this case the state $q_N^\dagger, a_N^\dagger$ at the bifurcation point need not be Benjamin–Feir unstable. In the other case, however, it is clear from eq. (3.39b) that at the point where the solution disappears $\varepsilon - b_1 q_N^2$ goes through zero, i.e. $q_N^\dagger$ coincides with the outer edge of the band of allowed wavenumbers, and hence is unstable. This happens at the left edge of the c_3 interval in fig. 12.

As the data points in fig. 12a illustrate, in the case $\varepsilon = -0.03$ localized initial conditions indeed evolve into fronts propagating with the nonlinear velocity $v^\dagger$, in the c_3-parameter range where $v^\dagger > 0$ and where the state $a_N^\dagger, q_N^\dagger$ is linearly stable. Moreover, outside the range of existence of nonlinear fronts, we observe stable $v = 0$ pulse solutions, as indicated by the crosses. As fig. 12b illustrates, for $\varepsilon = 0.03 > 0$ there are of course no stable pulse solutions, and one obtains fronts propagating with $v^\dagger$ or v^*, whichever is greatest, in agreement with our conjectures.

The open symbols in fig. 12 show that slightly beyond the point $c_3^{(BF)}$ where the state $a_N^\dagger, q_N^\dagger$ becomes Benjamin–Feir unstable, fronts still propagate with an average velocity close to $v^\dagger$. The behavior of the front velocity as a function of time for $\varepsilon = 0.03$, (with $c_3 = 0.1$ and $c_3 = 0.05$) is shown in fig. 13. In these examples, the velocity is measured at the point where the amplitude $a = 0.02$, and the velocity in these two cases is seen to be remarkably periodic; this was somewhat unexpected, since the Benjamin–Feir unstable state generated by the front eventually does lead to an irregular pattern. Presumably, the (nearly) periodic behavior of the front velocity is associated with the fact that at these parameter values the nonlinear state is only weakly unstable. By contrast, in fig. 14 we show a snapshot of a front for

[#16]Note that even if the equations can be solved for all $\varepsilon > \varepsilon'$, this does not imply $|\kappa^\dagger| > |\kappa^*|$, so the range over which the nonlinear front is selected will depend on ε.

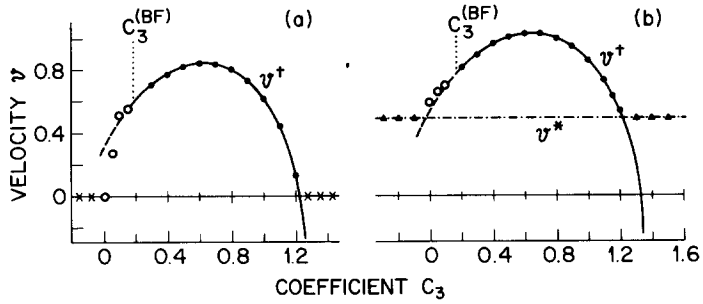

Fig. 12. Front velocity vs. parameter c_3 of the complex Ginzburg–Landau equation (2.10), for fixed $c_1 = 1$, $c_5 = -0.8$, and (a) $\varepsilon = -0.03$, (b) $\varepsilon = +0.03$. The velocity $v^\dagger$ obtained from the ansatz (3.38) is shown by the solid line, and the linear marginal stability velocity v^* is given by the dot-dashed line. For $c_3 < c_3^{(BF)}$ the nonlinear state $a_N^\dagger, q_N^\dagger$ produced by eq. (3.38) is Benjamin–Feir unstable. The symbols represent numerical solutions of eq. (2.10). Solid circles and triangles correspond to fronts with constant velocity, open circles are the average velocity of fronts with time-dependent velocity, and crosses indicate that pulses were formed. These results confirm the conjectures made in section 4.

different parameter values, leading to a strongly unstable state, and in this case the measured front velocity shown in fig. 14b is much more irregular.

The velocity as a function of time near the point where the front velocity crosses over from $v^\dagger$ to v^* in the case $\varepsilon = 0.03$ is shown in fig. 15 for the parameter values of fig. 12b and $c_3 = 1.3$ and 1.4. In these two cases, $v^* > v^\dagger$. Remarkably, however, we find that the front velocity initially oscillates around $v^\dagger$ (these oscillations are *not* associated with an instability behind the front, since the $q_N^\dagger, a_N^\dagger$ state at these parameter values is still linearly stable), but finally does approach v^*. The transient behavior is longer for the run in which c_3 is closer to the crossover value. In passing, we note that the long-time front velocity appears to approach v^* from *above* in fig. 15, in disagreement with the asymptotic behavior predicted by van Saarloos [11] and by Powell et al. [43], and observed in the nonlinear diffusion equation.

We now illustrate the fact that in regions of parameter space where there is no nonlinear front with $v^\dagger > 0$, the long-time dynamics depends sensitively on the initial conditions. Figure 16 shows a calculation for parameter values corresponding to the first quadrant of the (c_3, c_5) plane of fig. 8, which are far from those where a nonlinear front exists, and for which all uniform amplitude states are Benjamin–Feir unstable. As fig. 16a illustrates, a rather extended initial condition leads to a transient behavior reminiscent of a two-pulse solution. Eventually, however, it approaches a stable single pulse solution. In

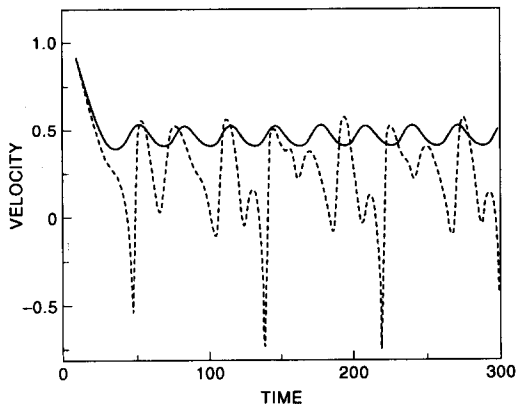

Fig. 13. Front velocity measured at the point where $a = 0.02$ for eq. (2.10) with $\varepsilon = -0.03$, $b_1 = 1$, $b_3 = -1$, $b_5 = 1$, $c_1 = 1$, $c_5 = -0.8$ and $c_3 = 0.1$ (solid line) and $c_3 = 0.05$ (dashed line). As shown in fig. 12a, at these values of c_3, $v^\dagger > 0$, but the state generated by the front is Benjamin–Feir unstable. The figure shows that the front velocity becomes time dependent, but the average velocity is relatively close to $v^\dagger$.

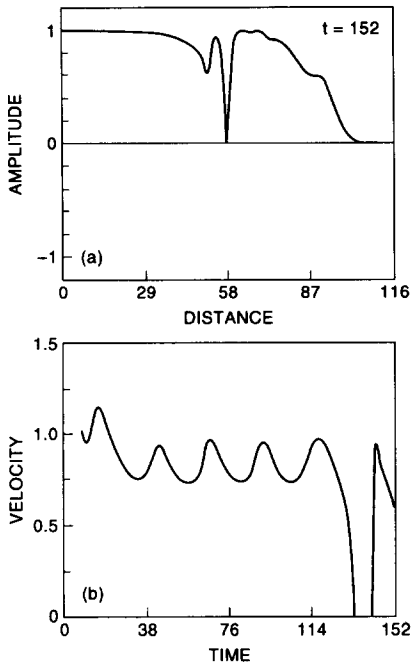

Fig. 14. Example of a chaotically propagating front for eq. (2.10) with $\varepsilon = 0$, $b_1 = -b_3 = b_5 = 1$, $c_1 = 1.25$, $c_3 = 0.375$, $c_5 = -1.25$. (a) The profile $a(x)$ for $t = 152$; (b) the front velocity measured at $a = 0.02$ as a function of time.

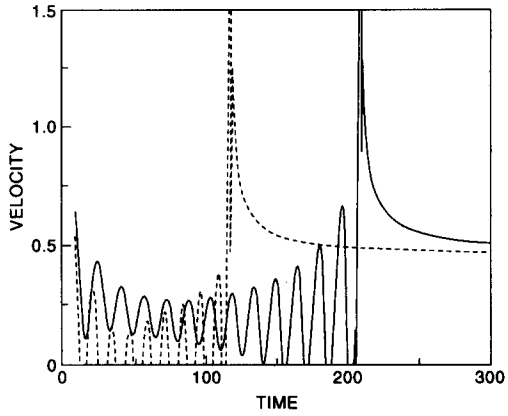

Fig. 15. Plot of the front velocity as a function of time for eq. (2.10) with $\varepsilon = 0.03$, $b_1 = -b_3 = b_5 = 1$, $c_1 = 1$, $c_5 = -0.8$ and $c_3 = 1.3$ (solid line), $c_3 = 1.4$ (dashed line). As fig. 12b shows, at these parameter values, $v^* > v^\dagger$. It is seen that the front velocity does indeed approach $v^* = 0.55$, but only after a relatively long transient.

fig. 16b, however, we show that starting with an even wider initial condition, the system does approach a stable bound state of two pulses at long times.

Deissler [48] has presented examples where smooth localized initial condition lead to chaotic dynamics in a localized region ("slugs"). Figure 17 shows that this behavior can coexist with stable pulse behavior for parameter values close to those of Deissler, at which all uniform amplitude states are strongly chaotic. (The pulse-like solution shown in fig. 17b at time 200 still has not fully relaxed, but we have checked that a stable pulse solution is approached eventually.)

We would expect that for arbitrary parameter values, chaotic "slugs" either shrink or spread. If they shrink, it means that these chaotic states are only transients, as they will evolve into either an $A = 0$ state or into (multiple) regular pulse solutions. If on the other hand they spread, they will eventually fill the whole system. We have performed a few exploratory runs that confirm this picture. In fig. 18 we show one example of a slug that dies away completely, as well as one obtained from a different initial condition, that settles into a stable pulse, for the same parameters as in fig. 17, except that ε was decreased to $\varepsilon = -0.02$. In these plots, we have used the quantity $\mathcal{N} = \int \mathrm{d}x\, |A|^2$ introduced in (3.1) to measure the size of the "slugs". In fig. 19, we show the same quantity at the larger value $\varepsilon = -0.005$ for the same initial conditions but with two different system sizes, $L = 300$ and $L = 600$. We used periodic boundary conditions and a pseudospectral code with 1024 and 2048 modes, respectively. It is seen that in each case, the chaotic regions spread till they fill the whole system, consistent with the fact that the long-time average value roughly doubles when the system size is doubled.

The above numerical results show evidence that stable pulses can coexist with spreading chaotic fronts. Although these findings do not contradict our rules and conjectures regarding the competition between

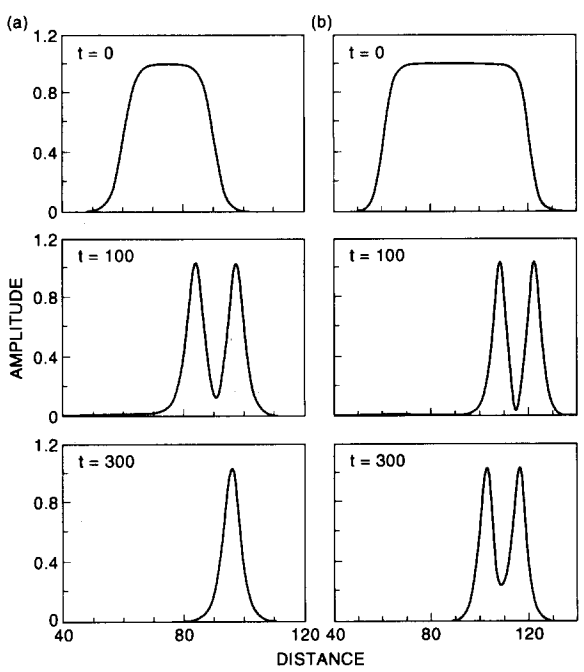

Fig. 16. Illustration of the dependence on initial conditions for eq. (2.10) with $\varepsilon = -0.03$, $b_1 = -b_3 = b_5 = 1$, $c_1 = 1.4$, $c_3 = 0.33$, $c_5 = 0.36$. For these parameter values, all uniform amplitude states are Benjamin–Feir unstable, and there is no nonlinear front (keeping all other parameters fixed, there is a nonlinear front for $-1.57 < c_3 < 0.15$). (a) The initial condition

$$A = \tfrac{1}{4}\exp(iqx)\left[1 + \tanh\left(\tfrac{1}{4}(x - x_1)\right)\right]\left[1 - \tanh\left(\tfrac{1}{4}(x - x_2)\right)\right]$$

with $q = 0.15$, $x_1 = 60$, $x_2 = 90$, goes through a transient solution reminiscent of a two-pulse state, but eventually evolves into a single pulse solution. (b) An initial condition of the same form with $x_1 = 60$, $x_2 = 120$ evolves into a two-pulse state. Similar behavior has been observed for $c_1 = 0.5$, $c_3 = 0.5$, $c_5 = 0.5$.

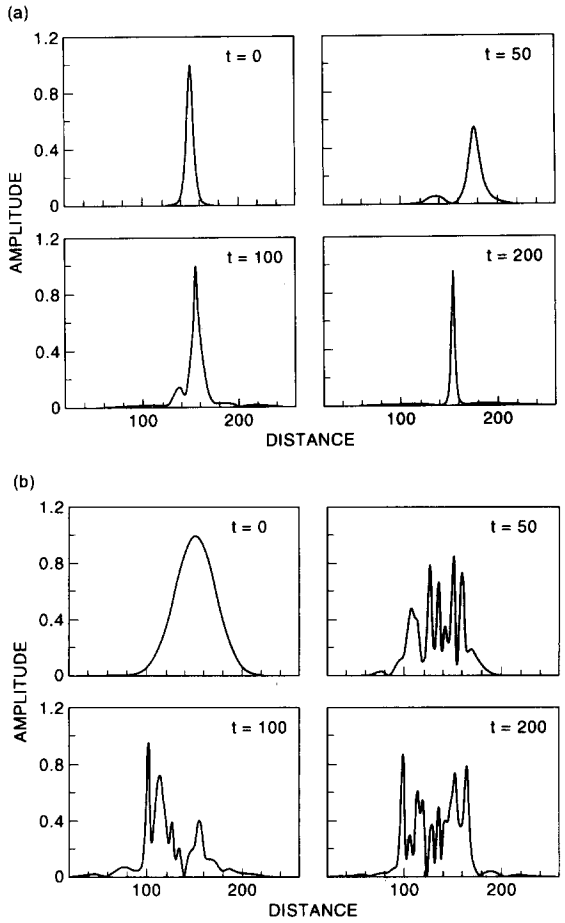

Fig. 17. Illustration of the dependence of the final state on initial conditions. For these runs $b_1 = -b_3 = b_5 = 1$, $\varepsilon = -0.01$, $c_1 = -2.2$, $c_3 = -0.5$, $c_5 = -2$ in eq. (2.10). These values are close to those of Deissler (fig. 8, ref. [48a]), corresponding to $\varepsilon = -0.0125$, $c_1 = -2.5$ and all other parameters the same. (a) The initial condition $\cosh^{-1}[\frac{1}{3}(x - 150)]\exp(iqx)$ with $q = 0.15$ converges to a single pulse. (b) The initial condition $\exp[iqx - ((x - 150)/\Delta x)^2]$ with $q = 0.15$ and $\Delta x = 30$ leads to chaotic behavior similar to that seen by Deissler.

pulses and fronts, the spreading of the chaotic fronts cannot be studied with the methods developed in this paper.

In section 4.2, we showed that for $\varepsilon > 0$ but small, there are large regions of parameter space where the linear marginal stability fronts cannot be uniformly translating in the quintic equation (2.10). The runs shown in figs. 17–19 were carried out in regions of parameter space where all nonlinear amplitude states a_N are strongly Benjamin–Feir unstable, and they therefore lead to chaotic behavior. For $c_1 > 0$, $c_3 < 0$, $c_5 < 0$, however, (i.e. in the third quadrant of the (c_3, c_5) plane of fig. 8) most nonlinear states are Benjamin–Feir stable. To explore the behavior of nonuniformly translating linear fronts in this regime

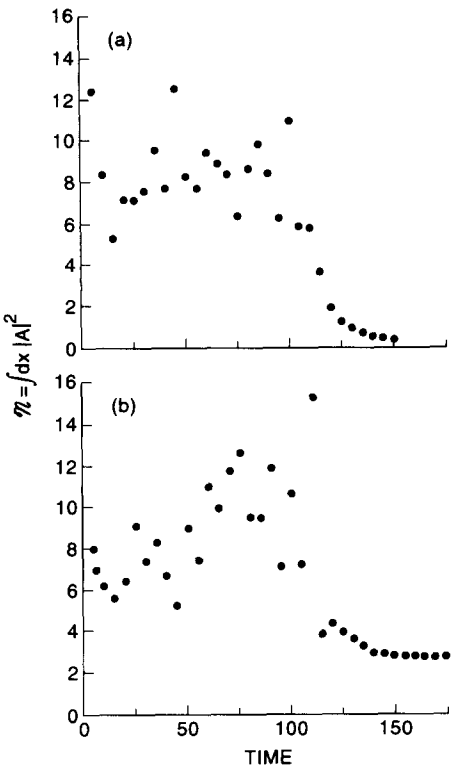

Fig. 18. Examples of chaotic transients that (a) die away ($A \to 0$ for all x) or (b) evolve into a stable pulse solution. In these plots, instantaneous values of $\mathcal{N} = \int dx\,|A|^2$ are shown for times $t = 5, 10, \ldots$, and the runs were made with the same parameter values as in fig. 17, except that $\varepsilon = -0.02$. The initial conditions were in both cases a Gaussian, as in fig. 17a, corresponding to $\mathcal{N}(t=0) = (\frac{1}{2}\pi)^{1/2}\Delta x$. (a) $q = 0.15$, $\Delta x = 20$ and $\mathcal{N}(t=0) = 25.07$; (b) $q = 0.15$, $\Delta x = 15$ and $\mathcal{N}(t=0) = 18.8$. Note that the initial condition with the smaller value of $\mathcal{N}$ leads to a stable pulse of size $\mathcal{N} = 2.8$.

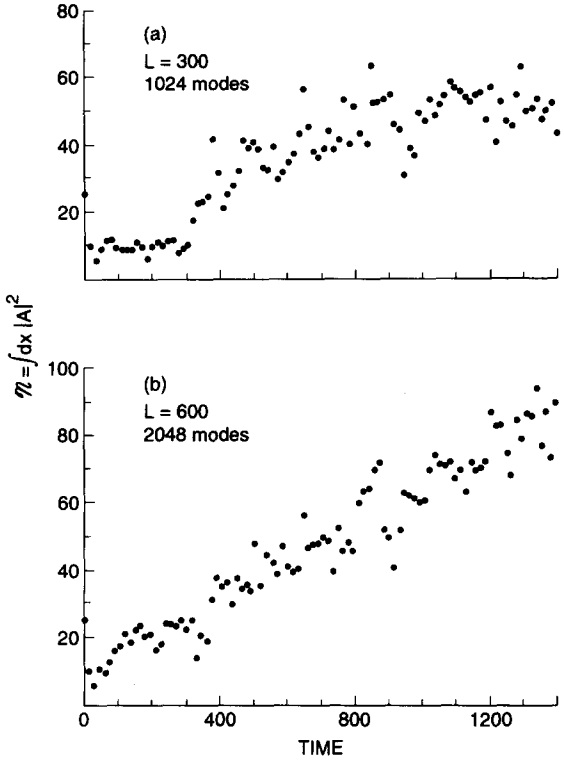

Fig. 19. Instantaneous values of $\mathcal{N} = \int dx\,|A|^2$ as a function of time for $\varepsilon = -0.005$ but otherwise the same parameters as in fig. 18. We used a pseudospectral code with 1024 modes and system size $L = 300$ in (a), and 2048 modes and $L = 600$ in (b). The initial conditions were a Gaussian as in fig. 17 with $q = 0.15$ and $\Delta x = 20$. This corresponds to $\mathcal{N}(t=0) = 25.07$. In part (a) the slug fills the whole system around a time of order 800. For $t \gtrsim 800$, $\mathcal{N}$ fluctuates around an average value of about 50. For part (b) with a system that is twice as long, the slug continues to spread. We have checked that in this case, the average of $\mathcal{N}$ saturates at a value of about 100 for $t \gtrsim 1600$.

we have carried out some runs for $b_1 = -b_3 = b_5 = c_1 = -c_3 = -c_5 = 1$ and $\varepsilon = 0.25$. It is easy to check that for these parameter values eqs. (4.9) have no solution. In fig. 20, we show snapshots of the resulting front at times $t = 100$, 150 and 200. It is seen that the front profiles consist of six regions: (i) a leading edge whose velocity approaches the marginal stability value $v^* = \sqrt{2}$ from below, roughly in agreement with the predictions of ref. [11]; (ii) a strongly nonlinear region where "space-time defects" (i.e. instantaneous zeroes of a) are created, at a rate of about 0.7 per unit of time; (iii) a region where both a and q are slowly varying functions of x, and where defects occur; (iv) a front propagating to the right into the slowly modulated state with speed $v \simeq 0.53$; (v) a well-defined nonlinear state a_N; and finally (vi) a region associated with our boundary condition at $x = 0$. Note that since the front (iv) propagates with a speed less than v^*, both regions (iii) and (v) are expanding. Because the generation of defects creates phase jumps we see no way of predicting the properties of region (v) from the linear marginal stability values that characterize region (i). Nevertheless, runs carried out with a number of different

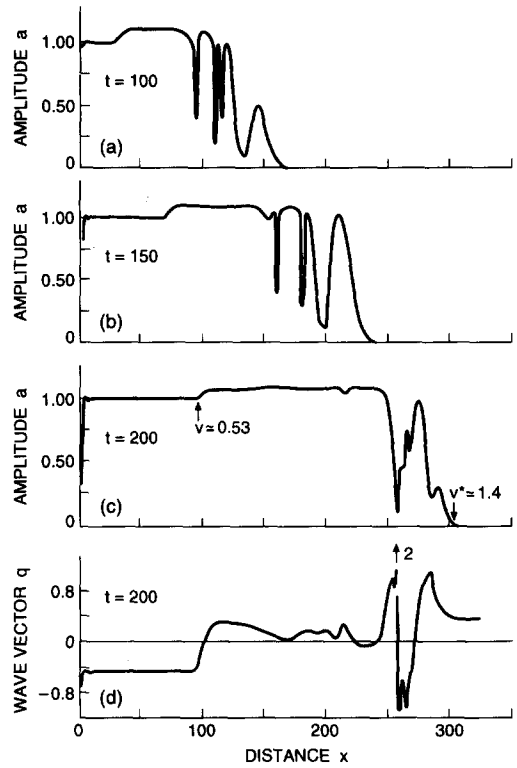

Fig. 20. Snapshots of a propagating front for $\varepsilon = 0.25$ and $b_1 = -b_3 = b_5 = c_1 = -c_3 = -c_5 = 1$ at times (a) $t = 100$, (b) $t = 150$ and (c) $t = 200$. The steep local minima in the profile result from space–time defects that have just been generated or that are about to occur. For $t = 200$ the local wavevector $q(x)$ is also shown in (d). The profile contains a front propagating with the predicted linear marginal stability velocity $v^* = 1.4$ in the leading edge ($x \gtrsim 300$), as well as a front propagating with velocity $v = 0.53$ in the nonlinear regime. We have no way of predicting this latter velocity theoretically.

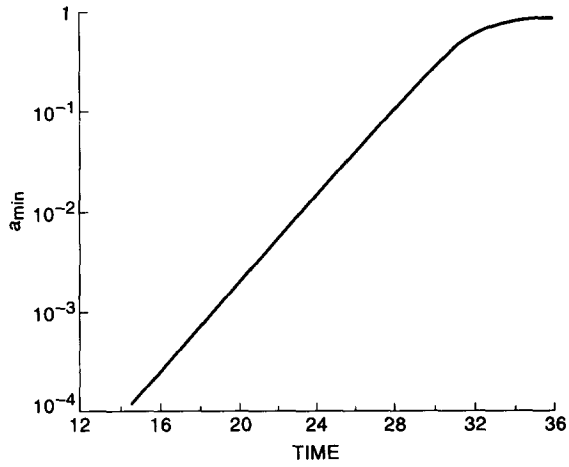

Fig. 21. Plot of the minimum amplitude a_{min} as a function of time in numerical integration of eq. (2.10) in the cubic case with $b_5 = c_5 = 0$, $\varepsilon = b_1 = b_3 = 1$, $c_1 = 0.3$ and $c_3 = -0.4$. The source solution eq. (3.57) of Nozaki and Bekki [25b] for which $a_{min} = 0$ was taken as initial condition. The exponential increase of a_{min} shows that this solution is linearly unstable. The simulations were performed with a pseudospectral code with 1024 modes, and the length L of the system was $L = 160$.

initial conditions (Gaussians with different widths) all lead to the same state in region (v). Hence it appears that the state in this region is uniquely selected.

We may point out that Powell et al. [43] attribute special dynamical significance to front profiles with zeroes that persist in time. In all our simulations, however, we observe front profiles that either have no zeroes, or that have zeroes associated with space-time defects, i.e. only at isolated points in time.

The stability of the source solutions (3.58) and (3.60) has very recently been investigated by Sakaguchi [49]. An isolated $v = 0$ source solution given by eq. (3.58) can be unstable in at least two ways: (i) The wave number q_N given by eq. (3.58d) can be Benjamin–Feir unstable. However, since these solutions are sources, small perturbations that grow due to the Benjamin–Feir instability propagate away from the core where $a \to 0$, and thus do not necessarily destroy the solution in this region. (ii) The core region itself can be unstable. One way in which this can happen, observed by Sakaguchi [49], is that the stationary source moves away, i.e. it becomes a propagating source solution (3.60). Another mechanism that we have found numerically, is that the minimum value a_{min} ($a_{min} = 0$ for the solution (3.58)) remains

essentially stationary, but grows exponentially in time (see ref. [50]). In fig. 21, we illustrate this for the supercritical case $b_1 = b_3 = 1$, $c_1 = 0.4$, $c_3 = -0.3$, $b_5 = c_5 = 0$. We see that $a_{\min}$ grows exponentially till it reaches a value of order unity, after which the solution relaxes to a uniform amplitude state $a = a_N$, $q = q_N$, $\kappa = 0$. (Note that since the Nozaki–Bekki source (3.58) has a wavevector q_N for $x \to \infty$ and a wavevector $-q_N$ for $x \to -\infty$, an additional structure has to be included in the initial conditions in order that the solution satisfies periodic boundary conditions. In our runs this was done by an additional sink structure a distance $x \approx \frac{1}{2}L = 80$ away from the source. This sink connects the q_N and $-q_N$ states and gives rise to a corresponding phase shift. We have checked that the presence of the sink does not perturb the source during the length of the simulations.) According to Sakaguchi [49a] there is actually a small region of parameter space for $c_1 c_3 < 0$ [near the line $c_1 = \frac{1}{2}(c_3 - 1)$] where the $v = 0$ sources are stable. Clearly, the phase diagram of both the stationary and the moving source solutions is extremely rich, and much further work is needed[#17].

Moreover, since the solution (3.58) is the extension of the fundamental dark soliton to the case $\varepsilon, b_1, b_3 > 0$, it would be interesting to explore[#17] the stability of stationary as well as moving sources perturbatively for $\varepsilon, b_1, b_3 \ll 1$.

We now wish to test the assertion, made in section 4, that the nonlinear front is selected only if $v^\dagger > v^*$ *and* $|\kappa^\dagger| > |\kappa^*|$. As a first example we consider the front solution (3.47) of Nozaki and Bekki [25b], which exists for $\varepsilon > 0$ in the case of a supercritical bifurcation. This front always turns out to have $|\kappa^\dagger| < |\kappa^*|$, but $v^\dagger$ is sometimes greater and sometimes less than v^*. According to our simulations, however, in all cases the asymptotic front velocity was v^*, in agreement with condition (4.14). Another example concerns the behavior of $v^\dagger$ for $\varepsilon \gg \varepsilon^\dagger$. It turns out that although for $\varepsilon \gtrsim \varepsilon^\dagger$ we have $v^\dagger < v^*$ (see fig. 7a), at very large values of ε there can be another crossing when $v^\dagger > v^*$, in which case one always has $|\kappa^\dagger| < |\kappa^*|$ (a similar behavior occurs in the real case for all $\varepsilon > \varepsilon^\dagger$; see ref. [11]). We have carried out a simulation of eq. (2.10) in the subcritical case with $b_1 = -b_3 = b_5 = 1$, $c_1 = -0.1$, $c_3 = 0.2$, $c_5 = 0.15$, $\varepsilon = 100$, for which $|\kappa_L^*| = 9.95$, $|\kappa_L^\dagger| = 5.98$, $v^* = 20.40$ and $v^\dagger = 22.61$, and found once again it is v^* and not $v^\dagger$ that is selected, in agreement with the criterion (4.14).

7. Conclusion

In this paper we have attempted a comprehensive analysis of coherent structure solutions of the one-dimensional complex Ginzburg–Landau equation, and a partial analysis for generalizations of that equation. There is an enormous literature covering such solutions, which we have tried to summarize, clarify and extend. Our primary result concerns the selection problem posed by the multiplicity of available solutions; we have formulated it as a set of conjectures regarding front/pulse competition, which reduce to previously known results in special cases. We have tested and verified the conjectures by numerical calculations and analytical perturbation theory for the complex Ginzburg–Landau equation.

Our primary focus has been on the behavior near subcritical bifurcations in order to elucidate the relation between front propagation and the existence of pulse solutions. In ref. [11], one of us conjectured that if the bifurcation is subcritical, front propagation into unstable states for $0 < \varepsilon \ll 1$ will be governed by nonlinear fronts, while near a supercritical bifurcation, front propagation is governed by linear marginal stability. This conclusion was based on the analysis of real equations of the form (2.66). Our present work on the complex Ginzburg–Landau equation requires us to rephrase these conjectures in the following way: In the case $b_3 > 0$, corresponding to a supercritical bifurcation, we have found no

[#17]The stability of source and sink solutions has recently been studied in the subcritical case [51].

nonlinear fronts (3.38) that satisfy (4.14). Thus, according to our rules and the result (4.11), the selected front above a supercritical bifurcation will indeed be a uniformly translating solution propagating with the linear marginal stability velocity v^*, as envisaged in ref. [11]. Now consider the case of a subcritical bifurcation, $b_3 < 0$. If a nonlinear front exists with $v^\dagger(\varepsilon = 0) > 0$, our conjectures imply that front propagation near $\varepsilon = 0$ will indeed be governed by this nonlinear front, and we will have $\varepsilon_3 < 0$. The new features not anticipated in ref. [11] are: (a) the nonlinear front does not necessarily exist. In this case the front dynamics (if fronts are created!) is still an open question. (b) Even if the nonlinear front exists but if it has $v^\dagger(\varepsilon = 0) < 0$, then $\varepsilon_3 = 0$ and we do not obtain fronts propagating into the $A = 0$ state. For $\varepsilon > 0$, fronts do propagate, though *not* with the velocity $v^\dagger < 0$; instead they have the linear marginal stability velocity v^*. Note that even though these fronts give rise to a finite amplitude state a_N^* (see fig. 7), they are extremely wide for small ε since according to eq. (4.8b) $|\kappa_L| \sim \sqrt{\varepsilon}$. Whether the linear fronts are uniformly translating or not depends on the parameters $\{\varepsilon, c_i\}$ in a known way, as illustrated in fig. 8.

The distinction between subcritical and supercritical bifurcations is made on the basis of the bifurcation behavior of the uniform amplitude solution $a_{N0} = a_N(q_N = 0)$. Whether or not stable pulses exist depends directly on whether this bifurcation is subcritical or supercritical. For front propagation, on the other hand, our results show that in the parameter ranges where there is no nonlinear front or where $v^\dagger(\varepsilon = 0) < 0$, the dynamical distinction between supercritical and subcritical bifurcations becomes less sharp. We will return to this question in section 7.2.

7.1. *Comparison with experiment*

Coherent structures have been observed experimentally in a number of systems with oscillatory dynamics, e.g. binary-fluid convection, [2] Taylor–Couette flow [4, 5], parametric waves in fluids [3], plane Poiseuille flow [20], optical waveguides [6] and oscillatory chemical reactions [7]. Amplitude equations in the form of Ginzburg–Landau models can be derived for most of these systems by expanding the basic equations near the threshold for the oscillatory instability. It is well known, however, that in many cases of experimental interest the states of the system lie outside the domain of applicability of the amplitude expansion, either because the bifurcation is subcritical with stabilization far from the linear instability, or because of the existence of "parasitic" small parameters that invalidate the expansion. Examples of the latter are the ratio of the mass diffusion and thermal diffusion coefficients called the Lewis number $\mathscr{L}$ in binary-fluid convection [52] (for that case both of the above mechanisms are operative!), or the ratio τ_1/τ_2 of the characteristic time scales of activator and inhibitor in oscillatory chemical reactions [7]. Even in cases where one might hope to have a controlled amplitude expansion, precise and controlled experiments on complicated time-dependent states are difficult to carry out, so there is not at present a body of relevant experimental data which one could hope to explain quantitatively by our theoretical model.

Under these circumstances we may ask whether we can understand the *qualitative* or semiquantitative aspects of the experiments. Apart from the very existence of pulse-like states in many of these systems, the most detailed and varied observations have been made in binary-fluid convection where pulses, fronts, sources and sinks have been reported [2]. An important aspect of this system, of course, is that it has a basic pattern with nonzero wavevector q_0 (type I_o in the classification of Cross and Hohenberg [1]), so that the simplest amplitude equation has the coupled form [53]

$$\partial_t A_R - s_0 \partial_x A_R = \varepsilon A_R + (1 + ic_1)\partial_x^2 A_R - (b_3 - ic_3)|A_R|^2 A_R + (b_2 + ic_2)|A_L|^2 A_R, \tag{7.1a}$$

$$\partial_t A_L + s_0 \partial_x A_L = \varepsilon A_L + (1 + ic_1)\partial_x^2 A_L - (b_3 - ic_3)|A_L|^2 A_L + (b_2 + ic_2)|A_R|^2 A_L, \tag{7.1b}$$

for right- and left-traveling waves. If one assumes that in the absence of wall reflection it is sufficient to consider a single direction of propagation (i.e. $A_L \equiv 0$), one is still left with an equation with the convective term $s_0 \partial_x A$. If this term is alone, as in eq. (7.1a) with $A_L = 0$, we can eliminate it by a Galilean transformation, but if $A_L \neq 0$, or if the nonlinear term $s_2 \partial_x(|A|^2 A)$ is added to eq. (7.1) (as it should in general), then we can expect the convective nature of the linear instability [53, 54] to have important physical consequences. Moreover, even in the absence of the nonlinear s_2 term the $s_0 \partial_x A$ term cannot be transformed away in *a finite* nonperiodic system.

With these caveats, let us ask how much of the behavior of pulses and fronts in one-dimensional binary-fluid convection experiments we can account for qualitatively by our model. The experimental detection of stationary pulses is an apparent confirmation of the theory, but of course it contradicts the predictions of eq. (2.10), since that equation refers to the frame moving with velocity s_0 rather than the lab frame. Thus according to eq. (2.10) pulses should move with velocity $-s_0$ in the lab frame. To account for the observations we invoke first geometrical imperfections which, as demonstrated by Kolodner [55], lead to trapping of the pulses near regions where the local velocity vanishes. This interpretation implies a nonzero pulse velocity $v_p(\varepsilon)$ in an ideal system, which one might try to explain [44] by appeal to the nonlinear term $s_2 \partial_x(|A|^2 A)$ added to eq. (7.1), using the arguments of section 5.2. From a qualitative point of view what needs explanation is the fact that for all experiments $v_p(\varepsilon) \ll |s_0|$, whereas the arguments of section 5.2 only say that in general $v_p(\varepsilon) \neq -s_0$.

The observation of stable pulses for $\varepsilon > 0$ is more problematical [2]. According to our hypotheses these should be destabilized by two different mechanisms. First of all by a positive front (either $v^\dagger$ or v^*) which leads to the spreading of the pulse. As the discussion of section 4.2 shows, unless the nonlinear dispersion terms nearly balance, we expect stable pulses to exist up to $\varepsilon_3 = 0$. For $\varepsilon > 0$, v^* will then be selected. A possible way in which the spreading might be inhibited if indeed v^* is selected, arises through finite-size effects, since the width of the linear front is large for small ε [$|\kappa_L^*| \sim \varepsilon^{-1/2}$ according to eq. (4.8b)]. The second mechanism for destabilizing pulses is the linear instability of the $A = 0$ state for $\varepsilon > 0$. Here again in a finite system, the convective nature of that instability might suppress its effects since disturbances do not grow large enough in an annulus before they are reabsorbed by the pulse [55]. This latter explanation, of course, hinges on the fact that pulses move with a velocity different from the group velocity s_0 of linear disturbances, so in order to substantiate it the nonlinear term $s_2(\partial_x|A|^2 A)$ must be taken into account. As noted in section 4.4 this term can be included in the analysis of the nonlinear fronts, but its effect on pulses can so far only be studied with the perturbative methods of section 5. In any event, the observation by Niemela et al. [2] that the exact pulse solution (3.51) fits their data, cannot at present be regarded as a quantitative confirmation of the theory.

The observation of stationary front pairs (Kolodner et al., Bensimon et al. [2]) has similar problems. If we assume that they are trapped by imperfections (contrary to the original interpretation given by the experimenters), we still need to understand how a front pair with equal and opposite q_N can be selected at the same value of ε (no source or sink was observed between the fronts). Here again, it seems to us likely that a qualitative understanding of the observations will have to take into account the nonlinear convective term [44] more explicitly.

7.2. *Open theoretical problems*

The most straightforward question we have not answered concerns the detailed behavior of the perturbation equations (5.20) for pulses near the generalized derivative Schrödinger limit. Since we have

not explicitly evaluated the nonlinear front solution (3.38) for that model, the detailed behavior for $\varepsilon > \varepsilon_3$ remains open, as does the bifurcation diagram for pulses as a function of ε, analogous to fig. 10. In particular, it would be interesting to find a case where the perturbation equations (5.20) lead to a limit cycle, and to simulate the full PDE near that limit. Would the system show oscillatory pulses, or is this an indication of some other behavior? An analogous situation was found for reaction-diffusion systems in ref. [46].

We also note that in the quintic-cubic Schrödinger equation (2.12) there are no pulse solutions in the third quadrant $c_3 < 0$, $c_5 < 0$ (with $c_1 > 0$) of figs. 4 and 9. Moreover, as fig. 8 illustrates, in the subcritical case $b_3 < 0$ nonlinear front solutions can only be found in the second and fourth quadrants of the (c_3, c_5) plane. Since there are no exact pulse solutions of the form (3.51) either [cf. fig. 5], we have at present no analytical information on the dynamics in this parameter range. Furthermore, we have found that even for $b_1 = -b_3 = b_5 = 1$ the range of existence of a nonlinear front with $v^\dagger > 0$ is concentrated near the plane $c_3 = -c_5$ in the $\{c_1, c_3, c_5\}$ parameter space. As discussed above, a partial cancellation of the nonlinear dispersion terms tends to favor nonlinear front propagation.

As we have pointed out in section 6, the behavior of both the stationary and the moving source solutions of Bekki and Nozaki [26] appears to be extremely rich. These solutions will have to be studied in more detail, both analytically, e.g. by perturbing around the dark soliton solutions, and numerically. Also, the very existence of a family of source solutions and its relation to symmetry properties deserve further study.

Another open problem concerns the asymptotic approach to the front velocity v^* in the linear marginal stability regime. According to the predictions of van Saarloos [11, 14] and Powell et al. [43], the front velocity should approach v^* from *below*. Numerical simulations for real equations of the form (2.66) are consistent with these results. Our simulations of the complex Ginzburg–Landau equation shown in fig. 15, however, indicate that here v^* is approached from *above*. A more detailed investigation of the asymptotics is clearly necessary, but we stress that all results on this and other models known to us are consistent with the conjecture that the asymptotic front speed is always larger than or equal to v^*. Such a result is also suggested by the intuitive arguments of ref. [11], though a more rigorous derivation is certainly desirable.

Since the selection problem for the complex Ginzburg–Landau model (2.10) is still only partially elucidated in parameter regions where there is no selected front, we have no general guidelines to help us understand whether a given initial condition will lead to a localized or extended state, and whether the solution will be regular or chaotic in those parameter regions. Generalizations to higher-order equations such as the Swift–Hohenberg model or more complicated models without a Lyapunov function would also be desirable, but from the work of Collet and Eckmann [56], Eckmann and Procaccia [57], and Aranson et al. [33] we know that the behavior can be quite rich indeed, and it is not clear whether the concepts we have developed will be useful in pursuing these questions. Finally, the corresponding problems in two and higher spatial dimensions [58] pose even greater challenges for the years ahead.

Acknowledgements

We wish to thank M.C. Cross for informative comments and discussions. P.C. Hohenberg acknowledges the hospitality of the Lorentz Institute, University of Leiden, where part of this work was carried out.

Appendix. Signs of the real parts of the roots of a cubic equation

In the study of stability properties, one often needs to know the signs of the real parts of the roots of a cubic equation. If the cubic equation is written as

$$\lambda^3 + \alpha\lambda^2 + \beta\lambda + \gamma = 0, \tag{A.1}$$

the signs of the real parts of the roots are given by

$$\text{For} \quad \gamma > 0 \quad \begin{cases} \text{if} \quad \alpha > 0 \quad \text{and} \quad \alpha\beta - \gamma > 0: \; - - -, & \text{(A.2a)} \\ \text{otherwise:} \qquad\qquad\qquad\quad + + -. & \text{(A.2b)} \end{cases}$$

$$\text{For} \quad \gamma < 0 \quad \begin{cases} \text{if} \quad \alpha < 0 \quad \text{and} \quad \alpha\beta - \gamma < 0: \; + + +, & \text{(A.2c)} \\ \text{otherwise:} \qquad\qquad\qquad\quad + - -. & \text{(A.2d)} \end{cases}$$

These formulas can, of course, be obtained from the well-known explicit expressions for the roots of a cubic equation [59]. More direct proofs of (A.2a) (and hence also (A.2c)) are, e.g. given by Pontrjagin [60] and Suter [61], and the other two results (A.2b) and (A.2d) then follow immediately from the fact that the product of the three roots of (A.1) is equal to $-\gamma$.

The above formulas can also be obtained directly by noting that (A.1) is equivalent to

$$(\lambda + a)(\lambda^2 + b\lambda + c) = 0, \tag{A.3}$$

with

$$\alpha = a + b, \qquad \beta = ab + c, \qquad \gamma = ac. \tag{A.4}$$

Consider e.g. the case $\gamma > 0$, so that we can either have $a < 0$, $c < 0$ or $a > 0$, $c > 0$. For $c < 0$, the quadratic form in (A.3) always has one root with a positive real part and one with a negative real part. Thus the structure of the case $a < 0$, $c < 0$ is always $(+ + -)$. When $a > 0$, $c > 0$, we see that for $\beta = ab + c < 0$ we necessarily have $b < 0$, and hence a $(+ + -)$ structure, while for $\beta > 0$ we have $\text{sgn}(\alpha\beta - \gamma) = \text{sgn}[b(a^2 + \beta)] = \text{sgn}\, b$, and so a $(- - -)$ structure for $\alpha\beta - \gamma > 0$ and a $(+ + -)$ structure for $\alpha\beta - \gamma < 0$. Thus, for $\gamma > 0$, the structure is always $+ + -$ except when both $\beta > 0$ and $\alpha\beta - \gamma > 0$. This is equivalent to the condition (A.2a, b).

References

[1] M.C. Cross and P.C. Hohenberg, in: Fluctuations and Stochastic Phenomena in Condensed Matter, ed. L. Garrido (Springer, New York, 1987); Rev. Mod. Phys., to be published.

[2] P. Kolodner, D. Bensimon and C.M. Surko, Phys. Rev. Lett. 60 (1988) 1723; D. Bensimon, P. Kolodner, C.M. Surko, H. Williams and V. Croquette, J. Fluid Mech. 217 (1990) 441;
E. Moses, J. Fineberg and V. Steinberg, Phys. Rev. A 35 (1987) 2757;
J.J. Niemela, G. Ahlers and D.S. Cannell, Phys. Rev. Lett. 64 (1990) 1365;
K.E. Anderson and R.P. Behringer, Phys. Lett. A 145 (1990) 323;
P. Kolodner and J.A. Glazier, Phys. Rev. A 42 (1990) 7504.

[3] J. Wu, R. Keolian and I. Rudnick, Phys. Rev. Lett. 59 (1987) 2744;
S. Douady, J. Fluid Mech. 221 (1990) 383.
[4] J.J. Hesgeth, C.D. Andereck, F. Hayot and Y. Pomeau, Phys. Rev. Lett. 62 (1989) 257.
[5] G. Ahlers and D.S. Cannell, Phys. Rev. Lett. 50 (1983) 1583;
M. Niklas, M. Lücke and H. Müller-Krumbhaar, Phys. Rev. A 40 (1989) 493.
[6] A. Hasegawa, Optical Solitons in Fibers (Springer, New York, 1989);
J.V. Moloney and A.C. Newell, Physica D 44 (1990) 1.
[7] S.L. Müller, T. Plesser, and B. Hess, Science 230 (1985) 661;
W.Y. Tam, W. Horsthemke, Z. Noszticzius and H.L. Swinney, J. Chem. Phys. 88 (1988) 3395;
G.S. Skinner and H.L. Swinney, Physica D48 (1991) 1;
J.J. Tyson and J.P. Keener, Physica D 32 (1988) 327; J.P. Keener and J.J. Tyson, Physical D 21, (1986) 307.
[8] W. van Saarloos and P.C. Hohenberg, Phys. Rev. Lett. 64 (1990) 749.
[9] E. Ben-Jacob, H.R. Brand, G. Dee, L. Kramer and J.S. Langer, Physica D 14 (1985) 348;
G. Dee and J.S. Langer, Phys. Rev. Lett. 50 (1983) 383.
[10] J.S. Langer, in: Chance and Matter, eds. J. Souletie, J. Vannimenus and R. Stora (North-Holland, Amsterdam, 1987) p. 629.
[11] W. van Saarloos, Phys. Rev. A 37 (1988) 211; 39 (1989) 6367.
[12] A. Bers, in: Handbook of Plasma Physics, eds. M.N. Rosenbluth and R.Z. Sagdeev (North-Holland, Amsterdam, 1983) Vol. 1;
P. Huerre, in: Instabilities and Nonequilibrium Structures, eds. E. Tirapegui and D. Villarroel (Reidel, Dordrecht, 1987) p. 141; in: Propagation in Systems Far From Equilibrium, eds. J.E. Wesfreid, H.R. Brand, P. Manneville, G. Albinet and N. Boccara (Springer, New York, 1988) p. 340.
[13] E.M. Lifshitz and L.P. Pitaevskii, Physical Kinetics, Course of Theoretical Physics (Pergamon, New York, 1981) Vol. 10, Chap. VI.
[14] W. van Saarloos, in: Nonlinear Evolution of Spatio Temporal Structures in Continuous Media, eds. F.H. Busse and L. Kramer (Plenum, New York, 1990) p. 499.
[15] A.C. Newell, Rocky Mountain J. Math. 8 (1978) 25;
Y.S. Kivshar and B.A. Malomed, Rev. Mod. Phys. 61 (1989) 763.
[16] B.A. Malomed, Physica D 29 (1987) 155.
[17] C. Elphick and E. Meron, Phys. Rev. A 40 (1989) 3226; Phys. Rev. Lett. 65 (1990) 2476.
[18] S. Fauve and O. Thual, Phys. Rev. Lett. 64 (1990) 282.
[19] N. Kopell and L.N. Howard, Stud. Appl. Math. 64 (1981) 1;
P. Holmes, Physica D 23 (1986) 84;
A. Doelman, Physica D 40 (1989) 156;
L. Sirovich and P.K. Newton, Physica D 21 (1986) 115.
[20] M.J. Landman, Stud. Appl. Math. 76 (1987) 187.
[21] M. Florjanczyk and L. Gagnon, Phys. Rev. A 41 (1990) 4478;
F. Cariello and M. Tabor, Physica D 39 (1989) 77.
[22] R.H. Fisher, Ann. Eugen. 7 (1937) 355.
[23] A. Kolmogorov, I. Petrovsky and N. Piscounov, Bull. Univ. Moscow Ser. Int. A 1 (1937) 1.
[24] L.M. Hocking and K. Stewartson, Proc. R. Soc. London A 326 (1972) 289;
N.R. Pereira and L. Stenflo, Phys. Fluids 20 (1977) 1733.
[25] K. Nozaki and N. Bekki, (a) Phys. Rev. Lett. 51 (1983) 2171; (b) J. Phys. Soc. Jpn. 53 (1984) 1581.
[26] N. Bekki and K. Nozaki, Phys. Lett. A 110 (1985) 133.
[27] D.G. Aronson and H.F. Weinberger, Adv. Math. 30 (1978) 33.
[28] T.B. Benjamin and J.E. Feir, J. Fluid Mech. 27 (1967) 417;
J.T. Stuart and R.C. DiPrima, Proc. Roy. Soc. London A 362 (1978) 27.
[29] V. Hakim, P. Jakobsen and Y. Pomeau, Europhys. Lett. 11 (1990) 19; a more detailed account of this work is given in V. Hakim and Y. Pomeau, Eur. J. Mech. B 10 (1991) 137.
[30] B.A. Malomed and A.A. Nepomnyashchy, Phys. Rev. A 42, (1990) 6009.
[31] C.K.R.T. Jones, T.M. Kapitula and J.A. Powell, P. Rs. Edin. A 116 (1990) 193.
[32] J.B. Swift and P.C. Hohenberg, Phys. Rev. A 15, (1977) 319.
[33] I.S. Aranson, K.A. Gorshkov, A.S. Lomov and M.I. Rabinovich, Physica D 43 (1990) 435.
[34] G. Dee, J. Stat. Phys. 39 (1985) 705; Physica D 15 (1985) 295.
[35] G. Dee and W. van Saarloos, Phys. Rev. Lett. 60 (1988) 2641.
[36] A.V. Gurevich and L.P. Pitaevskii, Sov. Phys. JETP 66 (1987) 490.
[37] D.J. Kaup and A.C. Newell, J. Math. Phys. 19 (1978) 798;
E. Mjolhus and J. Wyller, Phys. Scr. 33 (1986) 442, and references therein;
Y. Ichikawa and Y. Abe, Prog. Theor. Phys. Suppl. 94 (1988) 128;

S.R. Spangler, J.P. Sheerin and G.L. Payne, Phys. Fluids 28 (1985) 104;
K. Ohkuma, Y.H. Ichikawa and Y. Abe, Opt. Lett. 12 (1987) 516;
M. Wadati, K. Konno and Y.H. Ichikawa, J. Phys. Soc. Jpn. 46 (1979) 1965.
[38] J.A.G. Roberts and G.R.W. Quispel, Phys. Reports, in press;
E.L. Hill, Rev. Mod. Phys. 23 (1951) 253.
[39] B.A. Malomed, Z. Phys. 55 (1984) (a) 241, (b) 249.
[40] L. Gagnon, J. Opt. Soc. Am. A 6 (1989) 1477.
[41] E. Montroll, in: Statistical Mechanics, eds. S.A. Rice and K. Freed (Univ. Chicago Press, Chicago, 1972);
P. Kaliappan, Physica D 11 (1984) 368;
K. Parlinski and P. Zielinski, Z. Phys. B 44 (1981) 317;
M. Otwinowski, R. Paul and W.G. Laidlaw, Phys. Lett. A 128 (1988) 483.
[42] A.V. Klyachkin, Modulational instability and autowaves in the active media described by the nonlinear equations of Ginzburg–Landau type, preprint (1989);
F. Cariello and M. Tabor, unpublished; J. Powell and M. Tabor, unpublished.
[43] J.A. Powell, A.C. Newell and C.K.R.T. Jones, Phys. Rev. A 44 (1991) 3636.
[44] H. Brand and R.J. Deissler, Phys. Rev. Lett. 63 (1989) 2801;
R.J. Deissler and H. Brand, Phys. Lett. A 146 (1990) 252.
[45] I.S. Aranson, L. Aranson, L. Kramer and A. Weber, unpublished.
[46] G. Dewel and P. Borckmans, in: Patterns, Defects and Materials Instabilities, eds. D. Walgraef and N.M. Ghoniem (Kluwer, Dordrecht, 1990) p. 63;
Y. Nishiura and M. Mimura, SIAM J. Appl. Math. 49 (1989) 481;
L.M. Pismen, J. Chem. Phys. 71 (1979) 462.
[47] D.W. McLaughlin and A.C. Scott, Phys. Rev. A 18 (1978) 1652.
[48] (a) R.J. Deissler, J. Stat. Phys. 54 (1989) 1459; (b) Phys. Lett. A 120 (1987) 334.
[49] H. Sakaguchi, Prog. Theor. Phys. (a) 85 (1991) 417; (b) 86 (1991) 7.
[50] G.B. Ermentrout and J. Rinzel, J. Math. Biol. 10 (1980) 97.
[51] G. Dewel and P. Borckmans, Europhys. Lett. 17 (1992) 523.
[52] D. Bensimon, B.I. Shraiman and V. Croquette, Phys. Rev. A 38 (1988) 5461.
[53] M.C. Cross, Phys. Rev. A 38 (1988) 3593.
[54] R.J. Deissler, Phys. Fluids 30 (1987) 2303;
M. Niklas, M. Lücke and H. Müller-Krumbhaar, Europhys. Lett. 9 (1989) 237.
[55] P. Kolodner, Phys. Rev. Lett. 66 (1991) 1165
W. Barten, M. Lücke and M. Kamps, Phys. Rev. Lett. 66 (1991) 2621.
[56] P. Collet and J.P. Eckmann, Instabilities and Fronts in Extended Systems (Princeton Univ. Press, Princeton, 1990).
[57] J.P. Eckmann and I. Procaccia, Phys. Rev. Lett. 66 (1991) 891.
[58] J.J. Rasmussen and K. Rypdal, Phys. Scr. 33 (1986) 481;
M.J. Landman, G.C. Papanicolaou, C. Sulem and P.L. Sulem, Phys. Rev. A 38 (1988) 3837;
V.E. Zakharov, N.E. Kosmatov and V.F. Shvets, JETP Lett. 49 (1989) 432;
L. Gagnon and P. Winternitz, Phys. Rev. A 39 (1989) 296.
[59] M. Abramowitz and I.S. Stegun, Handbook of Mathematical Functions (Dover, New York, 1972).
[60] L.S. Pontrjagin, Ordinary Differential Equations (Addison–Wesley, London, 1962) pp. 57–62.
[61] R. Suter, Z. Angew. Math. Phys. 34 (1983) 956.